UCL Université catholique de Louvain

Center for Systems Engineering and Applied Mechanics

Rehabilitation and Physical Medicine Unit.

The Gravitational Forces as Fundamental Input for Sensorimotor Coordination

F. Crevecoeur

Doctoral Dissertation presented
in partial fulfillment of the requirements for
the degree of Doctor in Applied Sciences

Prof. P. Van Dooren (chair), Univ. catholique de Louvain, Belgium
Prof. P. Lefèvre (supervisor), Univ. catholique de Louvain, Belgium
Dr. J. McIntyre, Univ. Paris Descartes, France
Prof. L. Plaghki, Univ. catholique de Louvain, Belgium
Prof. J-L. Thonnard (supervisor), Univ. catholique de Louvain, Belgium
Prof. S. Stramigioli, Univ. of Twente, Netherland

Acknowledgements

Ce travail n'aurait pas été possible sans la contribution d'un grand nombre de personnes. Je n'ose pas faire de liste exhaustive car le risque d'un oubli est trop élevé alors que j'entretiens avec vigueur le souvenir de chaque rencontre, si nombreuses soient-elles.

Tout d'abord, je souhaite exprimer à Jean-Louis et Philippe toute ma gratitude. Pour l'accompagnement, le soutien, la confiance et l'amitié dont vous avez si généreusement fait preuve durant ces années, merci.

Merci à Joe et Léon, pour avoir témoigné votre intérêt pour mon travail depuis le début de mes années de recherche en faisant partie de mon comité d'encadrement. Merci également à Stefano et Paul pour avoir accepté de faire partie du jury, qui restera un souvenir de grande valeur.

Merci à Thibaut pour avoir partagé chaque étape de cette aventure, les vols, les voyages, les hauts et les bas. Notre évolution côte à côte a été une réelle source de motivation.

Merci au CESAME, à Eyelab et et à l'unité READ pour l'ouverture et la richesse scientifique dont j'ai pu bénéficier et qui contribuent à créer un cadre de travail unique. Merci surtout pour tout ce qu'on a vécu en dehors de nos bureaux.

Je souhaite également remercier ma famille (étendue) pour leur soutien infallible, et mes parents en particulier qui ont absorbé tellement de stress de nous imaginer dans un avion en chute libre que nous avons pu voler tranquillement.

Enfin, merci à toi, Julie, pour ta présence, ta force et ton ecouragement qui m'ont guidé chaque jour.

Contents

1 Contribution **9**

1.1 Executive Summary 9

1.2 Publications and Communications 13

2 General Introduction **17**

2.1 The Scope of this Work 17

2.2 How to Model This 19

2.2.1 Prediction 19

2.2.2 Estimation 22

2.2.3 Control 25

2.2.4 Global Model 31

2.3 Where does Gravity Come into Play? 34

3 Movement control I: Hypergravity **37**

3.1 Introduction 38

3.2 Materials and Methods 41

3.3 Results 51

3.4 Discussion 62

3.5 Addendum 68

4 Forward models I: Hypergravity **69**

4.1 Introduction 70

4.2 Material and Methods 73

4.3 Results 77
4.4 Discussion 85

5 Forward models II: Microgravity 89
5.1 Introduction 90
5.2 Experimental Procedures 93
5.3 Results 99
5.4 Discussion 107

6 Optimal State Estimation 113
6.1 Introduction 114
6.2 Problem Definition and Assumptions 115
6.3 Control Algorithm 117
6.3.1 Optimal Controller 117
6.3.2 Optimal State Estimator 121
6.3.3 Recursion Formulas 122
6.3.4 Feedback Delay 124
6.4 Application 125
6.4.1 Model 125
6.4.2 Simulation Results 127
6.5 Conclusion 129

7 Movement control II: Microgravity 131
7.1 Introduction 132
7.2 Material and Methods 135
7.3 Results 144
7.4 Discussion 154

8 Conclusions and Future 161
8.1 Major Contributions 161
8.2 Limitation of Optimal Feedback Control 163
8.3 Open Questions and Perspectives 164

8.3.1 Long-term Adaptation 164
8.3.2 Optimal Control vs. Impedance Adjustments . . . 165
8.3.3 Horizontal vs. Vertical 167
8.3.4 Gain Up vs. Gain Down 168
8.4 Concluding word 169

A Control theory **171**
A.1 Introduction 171
A.2 Deterministic Systems, Continuous Time 172
A.2.1 Linear Systems 173
A.2.2 Optimal Control 174
A.2.3 Delayed Systems 178
A.3 Stochastic Dynamics, Discrete Time 180
A.3.1 Random Motion 180
A.3.2 Optimal Control 182
A.4 Towards Neuroscience 186

B Parabolic Flights **189**
B.1 Introduction 189
B.2 Data collection 189
B.3 Results and Conclusion 191

Chapter 1

Contribution

"Research is what I am doing
when I do not know what I am doing."

W von Braun.

1.1 Executive Summary

To achieve any movement, the brain must continuously decode sensory information, estimate the state of the body and send motor commands generating muscular forces and joint torques in order to bring the movements to the intended goal. Various sensory modalities are influenced by the action of gravity on the body. Notably, proprioception[1] informs the Central Nervous System (CNS) about the forces acting on the body, of which the gravitational forces.

However, sensory perception of these forces cannot be used as they are in order to calibrate the motor commands. Indeed, the presence of significant time delays affecting the transmission of neural signals and the presence of uncertainty, or sensorimotor noise, are potential sources of poor movement performance. In order to compensate for both time delays and noise, the CNS must develop control strategies based on an

[1]The proprioception can be defined as the perception of motion, position and forces of the body or a limb via sensory transducers found in muscles, tendons and joints (Shadmehr and Wise, 2005).

internal knowledge of the input-output relationship of a given system, like e.g. the effect of a motor command on the limb and/or object dynamics. This is thought to be ensured by groups of neurons, called internal models, that can mimic physical properties (see Kawato, 1999, for review). Internal models for motor control and sensory information will be presented and discussed in details in the following chapter (Chapter 2). Thus, motor learning and adaptation can be viewed as building internal models of the novel tool or environment dynamics.

Given the omnipresent action of gravitational forces on the body and on the objects that we manipulate, gravity plays a fundamental role in the internal models of dynamics. The goal of the two chapters presented hereafter is to better understand and model this role.

- In Chapter 3, we show that the movement pattern adapts rapidly to the hypergravity condition. A main result of this study is that the subjects did not show any tendency to recover a movement profile similar to the baseline condition (Earth gravity, 1g). Rather, the change in kinematic profile was consistent with the hypothesis of minimum total motor cost. We conclude that the CNS takes into account the action of gravity on the body in order to optimize the motor commands.

- Chapter 4 further argues that the hypergravity condition has little impact on the internal models of arm dynamics. Indeed, the coordination of grasping forces with changes in loads induced by voluntary movements shows performances that are comparable to the 1 g condition. In particular, the experimental results argue that the weight of a manipulated object is an input to the internal models of loads arising when the object is accelerated. The hypergravity condition also revealed that the subjects expected greater loads, as if the mass was increased instead of the gravity.

These two chapters strengthen the hypothesis that optimality principles apply to the role of gravity in the internal models. In addition, the weight of the interacting objects is an input that calibrates the motor gains for anticipating the consequences of motor actions.

The second part of the thesis addresses the problem of sensorimotor coordination in weightlessness (0 g). What is the motor strategy in this condition? How do internal models adapt when the gravitational input is lost? A summary of the three related chapters is given hereafter.

- Chapter 5 examines the anticipation of inertial loads induced by voluntary movements by looking at the grip force modulation applied by the subjects to the object manipulated under 0 g condition. Subjects had the inertial loads, proportional to the acceleration, as only information for adapting the internal models, since the weight of the object was zero. The results show that the inertial loads are continuously predicted, and that the grip force is adjusted accordingly.

- Chapter 6 presents an improvement of the computational model utilized in the present study. This model based on optimal feedback control allows to formulate the presence of sensory feedback delays, the presence of motor noise and the position and motor costs in a single sensorimotor process (Todorov and Jordan, 2002). The advantages and limitations of this model for sensorimotor coordination will be presented in the following chapter. Based on our previous results, this model was naturally retained for testing our hypothesis on the control strategy in weightlessness.

  Practically, we improve the state estimation of a stochastic process of which only delayed, noisy and possibly incomplete measurements are available. With a better estimate of the state of the system at each point in time, the controller achieves better

performance in terms of movement accuracy and variability.

- The technique developed in Chapter 6 was employed in Chapter 7 in order to test the hypothesis of control gain reduction in order to maintain the movement stability. Indeed, although the internal models adapt to this condition (see Chapter 5), the data indicate that the output of internal models may present more variability, or be considered as less reliable at a central level. Therefore, movement performance cannot be similar to the normal gravity condition where internal models are well calibrated. This can be translated as authorizing the movement to be less precise and limit the intensity of motor corrections when the arm deviates from the intended position. The optimal feedback control theory allowed us for directly testing this hypothesis in a well-defined computational framework. We modulated the cost function following the alteration of the internal model and reproduced the change in movement kinematics that we observed experimentally, in quantitative agreement.

These results are discussed in the last chapter where the differences between hypergravity and microgravity are put forward. In light of our results, we suggest that the CNS uses the effect of gravitational forces to tune the sensorimotor loop and adjust the motor gain. In other words, the objects and body weight is a guidance for the movement. For this reason, the microgravity condition has an effect that dramatically differs from the effect of the hypergravity condition, despite a similar absolute change in the gravity level. In the former, the guidance is lost, forcing the CNS to rely more heavily on the sensory afferents[2] rather than internal models. We show that adjusting the intended performance can preserve movement stability. We suggest that this strategy can be

[2]The afferents are the set of neurons carrying neural inputs from receptors or sense organs towards the central nervous system.

a general mechanism in motor learning. A series of open questions and perspectives emanating from these results is proposed to close the core of the present thesis.

1.2 Publications and Communications

Published:

- Crevecoeur F., Thonnard J-L., Lefèvre P. (2009) Optimal integration of gravity in the trajectory planning of vertical pointing movements. *Journal of Neurophysiology*, 102: 786 - 796.

- Crevecoeur F., Thonnard J-L., Lefèvre P. (2009) Forward models of inertial loads in weightlessness. *Neuroscience*, 161: 589 - 598.

Under Revision:

- Crevecoeur F., McIntyre J., Thonnard J-L., Lefèvre P. Movement stability under uncertain internal models of dynamics.

- Crevecoeur F., Sepulchre R., Thonnard J-L., Lefèvre P. Improving the state estimation for optimal control of stochastic processes subject to multiplicative noise.

- Crevecoeur F., Thonnard J-L., Lefèvre P. Sensorimotor mapping for anticipatory grip force modulation.

Proceedings:

- Crevecoeur F., Thonnard J-L., Lefèvre P. (2008) Feed forward compensation of hyper gravity in vertical pointing movements. *IFMBE Proceedings*, 22: 2109 - 2112.

Oral presentations and posters:

- Crevecoeur F, Thonnard JL, Lefèvre P. Movement slow-down in weightlessness: a stabilization mechanism to compensate for sensory feedback delays. *Workshop on Human Behaviour and Performance in Analogue Environments and Simulations*, Noordwijk (ESTEC-European Space Agency) 2009 (Poster).

- Crevecoeur F, Thonnard JL, Lefèvre P. Using delayed feedback to learn new dynamics: implication for motor control and application to pointing movements in weightlessness. *Annual meeting of the Society for Neuroscience*, Chicago 2009 (Poster).

- Crevecoeur F, Thonnard JL, Lefèvre P. How do astronauts control arm movements in space? *17th IAA Human in Space Symposium*, Moscow 2009 (Oral Presentation).

- Crevecoeur F, Thonnard JL, Lefèvre P. Motor commands are optimized in the gravity field. *28th Bénélux Meeting on Systems and Control*, Spa 2009 (Oral Presentation).

- Crevecoeur F, Thonnard JL, Lefèvre P. Influence of changes in gravity on the trajectory planning of vertical pointing movements. *Annual meeting of the Society for Neuroscience*, Washington 2008 (Poster).

- Crevecoeur F, Thonnard JL, Lefèvre P. Feed forward compensation of hypergravity in vertical pointing movements. *4th European congress on Biomedical Engineering*, Antwerp 2008 (Oral Presentation).

- Crevecoeur F, Thonnard JL, Lefèvre P. Eye-hand coordination in a pointing task performed during short exposure to weightlessness. *Annual meeting of the Society for Neuroscience*, San Diego 2007 (Poster).

- Crevecoeur F, Thonnard JL, Lefèvre P. The control of Grip-Force in a point-to-point task performed during short exposure to weightlessness. *Annual meeting of the Neural Control of Movement society*, Sevilla 2007 (poster).

Chapter 2

General Introduction

"A mathematician is someone who can take a cup of coffee and turn it into a theory."

P Erdos.

2.1 The Scope of this Work

Consider the problem of reaching to grasp for an object of interest, like a cup of coffee. There are at least two ways to solve it. First, one can write down the mechanical equations describing the motion of the musculo-skeletal system, add a physiological model for muscular contraction and force production, make hypotheses on the control strategy used by the brain, and compute a solution of the reach-for-a-cup problem. Such a solution would be certainly efficient, but it would be based on extremely simplifying assumptions; for instance a single joint reach-for-a-cup in the horizontal plane would help a lot, for non-linear dynamics concerns. In addition, it is likely that under a head-roll condition (e.g. answering a phone call), the solution of the reach-for-a-cup should be re-computed, in order to account for the novel head position and orientation relative to the cup.

The second way to solve this problem is to actually grasp the cup and drink. This is done thousands of times by the best engineers while

they are setting up and implementing the best control algorithms for the first attempt to solve the reach-for-a-cup problem. This suggests that the brain regions responsible for the mathematical and engineering solutions are much slower than the regions responsible for motor control. But, this is not a result of the present work. This thesis uses the first approach to investigate the effect of changes in gravity on the control of arm movements.

This example illustrates that the brain solves a fascinating amount of complex problems that would represent very hard challenges for engineers if robots were similar to the human motor system. Despite the precision of the computers and the electro-mechanical devices employed in robotic applications, robots are still clumsy and their movement repertory is limited. Counter to this observation, humans and animals achieve complex motor tasks with a disconcerting ease. For decades, many research efforts have therefore been dedicated to the understanding of how the brain controls a movement.

The complexity of the mechanisms underlying the control of movement is further disconcerting when one carefully considers the physical and physiological constraints that act on the body. Some of these constraints are due to the geometry of the limbs, some are induced by self-motion (e.g. Coriolis acceleration during body rotation) and others are applied externally by the environment. Among the external constraints, gravitational forces (and Sir Isaac Newton) condition the dynamics of our movements since we are born. In this respect, it is likely that the presence of gravity plays a fundamental role in motor control, but this role is still far from being fully understood. Is this force needed for motor systems at maturity? Or is it a constraint, in the sense that its action penalizes the movements? Are humans able to move efficiently in other gravitational fields? Do the adaptive mechanisms depend on the level of gravity?

The following chapters address these questions by investigating motor behavior of healthy human subjects in various gravitational contexts induced by parabolic flights. This experimental environment allowed for testing adaptation to both hypergravity and microgravity. The studies reported hereafter present relevant pieces of answers on the role played by gravity in the control strategy used by the Central Nervous System (CNS).

Before entering into the details, the following sections review the state-of-the-art models for motor control, address the role of gravity in motor control and give a summary of the contents of this thesis.

2.2 How to Model This

This section surveys the scientific hypothesis formulated in the modeling approach of motor control. The theory is divided into three distinct processes: prediction, estimation and control. These processes are not independent, and are generalized in a global model of sensorimotor coordination. However, they constitute distinct stages in the control of a movement; they are thus presented accordingly.

2.2.1 Prediction

The signal conduction along the nerves delays the sensory information conveyed from the periphery to the central nervous systems. The presence of feedback delay is a potential source of instability and poor performance for the achievement of a movement. In order to compensate for feedback delays, there is consensus on the fact that the brain predicts the sensory consequences of a self-generated action (Wolpert and Flanagan, 2001). Such prediction allows the brain to anticipate the effect of the ongoing motor commands.

Evidence for the predictive control process is given by the grip force

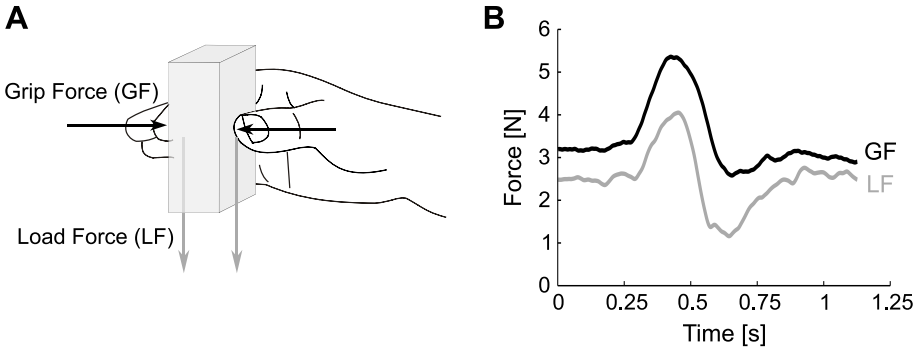


Figure 2.1: (A) Illustration of a precision grip, the object is held between the thumb and the index finger. The grip force (GF) is the mean of the force components normal to the finger-object interface and the load force (LF) results from the tangential constraints at the finger-object interface. (B) Typical grip and load forces profiles as a function of time during one vertical point-to-point movement.

modulation during object manipulation. When healthy subjects move an object held between the thumb and the index finger, the increase in load due to the object acceleration is properly anticipated by an increase in the grip force applied by the fingers normally to the object surfaces (Flanagan and Wing, 1993, 1995). The modulation of grip force is synchronized with the variation of inertial loads, which would be impossible if the CNS would rely on tactile and proprioceptive feedback. In addition, the amplitude of the modulation correlates with the amplitude of load variation, suggesting that the inertial load is predicted for each individual movement.

The coupling between the grip force and the load force is shown in Fig. 2.1A illustrates the forces on a representation of a precision grip. Fig. 2.1B shows the grip force and the load force as a function of time during one typical vertical point-to-point movement. Such movement consists of a stable phase, followed by a dynamic phase during which the subject was asked to move the held load following a vertical axis,

before another stable phase. At the beginning of the trial (from 0 to 250 ms), the arm is stable and the resulting tangential constraint equals the weight of the object ($\sim$ 2.5 N for 250 g). Then the load force increases proportionally to the upward acceleration. The grip force clearly anticipates the increase in load force and consequently presents a peak in phase with the load force peak.

This predictive mechanism is formulated as a forward model: an internal model within the CNS that can simulate the limb dynamics and predict the consequences of the ongoing arm motor command (Miall and Wolpert, 1996). Thus, the motor command is sent to the limb and to the forward models as a corollary discharge, also called efference copy, for internal processing.

Internal prediction based on forward models is processed in other contexts. It is known that the brain predicts the change in visual space provoked by a saccadic eye movement and remaps the location of surrounding stimuli relative to the novel eye position (Duhamel et al., 1992). This mechanism allows for differentiating the objects moving relative to the body from the apparent motion of stationary objects induced by self-movements. Similarly, reaching movements performed during active trunk rotation are not affected by the Coriolis acceleration, whereas Coriolis force induced by passive rotation markedly altered the motor performances (Pigeon et al., 2003; Lackner and Dizio, 1994). These results show that the CNS predicts the self-generated Coriolis force field and adjusts the reach motor commands accordingly, in an anticipative way.

At a neural level, body of evidence is growing that the prediction based on internal models is processed in the cerebellum via the cortico-cerebellar loop (Miall et al., 1993; Wolpert et al., 1998b; Kawato et al., 2003; Nowak et al., 2007).

2.2.2 Estimation

Many parameters of the body and its environment must be continuously estimated in order to produce adequate motor behavior. For instance, when the engineers are drinking while they are reading an error in the source code of the implementation of arm dynamics, the grip and arm motor commands will depend on the expected object weight. This expectation is based on the knowledge of whether the cup is full or almost empty, and possibly corrected if the weight experienced after grasping the cup differs from the expected weight. In such context, the use of Bayesian statistics for maximum likelihood estimation has been proposed as powerful model for multi-sensory integration.

Indeed, the best strategy to estimate a given parameter is to combine all sources of information (including sensory afferents and prediction), and allocate each of them a relative weight that depends on their level of reliability. The resulting estimate is unbiased with minimum uncertainty (i.e. minimum variance). The Bayesian integration model is an adequate framework to describe how prior expectations (i.e. knowledge based on previous experience) and sensory feedback (the actual weight encoded from tactile and proprioceptive feedback) are combined in a optimal weight estimate. Many experimental results evidence strong similarities between this model and the strategy used by the CNS in sensorimotor learning and state estimation (Kording and Wolpert, 2006).

Formally, Bayes' theorem gives the posterior distribution of an event, A, given a conditional measurement B through the following relation:

$$P(A|B) = \frac{P(B|A)P(A)}{P(B)}. \tag{2.1}$$

In our example, the left hand side of Equation 2.1 is the probability distribution of the weight of the cup (represented by A), given the sensory feedback (called B). This distribution depends on the conditional probability distribution of the sensory feedback given A, $P(B|A)$, multiplied

by the prior distribution of A. The denominator is the marginal distribution of B ensuring that the posterior distribution integrates to 1. In filtering applications, the problem consists in estimating the posterior distribution of the state of a process at time t, say x_t, by taking into account a collection of noisy measurements (y_1, y_2, $\ldots$, y_t). Based on Equation 2.1, one can write:

$$f(x_t|y_1, \ldots, y_t) = \frac{f(y_t|x_t)f(x_t|y_1, \ldots, y_{t-1})}{f(y_t|y_1, \ldots, y_{t-1})}. \tag{2.2}$$

In other words, the probability density of the state given the feedback is computed from a prediction of the state distribution based on the last feedback $f(x_t|y_1, \ldots, y_{t-1})$, which is updated by taking into account the current feedback (y_t in Equation 2.2). In the particular case of linear functions for the process dynamics and the feedback, and Gaussian distribution at each time step, it can be proven that the resulting posterior is also Gaussian with mean and covariance given by the Kalman filter (see the Appendix A). Finally, one can show that the optimal state estimate in the sense of minimum variance (i.e. maximum likelihood) is the conditional expectation computed from the posterior distribution (Jazwinski, 1970, pp. 148).

These mathematical considerations define a general framework for integration of internal representation based on prediction and state estimation in general. This theory successfully modeled the strategy in sensorimotor integration (Wolpert et al., 1995; Kording and Wolpert, 2004), the estimation of force production (Kording et al., 2004), or the combination of remapped and peripheral retinal information (Vaziri et al., 2006). The Bayesian estimation is closely related to the maximum likelihood estimation that is a robust strategy of the CNS: Singh and Scott (2003) showed that a perturbation of the elbow dynamics, that correlated with the elbow velocity, was locally attributed to this joint, although is was actually depending on the shoulder velocity. This

strategy vanished when the correlation between the joint dynamics and the perturbation decreased, arguing for a strong reliability on maximum likelihood principles within the CNS. More recently, Berniker and Kording (2008) demonstrated that the Bayesian integration in estimation of whether dynamics parameters were due to either body or environment changes accounted for many features of motor learning, including generalization and skill transfer across workspaces and limbs.

At a neural level, the parietal cortex[1] is thought to play a central role in the state estimation process. Damages to the parietal cortex were associated to an impaired ability to maintain an internal representation of the state of the body (Wolpert et al., 1998a). In the context of reaching movements, the parietal cortex was proposed as sensorimotor interface for the online movement control (Desmurget et al., 1999; Buneo and Andersen, 2006), and the representation of visual and proprioceptive feedback are present in the parietal lobe (Filimon et al., 2009). The cerebellum is also involved in the estimation process as demonstrated by Miall and colleagues (Miall et al., 2007; Miall and King, 2008). These results are consistent with the hypothesis that the state estimate at a given point in time will be composed of a predicted estimate from the cerebellum, completed with feedback information of weighted sensory signals from the parietal cortex. The anatomy of the parietal lobe further supports this view: the parietal cortex receives projections from the visual cortex, from the somatosensory cortex and from the cerebellum via the thalamus (Amino et al., 2001). The parietal lobe projects in turn to the motor and premotor areas involved in the control of movements (Battaglia-Mayer et al., 2003).

[1]The parietal cortex is the brain region situated behind the frontal lobe and above the occipital lobe. See Figure 2.2 section 2.2.4 for a better localization.

2.2.3 Control

The control problem in this context can be defined as follows: what does the brain send to the muscles? How does the CNS compute the motor command sent on the hard wires? This general problem is intrinsically hard to define because it covers many subproblems, each of them involving unknown parameters: What is the control strategy? In which frame of reference are the movements planned? What are the state variables taken into account? What are the relevant criteria that constitute the "goal of the movement"? Each problem has recruited many research efforts, yielding the following hypotheses for the process of movement control.

Equilibrium-point Control

The equilibrium-point hypothesis is based on the similarity between springs and muscles. This property allows for stabilizing the body in a given position, called equilibrium-point. A change in equilibrium point will therefore modify the stiffness of muscles in order to stabilize in the novel equilibrium position, which will generate a movement. In this framework, the control of movement was seen as a series of equilibrium-points and the movement results from shifting from one point to another as consequence of the change in the spring-like configuration of the muscular system (Polit and Bizzi, 1979; Bizzi et al., 1992; McIntyre and Bizzi, 1993).

The implications of this hypothesis grounded many research avenues. First, the series of equilibrium-points suggests that an internal representation of the movement (called "virtual trajectory" by Bizzi and colleagues) is available within the CNS. Such concept of internal desired trajectory is largely used in other computational models for motor control. Second, the change in spring-like configuration suggests that

the CNS controls the mechanical impedance of the arm. Evidence for impedance adjustments in motor learning and adaptation were found in subsequent studies.

However, some studies raised objections. Based on measurements of the arm stiffness during a movement, Gomi and Kawato (1996) computed the corresponding virtual trajectory under the equilibrium-point hypothesis. The estimated trajectories were very different from the experimental data. Another concern is raised by motor adaptation to velocity dependent force fields. Before adaptation, subjects exposed to viscous or Coriolis force fields generate movements that deviate from the straight trajectory observed when no force field is present (Lackner and Dizio, 1994; Shadmehr and Mussa-Ivaldi, 1994). These movements fall aside of the target. However, according to the equilibrium-point hypothesis, the final position should be the same since the effect of the velocity dependent force field vanish when the velocity decrease. However, the data clearly indicated that the movements fell aside of the target despite identical loading condition at very low velocity.

These results suggest that the time course of the motor commands was adapted to the dynamical interaction with the external force across the movement, which can be directly attributed to an internal model.

Inverse Models

A possible control strategy is that the CNS possesses internal models that invert the arm dynamics in order to map a desired trajectory into a motor command (Kawato, 1999; Wolpert and Ghahramani, 2000). In this context, the inverse models can process any desired trajectory and compute the motor commands that will generate the corresponding movement.

After adaptation, the removal of the velocity dependent force fields

provoked mirror effects as observed in the initial exposure to the perturbing field (Lackner and Dizio, 1994; Shadmehr and Mussa-Ivaldi, 1994). It means that the CNS had learned the novel dynamics of the arm and calibrated the motor commands in order to reproduce movement paths similar to the unperturbed condition. The internal representation of the novel dynamics is evidenced by the after-effect observed upon removal of the perturbing field. These results suggest that the internal processing of a motor command depends on the limb and interaction dynamics throughout the whole intended trajectory, which is the definition of an inverse model.

However, how the desired trajectory is selected remains an open question, addressing the coordinate frame of reference in which movements are planned. It has been proposed that the brain optimizes the movement smoothness (Flash and Hogan, 1985), the joint-torque changes (Uno et al., 1989; Nakano et al., 1999) or the inertial forces (Nishikawa et al., 1999). Specific and independent models were also proposed for kinematic and dynamic control adaptation (Krakauer et al., 1999).

These models predicted many features of movement properties (bell shape velocity profiles, no abrupt changes, etc.), but failed to explain the trial to trial variability. An alternative model suggested that the motor sequence is determined by the presence of signal-dependent noise if the controller aims at minimizing the end-point variability (Harris and Wolpert, 1998). The signal-dependent noise is the property of sensory and motor systems that the variability of a process (such as a muscular contraction) increases with its intensity (Jones et al., 2002; Todorov and Jordan, 2002). The minimum end-point variance model accounts for the presence of stochastic dynamics in the motor systems but, again, fails to explain the online motor adjustments observed on a single movement basis. In general, the common denominator of these models is that the brain does neither like useless expenditures nor variability.

The formation of internal inverse models is also an open question. A simplistic view consists in adjusting the motor commands based on the error feedback between the actual and intended path. A more realistic approach is based on the adjustment of mechanical impedance. Indeed, the CNS can tune the arm stiffness in the direction of instability (Burdet et al., 2001; Franklin et al., 2004). In addition, adjustments of mechanical impedance based on unexpected changes in muscle length can be the mechanism for building internal models (Franklin et al., 2003, 2008). Other studies support the hypothesis that the movement is controlled in terms of impedance (e.g. Damm and McIntyre, 2008)

The limitation of the inverse models approach is that it assumes that motor commands can be computed a-priori and that the execution of the motor plan (output of the inverse model) can be processed independently. However, experimental results presented hereafter show that, on a single movement basis, planning and execution cannot be dissociated. The optimal feedback control theory was then proposed and considered planning and execution as a single sensorimotor process.

Feedback Control

It was shown that the CNS is capable to limit the variability that interferes with the task objective, whereas variability that is irrelevant relative to the objective is less controlled. For instance, when subjects are asked to track a trajectory by passing through a given set of via-points, the trajectory variability decreases when the number of via-points along the trajectory increases (Todorov and Jordan, 2002). This suggests that planning and execution are not independent and are continuously processed during a movement. This control strategy, known as the “minimum intervention principle”, is captured by the computational framework of optimal feedback control.

The general assumption of optimal feedback control is that, at each point in time, the CNS must estimate the state of the body based on internal prediction and sensory feedback. Then, the CNS sends a motor command that is a function of the current estimate. The optimal feedback control theory is currently a powerful model for motor control, including aspects related to flexibility and online processing in target jump paradigms (Liu and Todorov, 2007; Izawa and Shadmehr, 2008), bimanual coordination (Diedrichsen, 2007), learning strategies in uncertain environments (Izawa et al., 2008), adaptability and object manipulation (Braun et al., 2009; Nagengast et al., 2009).

The main advance of this theory is the well defined computational model integrating the fact that motor output continuously depends on the sensory inflow. But, it has its own limitations. For instance, going back to the experiment from Polit and Bizzi (1979), they showed that when a robot placed monkey's arms on the target prior to the movement onset, the animals realized movements towards the initial position and ended the trajectory as in the normal condition. According to the optimal feedback control theory, a better strategy would be simply to stay on the target. This result is closely related to the concept of desired trajectory that was sought by the monkey despite that goal was already attained (and the probability of reward was very high). This is hardly captured by the optimal feedback control theory, unless via-points, constituting the desired trajectory, are specified in the cost function.

Neural Basis

The complexity of neural processing underlying the control of movements reflects the diversity of subproblems included in this topic. One view argues for a hierarchical transformation of task goals defined in rather abstract *extrinsic coordinates* (e.g. movement direction) to a

coding in *intrinsic coordinates* (muscular joint contractions). A simple view is that this hierarchy is serially implemented from the premotor cortex for abstract (extrinsic) movement representation like e.g. movement direction (Kakei et al., 2001), then by the primary motor cortex (M1) that encodes the movement variables in intrinsic coordinates (Scott and Kalaska, 1997), projecting to the spinal interneurons for muscular coding (Yanai et al., 2008).

The transformation from extrinsic to intrinsic coordinates must necessarily be computed prior to generating accurate control commands, but the serial implementation is a too simplistic model, given that neurons in the premotor areas are also sensitive to changes in arm configuration for invariant hand paths (Scott et al., 1997), and that neural correlates with kinematics features of the movement, including extrinsic movement parameters such as movement direction and speed, can be found in the primary motor cortex (Kakei et al., 1999; Scott, 2003). In addition, the serial transformation does not take into account the parallel processing given the contribution of the premotor areas to the corticospinal projections (Dum and Strick, 1991). In principle, neural correlates of high level parameters of movements (e.g. direction and speed) can be explained by a direct control of muscular activation encoded in M1 (Todorov, 2000), but M1 activity also evokes complex behaviors involving multi-joint dynamics (Graziano, 2006).

Hence, although the precise role of M1 is still the subject of animated debates, its activity is closely related to the control process, and in feedback control in particular (Scott, 2004, 2008). Indeed, in the context of optimal feedback control, an internal representation of the state of the body, including task objectives and variables of higher order, is necessary for the computation of adequate motor commands.

2.2.4 Global Model

The model is represented in Fig. 2.2A. It was simplified from Shadmehr and Krakauer (2008) in order to focus on the three processes described in the previous sections. The general view is that a controller generates the motor commands (based on inverse models and on feedback control policies), which are sent to the limb and to the forward model for internal processing. The prediction computed from the forward model is combined with the sensory feedback in order to produce the current state estimate that is used for online feedback control. The current state estimate must be updated in the forward model in order to process the computation of the next prediction.

Fig. 2.2B illustrates the interaction between key regions involved in the planning and execution processes of a movement. This schematic representation shows that the anatomy of neural regions is consistent with the computational problems identified in motor control.

The central role played by M1 is emphasized by the projections received from the premotor areas for more abstract movement representation, from the primary somatosensory cortex (S1) and the parietal cortex for feedback control based on sensory feedback and current state estimation, and from the cerebellum. Many features of the network map were omitted for clarity, such as the interaction with subcortical structures like the thalamus acting as relay in the cerebello-cortical projections. It should also be emphasized that an optimal control policy must be based on expected rewards and motor costs, which are not represented in the model of Fig. 2.2 (and implicitly embedded in the "Goal"). The basal ganglia may be responsible for the implicit attribution of cost and rewards to a given action (Mazzoni et al., 2007).

From a computational point of view, let us first assume that the

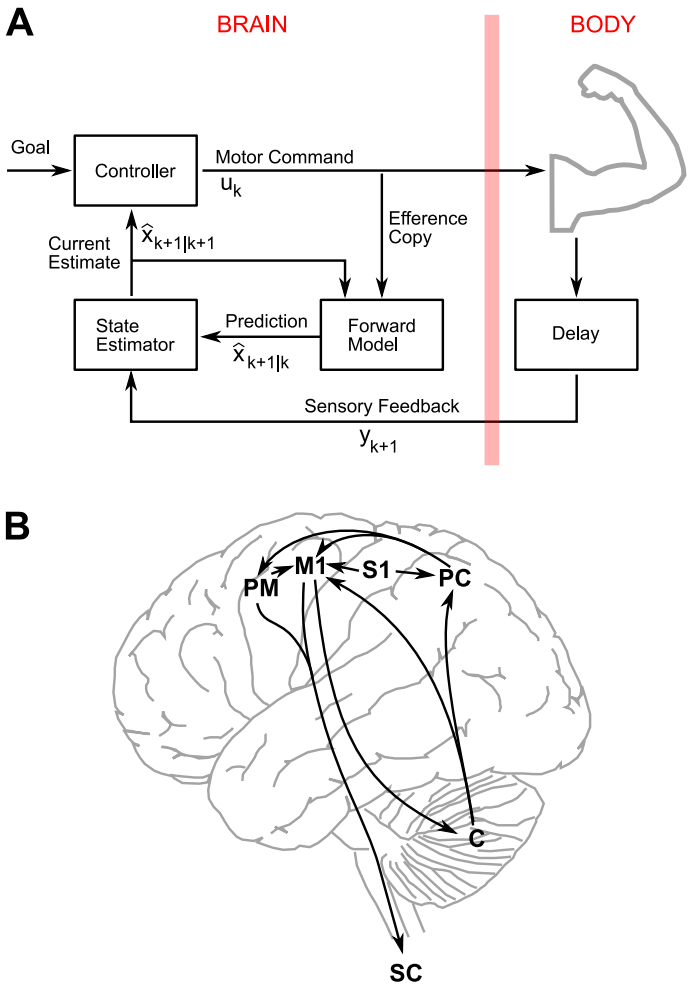


Figure 2.2: (A) Computational model for motor control (see text for detailed description). (B) Extremely simplified illustration of the interactions between the main regions involved in the control of movements. The arrows represent neural projections, the regions represented are the primary motor cortex (M1), the premotor cortex (PM), the primary somatosensory cortex (S1), the parietal cortex (PC), the cerebellum (C) and the spinal cord (SC).

system dynamics and feedback are linear and described by:

$$\begin{aligned} x_{k+1} &= Ax_k + Bu_k + \text{noise}, \\ y_k &= Hx_k + \text{noise}. \end{aligned}$$

In these equations, x is the state vector (e.g. position, velocity and joint torque), u is the control, and y is the feedback measurement (the discrete time formulation is required by the presence of noise). It is further assumed that the controller will minimize a cost expressed as a quadratic form in the state and control variables defined along the whole trajectory as follows:

$$J(x,u) = \sum_k x_k^T Q_k x_k + u_k^T R u_k. \tag{2.3}$$

Assuming that the controller possesses an internal model (i.e. knows A, B and H), a prior estimate of x_{k+1} can be computed from the corollary discharge and the current state estimate noted $\hat{x}_{k|k}$:

$$\hat{x}_{k+1|k} = A\hat{x}_{k|k} + Bu_k.$$

It is the maximum likelihood expected next state, given the current estimate ($\hat{x}_{k|k}$) and the corollary discharge (assuming Gaussian noise distributions). Based on Bayes' theorem, the optimal state estimate at time $k+1$ will be a combination of the prior estimate and a correction that depends on the difference between the actual and expected sensory feedbacks (Kalman filter):

$$\hat{x}_{k+1|k+1} = \hat{x}_{k+1|k} + K_{k+1}\left(y_{k+1} - H\hat{x}_{k+1|k}\right). \tag{2.4}$$

Fig. 2.2A illustrates these variables. Under these assumptions, the optimal control policy turns out to be a linear function of the state only, linking directly the estimation and control:

$$u_k = -L_k \hat{x}_{k|k}. \tag{2.5}$$

The optimal control policy (L_k) and Kalman gains (K_k) are fully determined analytically by the cost matrices (Q_k and R_k, Equation 2.3), the variance of the noise and the matrices describing the state-space representation of the system (A, B and H). Detailed mathematical developments can be found in the Appendix on mathematical control theory.

The advantage of the optimal feedback control framework is to provide a strong theoretical framework as a general model of sensorimotor coordination. When the system presents nonlinear dynamics, the optimal control policy may contain terms that do not depend on the state estimate (i.e. an affine control law (Li and Todorov, 2007)), in accordance with the hypothesis of inverse models.

2.3 Where does Gravity Come into Play?

Everywhere. The feed forward motor commands, the feedback responses and the long latency reflexes share internal models (Wagner and Smith, 2008; Kurtzer et al., 2008), suggesting that the internal representation of the limb dynamics is a crucial component at distinct levels of movement control. Similarly, accurate predictions, and consequently estimations, depend on the accuracy of the internal forward models. Therefore, changes in the limb dynamics following a change in gravity potentially alter all stages of sensorimotor processing.

Previous results indicate that the CNS uses internal representations of the effect of gravity on the body and on surrounding objects in various contexts including body orientation, catching falling objects or mass estimation (Lackner and DiZio, 2009; McIntyre et al., 2001; Ross et al., 1984). The effect of short- and long-term exposures to weightlessness on the control of movement was investigated in various experimental paradigms. There is an agreement on the presence of an effect but the

results seem inconclusive. A tendency for reduction of movement speed followed by increased execution time was reported in visuomotor tasks (Berger et al., 1997; Papaxanthis et al., 1998a; Sangals et al., 1999); and a reduction in movement amplitude was observed in single joint elbow rotation (Fisk et al., 1993).

Despite some convergence, a unifying hypothesis explaining the effect of exposure to weightlessness on the control of movement is currently lacking (Bock, 1998). In this previously cited review, Bock argued that the adaptation to the 0 g condition requires the suppression of no longer adapted motor commands, and that the learning of the novel input-output relationship of the motor systems is highly demanding from a computational point of view. The demanding process can be at the origin of the tendency for movement slow down observed under a 0 g condition. Such hypothesis is of course tenable but the mechanisms supporting the adaptation to changes in gravity and their interpretation in the current model for motor control is currently missing.

A recent study on oscillatory movements showed that human subjects responded to changes in gravity by changing the movement frequency as a resonance phenomenon of a pendulum (White et al., 2008). This result suggests that the CNS can take advantage of the dynamic interaction with the environment and gravitational forces on the limb in particular. It also enhances the challenge of moving in 0 g under the hypothesis that the CNS exploits gravitational forces.

A reduction of movement speed and acceleration accompanied by an increase in movement duration was also reported during prolonged exposure to weightlessness (Mechtcheriakov et al., 2002). In the latter reference, the authors showed that the visual feedback limited the movement error, but without modifying the tendency for movement slowing, arguing for the use of sensory feedback for movement stabilization. However, they did not provide any evidence that this was computationally

plausible under signal-dependent noise and delayed state feedback characterizing the motor system.

On the contrary, the effect of changes in gravity on the dynamics of prehension in both rhythmic and discrete movements revealed fast timescales of adaptation. Subjects performing oscillations in the vertical plane showed flexible and adapted patterns of grip force (Hermsdorfer et al., 2000). The pattern of grip/load forces coupling in naive subjects was comparable to those of expert subjects after a short exposure time (5 parabola, $\sim$ 100 cycles, (Augurelle et al., 2003a)). In a similar task, changes in gravity emphasized that the arm and grip motor commands were dissociated. In other words, the grip force adjustments were based on the actual load force variation, despite distinct combinations of inertial, gravitational and mass constraints (White et al., 2005).

The following chapters address some of the open questions raised above: we investigated the role played by gravity in movement control in the context of point-to-point movements in order to better contextualize the problem of moving in weightlessness. Then, we investigated the quality of the prediction of inertial loads in both hyper and microgravity to address the problem of adaptation of forward models for state estimation. The results on forward models from anticipatory grip force adjustments revealed the sensorimotor strategies for state estimation in changed gravity, yielding the hypothesis of re-optimization of the motor commands in hypergravity and the reduction in control gains in microgravity. As a whole, our results provide a general framework for understanding the contribution of gravitational forces for sensorimotor coordination and interpret the effect of changes in gravity in the general context of optimal control and state estimation.

Chapter 3

Optimal integration of gravity in trajectory planning of vertical pointing movements

"As far as the laws of mathematics refer to reality, they are not certain; and as far as they are certain, they do not refer to reality."

A Einstein.

[1]**Abstract.** The planning and control of motor actions requires knowledge of the dynamics of the controlled limb in order to generate the appropriate muscular commands and achieve the desired goal. Such planning and control implies that the Central Nervous System must be able to deal with forces and constraints acting on the limb, such as the omnipresent force of gravity. The present study investigates the effect of hypergravity induced by parabolic flights on the trajectory of vertical pointing movements in order to test the hypothesis that motor commands are optimized with respect to the effect of gravity on the limb. Subjects performed vertical pointing movements in normal gravity and hypergravity. We use a model based on optimal control to identify the role played by gravity in the optimal arm trajectory with minimal motor

[1]Journal of Neurophysiology (2009), 102:786-796.

costs. First, the simulations in normal gravity reproduce the asymmetry in the velocity profiles (the velocity reaches its maximum before half of the movement duration), which typically characterizes the vertical pointing movements performed on Earth, whereas the horizontal movements present symmetrical velocity profiles. Second, according to the simulations, the optimal trajectory in hypergravity should present an increase in the peak acceleration and peak velocity despite the increase in the arm weight. In agreement with these predictions, the subjects performed faster movements in hypergravity with significant increases in the peak acceleration and peak velocity, which were accompanied by a significant decrease in the movement duration. This suggests that movement kinematics change in response to an increase in gravity, which is consistent with the hypothesis that motor commands are optimized and the action of gravity on the limb is taken into account. The results provide evidence for an internal representation of gravity in the central planning process and further suggest that an adaptation to altered dynamics can be understood as a re-optimization process.

3.1 Introduction

The investigation of the skillful and smooth movements that we achieve so many times a day intends to clarify how movements are controlled by the Central Nervous System. There are an infinite number of feasible trajectories and kinematics that allow individuals to perform a basic movement. However, in general, little variability is observed between repeated movements. Why is this? Is there any reason why one particular movement is realized among an infinite number, and why this movement is stable across repeated executions? To answer this question, one should identify the criteria taken into account when the movements are planned and controlled and how the system responds to a change in the

environment.

For this purpose, the concept of optimality has long been associated with mechanical parameter adjustments (Burdet et al., 2001) and with movement planning and control, assuming that motor actions were optimal with respect to a cost defined along the movement. Kinematics and dynamics costs have successfully modeled real movements (Flash and Hogan, 1985; Nakano et al., 1999; Uno et al., 1989) as well as the costs related to the movement variability and sensorimotor noise (Harris and Wolpert, 1998). Feedback control has also been proposed to rely on optimal strategy, maximizing locally the expected reward related to the next state at minimum cost by taking into account an estimate of the current state (Todorov, 2004; Todorov and Jordan, 2002). The optimal feedback control framework, supported by the neural basis, finely models the movement strategies, flexibility and learning properties of motor control (Izawa et al., 2008; Liu and Todorov, 2007; Scott, 2004; Shadmehr and Krakauer, 2008).

These models assume that the Central Nervous System has access to the internal representations of the limb dynamics and state (position, velocity, etc.) thanks to internal models (Kawato, 1999; Wolpert and Ghahramani, 2000) that are necessary for the computation of motor commands in the both feed forward and feedback control schemes (Wagner and Smith, 2008). Indeed, the generation of an appropriate motor command must rely on the knowledge of limb dynamics and its interaction with the environment through external constraints including that omnipresent force field in which we have learned to move from our earliest childhood: the gravity field.

Gravity has multiple implications for motor control. It influences reference frames for body orientation in the environment and for interaction with moving objects (McIntyre et al., 1998, 2001; Pozzo et al., 1998). Changes in motor responses following changes in gravity were

observed from various contexts such as the synchronization of grasping forces and isometric force production (Augurelle et al., 2003a; Crevecoeur et al., 2009a; Girgenrath et al., 2005; Mierau et al., 2008; White et al., 2005). In the context of vertical pointing movements, the characteristics of arm kinematics in Earths gravity led to the hypothesis that the gravitational constraint is internally represented in the planning process of motor actions (Atkeson and Hollerbach, 1985; Papaxanthis et al., 1998b). Vertical pointing movements typically exhibit skewness in the velocity profile, with the peak velocity occurring before the middle of the movement. This is in contrast to the horizontal pointing movements, which demonstrate symmetric velocity profiles (Gentili et al., 2007). In addition, simulations of arm trajectories with minimal absolute mechanical work reproduce the skewness in the velocity profiles (Berret et al., 2008), suggesting that the Central Nervous System accounts for the action of the gravitational torque on the limb in order to optimize the motor commands.

In the present paper, we test the hypothesis that motor commands are optimized in the gravity field by investigating how subjects adapt vertical pointing movements in a perturbed environment where the terrestrial gravity was nearly doubled. The analyses combine experimental and modeling approaches with simulations of arm trajectories with minimal control input to theoretically test the effect of an increase in gravity on the optimal trajectory. In particular, the simulations predicted changes in the kinematics profiles in hypergravity as compared to the optimal trajectories computed in normal gravity. The data strongly indicate that the subjects behavior in hypergravity was adjusted accordingly, providing further evidence to the theory that the arm motor commands are optimized with respect to the action of gravity on the limb, and that adaptation can be seen as a re-optimization process (Izawa et al., 2008).

3.2 Materials and Methods

Subjects

Ten right-handed volunteers (four males, six females) between the ages of 25 and 52 years with no neurological disorders gave their informed consent to take part in this experiment. They complied with the medical requirements to participate in the parabolic flights (Belgian Center for Aerospace Medicine, class II medical examination). The experimental protocol was approved by the ethical and biomedical requirements for experimentation on human subjects from the European Space Agency (ESA) Medical Board Committee and the French Comit pour la Protection des Personnes, which reviews life science protocols in accordance with French law.

Parabolic flight

The experiment was performed during the 47^{th} and 48^{th} ESA Parabolic Flight Campaigns. Parabolic maneuvers generate sequences of 20 s of hypergravity (1.8 g), followed by approximately 22 s of weightlessness (0 g) before another period of 20 s of hypergravity. The aircraft ran a sequence of 30 parabolas per flight, which permitted us to evaluate each subject during 15 consecutive parabolas. In the following sections, one block refers to the set of trials performed during one parabola.

Experimental Procedures

The subjects sat in front of three visual targets that were aligned vertically with respect to the aircraft floor and that were separated by 18 cm. The center target was in front of the subjects shoulder and

defined the horizontal arm position. They were asked to grasp a manipulandum (mass 250 g, grip aperture 4.5 cm) with the right hand and to perform visually guided pointing movements towards the current target with arm-straight rotations around the shoulder[2]. Upward movements (from the center to the top) and downward movements (from the center to the bottom) were randomly interleaved in order to avoid anticipatory movements. All of the subjects performed control experiments in normal gravity conditions (1 g) prior to the in-flight experiment. The subjects performed the task during the 0 g and subsequent 1.8 g phases of each parabola (they did not perform the task under normal gravity conditions during the flight). Each subject performed from 60 to 80 trials in each direction and in each gravitational condition. The analysis reported in the present study focuses on the data acquired during the hypergravity phases. The data collected during the 0 g phases of the flights will be addressed in another study. Indeed, previous studies suggest that the adaptation to other gravity levels do not generalize to zero gravity (Mireau et al. 2008; White et al. 2008), which means that this condition should be considered as a singularity where the adaptation relies on distinct mechanisms.

Data Acquisition and Post Processing

Gravity was sampled at 800 Hz with a three-dimensional accelerometer (ADXL330, Analog Devices). This signal was utilized to check that the gravity was stable during the movement executions. The trials performed at the transition phases between 0 g and hypergravity were removed because the gravity was unstable. The three-dimensional po-

[2]The subjects were explicitly asked to perform natural movements with clear stable phases before and after each trial. They also received the instruction to perform movements that were not interrupted between the two targets.

sitions of the shoulder and the hand held load were acquired at 200Hz (Codamotion, Charnwoods Dynamics, Leicestershire, UK).

The gravity and position signals were digitally low pass filtered with a zero phase-lag Butterworth filter of order four with a cut-off frequency set to 20Hz. The position of the held load and the shoulder permitted us to compute the elevation angle of the arm with respect to the horizontal axis as illustrated in Fig. 3.1A. The black dots represent the infrared markers placed on the shoulder and the manipulandum for the acquisition of the position signals. Fig. 3.1B represents a 2D reconstruction of a single upward movement with each line joining the held load and the shoulder marker every 25ms. The angular velocity and angular acceleration signals were computed from numerical differentiation of the position signals. Fig. 3.1C to Fig. 3.1H show the elevation angle, angular velocity and angular acceleration of two trials presenting typical overshoot (Fig. 3.1C to E) and undershoot (Fig. 3.1F to H) profiles.

The movement onset and end were computed with the following procedure illustrated in Fig. 3.1D. The velocity profile was linearized around the intersection with the threshold equal to 10% of the peak velocity (threshold: V_T) computed for each trial (linear regressions computed on five time steps). The onset (t_0) and offset (t_f) were then determined by the intersection of the linear regressions with the horizontal axis (red dots). The movement duration was defined as the elapsed time between t_0 and t_f. The procedure to detect the overshoots and undershoots was based on the acceleration profile. For an overshoot, as indicated in Fig. 3.1E, the acceleration presented a local maximum (red dot) occurring after the movement end (Fig. 3.1E, t_{OSH}). We let $\theta(t)$ be the elevation angle of the arm as a function of time, and defined the overshoot as the percentage of the displacement from t_f to t_{OSH} with

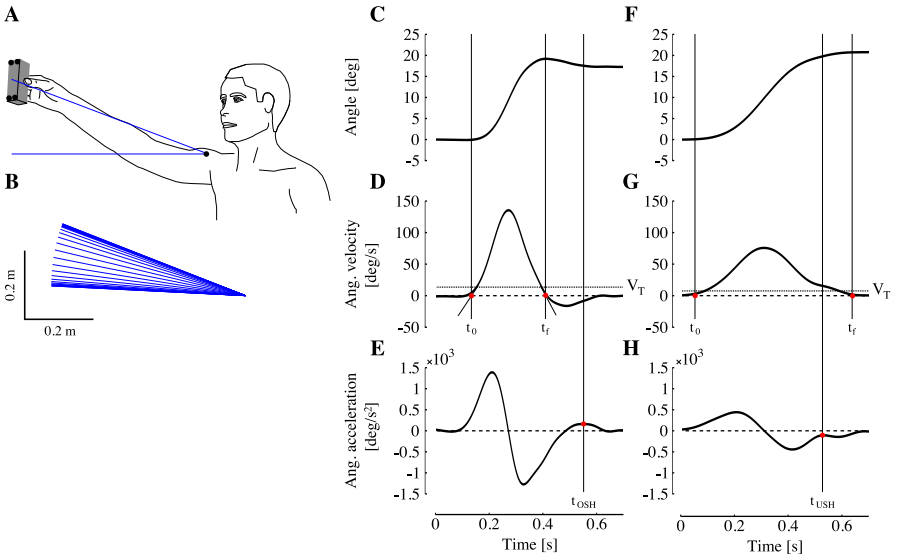


Figure 3.1: Illustration of a subject performing the task. B: 2D reconstruction of an upwards movement. One line joining the shoulder marker and the center of the held load is drawn every 25ms. C, D, E: The elevation angle, angular velocity and angular acceleration as a function of time of a movement presenting a typical overshoot profile. V_T is the threshold of 10% of the peak velocity computed to linearize the speed profile and estimate the movement onset and movement end. F, G, H: The elevation angle, angular velocity and angular acceleration as a function of the time of a movement presenting a typical undershoot profile. The local maxima of the angular acceleration used to compute the overshoot and undershoot are shown in panels E and H, respectively.

respect to the total displacement from t_0 to t_f:

$$OSH = 100\frac{\theta(t_f) - \theta(t_{OSH})}{\theta(t_f) - \theta(t_0)}. \tag{3.1}$$

The elapsed time between t_f and t_{OSH} was limited to 150 ms in order to exclude corrective movements.

Similarly, an undershoot strategy typically presented a local maximum in the acceleration profile before the end of the movement (t_{USH}, Fig. 3.1H). When such a maximum was detected, the undershoots were defined exactly like the overshoot in Equation 3.1, replacing t_{OSH} by t_f and t_f by t_{USH}. With these definitions, the overshoots and undershoots

are positive and negative, respectively. Trials presenting an undershoot detected before 150 ms prior to movement end were considered missed trials, given that the amplitude of the correction was not negligible as compared to the total movement amplitude. Such trials must therefore be considered to be composed of at least two distinct movements realized prior to reaching the target. This criterion revealed that one subject actually did not meet the task requirements. The success rate for this subject was 57% for the upward movements and less than 15% for the downward movements. Accordingly, this subject was removed from the subsequent analysis and the results section reports the data concerning the nine remaining subjects. A direct application of these procedures may provoke the detection of an undershoot and overshoot for the same movement. To avoid this situation, the undershoot strategy was considered to take precedent on the overshoot, which means that the detection of an undershoot implied that no overshoot was recorded for the corresponding trial.

Finally this study analyzes the skewness of the velocity profiles defined as the ratio of the acceleration duration to the total movement duration (AD/MD). Equivalently, this ratio is equal to the relative time from the movement onset to the peak velocity. For a symmetric velocity profile with a peak velocity arising at the middle of the movement, the AD/MD equals 0.5. For the analysis of the AD/MD, the trajectories were interpolated with cubic splines on discretized time intervals of identical size (200 samples) in order to compare the AD/MD ratios measured with identical resolution.

Mechanical and Physiological Model

The model of the arm was one rigid body composed of the arm, the forearm, and the hand. The motion of the system was constrained to

the rotation around one single axis (1 degree of freedom). The length and mass of the three components were computed for each subject as a fraction of the total body height and mass. The ratio was obtained from classical average anthropometric tables (Winter, 1979)[3]. The hand length was divided in half in order to mimic the grasp posture. The held load was added to this model as a point mass body located at the same coordinate as the hand center of mass. We assumed that three torques were acting on the limb: the muscular torque $T(t)$, the gravitational torque, and a viscous friction torque. In addition, the model assumes that the muscular torque is a first-order, low-pass filtered response of the motor command, $u(t)$, being the control signal. This control can take positive and negative values to model a pair of agonist-antagonist muscles. Let us first consider the unperturbed system in continuous time, the equations for the deterministic case are:

$$I\ddot{\theta} = T - mgl\cos(\theta) - k_v\dot{\theta} \tag{3.2}$$

$$\dot{T} = \frac{1}{\tau}(k_u u - T). \tag{3.3}$$

The explicit dependency on time was omitted for clarity. The viscous constant k_v was set to $0.63+0.095T_M$ where T_M is the average joint torque across the movement Nakano et al. (1999), the time constant τ was set to 40 ms and g was equal to 9.81 m/s^2 for the 1 g simulations or 17.658 m/s^2 (1.8 g) for the hypergravity simulations. The parameter m is the mass of the whole system, I is its inertia and l is the distance between the center of mass and the shoulder rotation axis. The control gain, k_u, permits us to have consistent units from the physical point of view. Assuming that the control input u represents the motor neuron discharge, then k_u is the steady state gain relating the torque output to the control input, which can be expressed in spikes density (δ). In prac-

[3]The anthropometric tables that can be found in this reference are due to the work of Dempster (Dempster, 1955; Dempster et al., 1959).

tice, the control was normalized between -1 and 1, and k_u was equal to 50 Nm/δ (after the simulations, we verified that the bounds were never active).

Optimal Control Problem and Re-optimization Hypothesis

The control problem for the unperturbed system is to find an admissible control function, $u(t)$, which drives the system described in Equations 3.2 and 3.3 from its initial to final position in a given amount of time. The minimum control input solution considered in this study is the solution of the control problem that minimizes the following cost:

$$J(u) = \int_{t_0}^{t_f} |u(t)|^2 dt. \tag{3.4}$$

The solutions were computed with Sequential Quadratic Programming (SQP) methods applied to direct multiple shooting (Bock and Plitt, 1984). The multiple shooting algorithm works as follows. The time span of the simulation is divided into n intervals $t_k - t_{k-1}$ where $0 = t_0 < t_1 < \ldots < t_n = t_f$. In each interval, the control policy is approximated by a constant value (say $\bar{u}_k$). In the discretized formulation, the cost function defined in Equation 3.4 becomes:

$$J(u) = \sum_{k=1}^{n} \bar{u}_k^2, \tag{3.5}$$

and the optimal control problem becomes a discrete constraint optimization problem. We initialize a guess of the state at each point of the time grid, $\bar{x}_k = x(t_k)$ where $\bar{x}$ represents the state variables (position, velocity and shoulder torque). Knowing the initial and final positions, the problem to solve is the minimization of the cost defined in Equation 3.5 such that the trajectory ends at $\bar{x}_k$ when the system is integrated from $\bar{x}_{k-1}$ with control $\bar{u}_{k-1}$. These are nonlinear constraints (given the nonlinear dynamics) ensuring the continuity of the state at each point t_k.

The size of the time sub-intervals was equal to 7.5 ms and the system was integrated in each interval with an adaptive step-size Runge-Kutta integrator of order four.

The optimal control sequence $\bar{u}_k$ constitutes the open loop control policy, which drives the unperturbed system along the optimal trajectory in the absence of noise or unexpected perturbation. However, the Central Nervous System must be able to correct for sensorimotor noise thanks to feedback control. To model this, we now consider a discrete time formulation enabling us to introduce additive and signal dependent noises characterizing the properties of the noise in the sensorimotor system. To this end, the system was linearized around the optimal open loop solutions, which permits us to derive a feedback law as a linear function of the state deviations. The optimal feedback gains were computed at each time step from the local linear approximation of the system dynamics. The stochastic dynamics of the deviations from the optimal trajectories are:

$$(x - \bar{x})_{k+1} = A_k(x - \bar{x})_k + B_k(1 + \varepsilon_k)(u - \bar{u})_k + \xi_k, \tag{3.6}$$

where

$$A_k = 1 + \Delta t \left(\frac{\partial f}{\partial \bar{x}_k} \right), \qquad B_k = \Delta t \left(\frac{\partial f}{\partial \bar{u}_k} \right), \tag{3.7}$$

and

$$f(x_k, u_k) = \begin{pmatrix} x_k^{(2)} \\ I^{-1}\left(x_k^{(3)} - mgl\cos(x_k^{(1)}) - k_v x_k^{(2)} \right) \\ \tau^{-1}\left(k_u u_k - x_k^{(3)} \right) \end{pmatrix} \tag{3.8}$$

defines the system dynamics. The noise terms, ε_k and ξ_k, are Gaussian random variables with zero mean and variances equal to 0.02 and 0.5 respectively. The cost per step associated to the motor cost and state deviation was:

$$J_k = r(u - \bar{u})_k^2 + w^T(x - \bar{x})_k^2, \tag{3.9}$$

and the optimal feedback gains were computed using the derivation given by Todorov (2005). The weighting factors for the control and state deviation in the cost function were: $r = 10^{-6}$ and $w^T = [10, 1, 0.2]$. In the second term, the square is computed component-wise. In summary, the stochastic system is driven by the following control policy:

$$u_k = \bar{u}_k - L_k(x - \bar{x})_k. \tag{3.10}$$

The first term is the open loop control sequence and the second term is the feedback correction to the local perturbations. This method is a simplified version of optimal control for nonlinear stochastic systems (Li and Todorov, 2007). For simplicity, we considered that there was no uncertainty about the state of the system, i.e. the state is fully observable and the feedback correction is computed on the true state. This model still makes the hypothesis that there is a feed forward optimization of the motor plan represented by $\bar{u}_k$. Indeed, the nonlinear dynamics do not allow computing an optimal control that is a linear function of the state only, and the feed forward component of the control must be added if one desires that the average trajectory of the stochastic system tends to the unperturbed optimal solution. Under the hypothesis of re-optimization, the feed forward component of the control law cost must be re-computed in hypergravity. Thus, in practice, the same criterion (Equation 3.4) is applied to the system (Equations 3.2 and 3.3) with a distinct value of g.

Non-optimizing Strategy

As an alternative, we simulated the following non-optimizing adaptation scheme. The solution of the control problem in normal gravity is primarily added to an offset to compensate for the static postural adjustment, and then corrected to attain the desired final position. That

is:

$$\bar{u}^{(1.8g)} = \bar{u}^{(1g)} + \alpha. \tag{3.11}$$

This formulation considers that the open loop component of the control policy ($\bar{u}_k$ in Equation 3.10) is not re-optimized in hypergravity, but only adjusted in response to the increase in arm weight.

Comparison between Models and Data

To compute the optimal trajectory in normal gravity, the simulation duration was adjusted in such a way that, for each individual subject, the durations measured in the data and in the simulation were identical. This adjustment corresponded to about the average movement duration plus 50 ms. To test the effect of hyper gravity on the optimal trajectory, the simulations were computed with all parameters kept constant, except the gravity. Thus, the same simulation duration was employed to compute the optimal trajectory in hypergravity. The simulations were computed for each subject with the inertia, mass, length, movement amplitude and duration adjusted to their individual values. The same procedure was used to measure the ratio AD/MD and the movement duration in the simulations and in the data.

3.3 Results

Testing the Model

The vertical trajectories performed in the normal gravity condition presented asymmetric velocity profiles. The AD/MD ratio was significantly smaller than 0.5 (t-test, $P < 0.01$). Our experiment also confirmed the difference between upward and downward movements: AD/MD was equal to 0.451 ± 0.053 for the upward movements and 0.463 ± 0.060 for the downward movements with a significant effect of the movement direction (all subjects pooled, ANOVA, $P < 0.01$). Despite its simplicity, the model captures this property. The asymmetry was computed on simulated trajectories of identical duration for upward and downward movement in normal gravity. The AD/MD ratio was equal to 0.475 ± 0.028 for the upward movements and 0.482 ± 0.027 for the downward movements (mean ± standard deviation computed across the simulations of the model with the parameters fitted to each individual subject). Fig. 3.2 presents the velocity profile for one subject computed from the model simulation (solid black, left) and the velocity profile collected in normal gravity condition averaged across the individual trials (solid grey, right). Both traces present a maximum velocity (vertical line) occurring before the middle of the movement. For comparison, Fig. 3.2 shows the symmetric velocity trace corresponding to the minimum jerk trajectory (dashed black), with an AD/MD ratio equal to 0.5. According to the model, the asymmetry can be directly attributed to the gravitational torque since the simulations for the horizontal movements (with $g = 0$) lead to an AD/MD ratio equal to 0.5 without the effect of the movement direction, as observed in the horizontal movements performed in normal gravity.

The effect of hypergravity on the optimal trajectories is illustrated

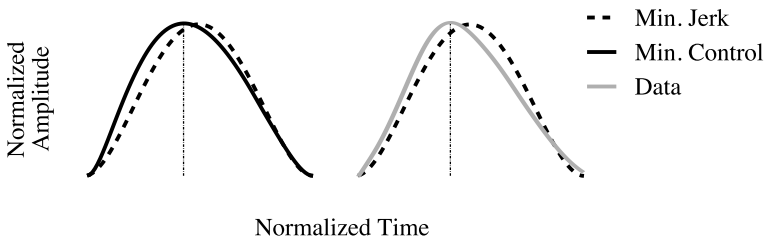


Figure 3.2: The skewness of the velocity profiles of the minimum control input model considered in this study (solid black) and observed in the data for one subject (solid grey). The velocity traces were normalized in time and amplitude. The minimum jerk trajectories with a symmetric velocity profile are shown for comparison (dashed black). The vertical dashed lines are aligned on peak velocity to illustrate the skewness of the corresponding curve.

in Fig. 3.3 showing simulations of upwards and downwards movements in both gravitational conditions for the same subject. The red and black traces correspond to the open loop trajectories in the two gravitational conditions. The shaded areas represent the standard deviations from the average trajectory when the system was simulated with noise (Equations 6, deviations computed on 100 simulations). The difference between the optimal solutions is due to the re-optimization of the feed forward component of the control policy. This difference in optimal trajectories can be directly attributed to the change in gravity since the only difference between the simulations was the value of g. Qualitatively, the main effects predicted by the model on the kinematics properties is an increase in the peak angular acceleration and in the peak angular velocity. As a consequence, the velocity profile in hypergravity changes, which leads to a difference in the estimation of the movement end, even for identical simulation durations. Therefore, the measurement of the movement duration applied to the simulations records a decrease in hypergravity. This is emphasized in Fig. 3.3B, where Δt_f illustrates the difference between the estimations of movements end in normal and hypergravity computed on the simulations.

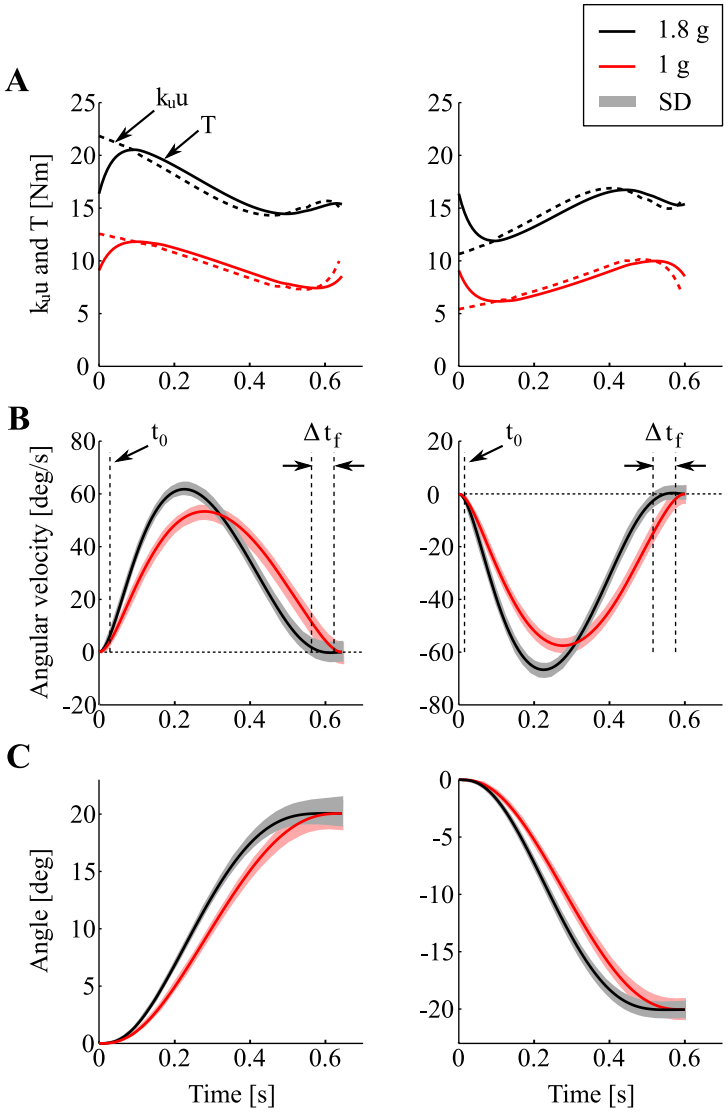


Figure 3.3: The plots of the optimal trajectories in normal gravity (red) and hypergravity (black) conditions for upward (left) and downward (right) movements. The dashed traces in panel A represent the optimal control policy and solid traces are the muscular response to the control input. B: The angular velocity of the simulated trajectories as a function of time. C: The optimal trajectories as a function of time. The shaded areas in panels B and C represent the standard deviation of the stochastic system around the optimal trajectories (solid black and red traces). The standard deviation was computed across 100 simulations.

Learning in Hypergravity

To investigate the effect of hypergravity on unperturbed and uncorrected trajectories, particular attention should be paid to the undershoot strategies, which typically reflect a distinct kind of movement planning and control. The detection of missed trials based on the presence of undershoots occurring 150 ms prior to movement end led to the removal of 5% of the trials for upward movements and 10% for downward movements. This failure rate was comparable to the behavior observed in normal gravity conditions where 8% and 4% of the trials had to be removed for the up and down trials, respectively. The evolution of the percentage of success trials across the blocks and a comparison with the average success rate in normal gravity are shown in Fig. 3.4 (averaged across the subjects $\pm$ the standard error). The performance was stable from the beginning for the upward movement, whereas a stable performance for downward movements was observed from the third block. The difference for the downward movements between normal and hypergravity in the first two blocks pooled together was significant (paired t-test, $P < 0.01$, grey rectangle in Fig. 3.4).

Effect of Hypergravity

The elevation angle and angular velocity as a function of time are shown in Fig. 3.5 in the two gravitation conditions. These data are shown for the same subject whose simulations were plotted in Fig. 3.2 and 3.3. All of the trajectories were aligned with respect to the movement onset in order to compute the average trajectory and standard error at every time step. For the upward movements (Fig. 3.5A and

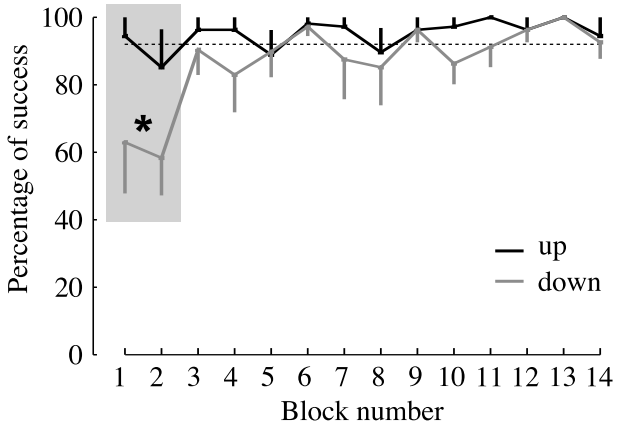


Figure 3.4: Success rate for hypergravity movements averaged across the subjects (N = 9) in both directions as a function of the block number. The horizontal dashed line is the average success rate in normal gravity for both movement directions. The grey rectangle illustrates the significant difference in the success rate between hyper and normal gravity for downward movements.

3.5B), any single trajectory (light grey) rapidly deviates from the average control trajectory (represented in red) and goes faster toward the target. This tendency is further confirmed by the average trajectory in hypergravity (black trace). This logically provokes the change in the speed profile illustrated in Fig. 3.5B. Similar comments may describe the effect on the downward trajectories (Fig. 3.5C and 3.5D) although the effect of hypergravity seems to have less of an impact on the downward movements than on the upward movements. Clearly, the effect is qualitatively similar to the model predictions shown in Fig. 3.3. The quantitative comparison will be addressed later in this analysis.

The statistical analysis revealed that the tendencies observed qualitatively in Fig. 3.5 were significant. The Wilcoxon Rank Sum test was chosen for testing whether the variations were significant given that the data were not normally distributed. For the upward movements, there was a significant increase in the peak angular acceleration followed by an increase in peak angular velocity and a significant decrease in the

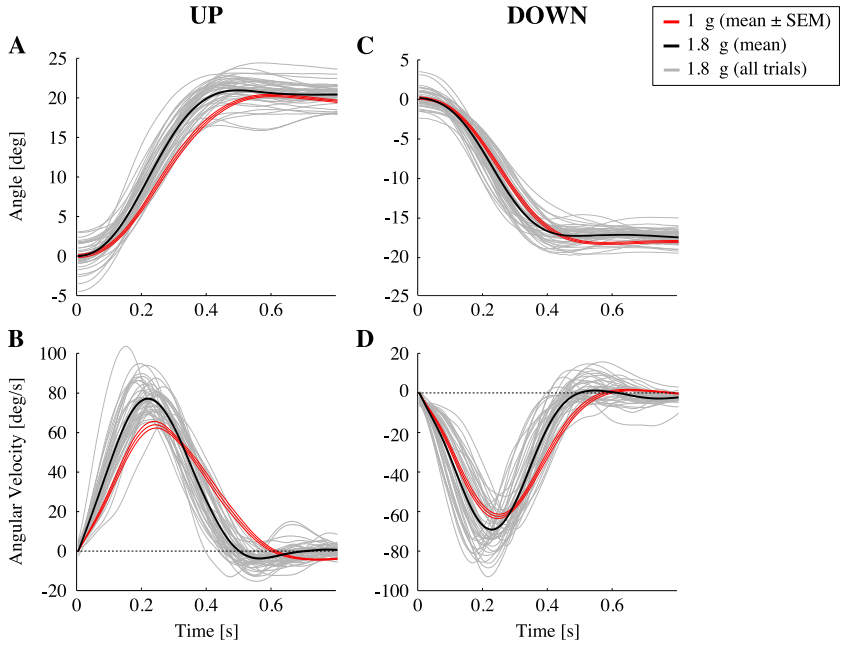


Figure 3.5: The elevation angle and angular velocities for one subject in the two directions. The red traces are the average 1 g trajectory plus and minus the standard error computed at each time step. The grey traces show all of the hypergravity trials for this subject, aligned on individual movement onsets. The black trace is the average trajectory in 1.8 g. The top panels indicate the angle as a function of time. The bottom panels indicate the angular velocity as a function of time.

movement duration ($P < 0.01$). The same significant effects on the kinematics parameters were observed for the downward movements. In addition, the effect of the movement direction was significant. This was evaluated by comparing the difference between the hypergravity data and the average in normal gravity across the two movement directions. In all of the cases (peak angular acceleration, peak angular velocity and movement duration), the variations in absolute value were larger for upward movements than for downward movements ($P < 0.01$). The magnitude of the effect is illustrated in Fig. 3.6A for the peak angular acceleration, in Fig. 3.6B for the peak angular velocity, and in Fig. 3.6C for the movement duration. All differences across the gravitational con-

ditions were significant (the data of the peak angular acceleration and velocity for the downward movements are presented as absolute values).

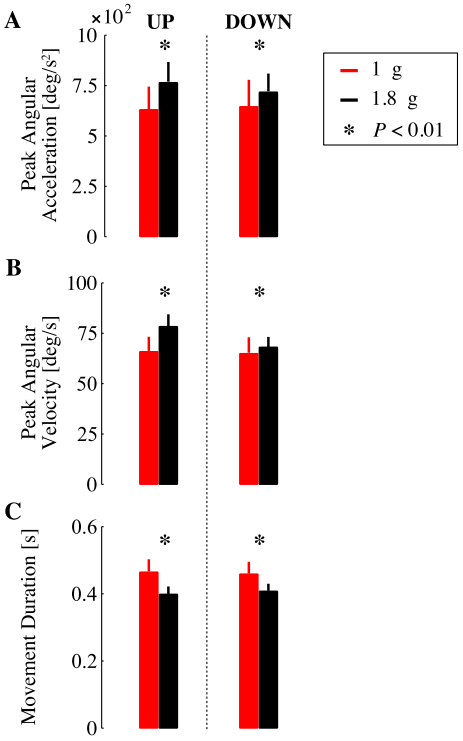


Figure 3.6: The variation of the kinematics parameters across the two gravitational conditions and in the two movement directions. The means of the peak angular acceleration (A), peak angular velocity (B), and movement duration (C) were averaged across the subjects. The error bars represent the inter-subject standard error of the mean. The data of the peak acceleration and velocity for the downward movements are presented as the absolute value. All of the differences between 1 g and 1.8 g were statistically significant.

The effect of the movement direction revealed that adaptation was not symmetrical for the two movement directions. The analysis of the overshoots and undershoots shown in Fig. 3.7 provides interesting insight on the strategies and enables us to better understand the difference observed between the up and down movements. For the upward movements, the subjects reinforced their tendency to overshoot with 77% of the trials against 73% in normal gravity. In addition, the amplitude of the overshoots was significantly increased in the 1.8 g condition ($P < 0.01$), as confirmed by the shift in the overshoots histogram of Fig. 3.7A. In this direction, the undershoots were detected in 6% of the trials in hypergravity as compared to 11% in normal gravity. For the

downward movements, there was no difference concerning undershoot trials (6% in hypergravity as compared to 7% in normal gravity without variation in amplitude), whereas the overshoots were observed in only 43% of the trials as compared to 72% in normal gravity (Fig. 3.7B).

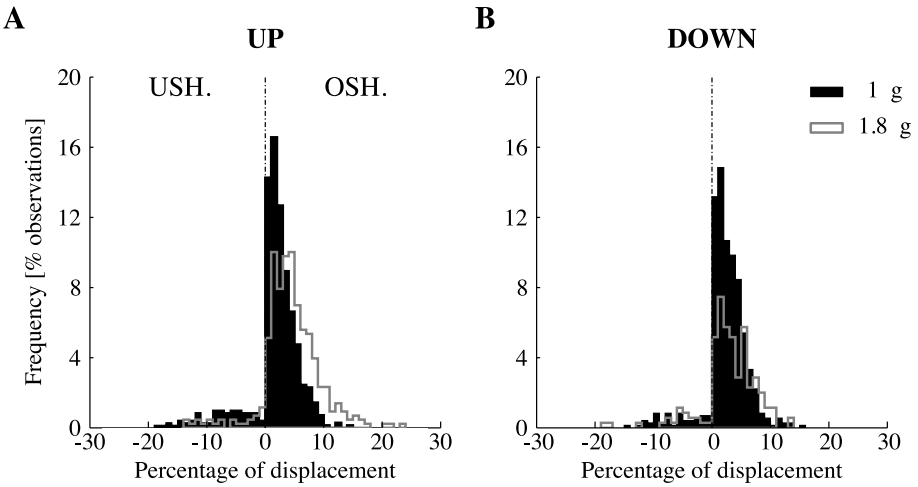


Figure 3.7: The overshoots (OSH) and undershoots (USH) in the normal and hypergravity conditions for the upward (A) and the downward (B) movements. The histograms show the frequency of the observation of trials with the corresponding percentage of displacement. Recall from the methods that the overshoots are positive and the undershoots are negative.

In summary, the subjects strategy was to globally reach the target faster in hypergravity and with a significant difference between the up and down variations and a preference for overshooting when going upwards.

Comparison with Model Simulations

For the upward movements, the simulations in hyper gravity predict a relative increase of 25% in the peak acceleration and 8% in the peak velocity. The prediction matched the data for peak acceleration: we observed a relative increase in the peak acceleration of 24% (averaged

across subjects). The relative increase in the peak velocity was equal to 19%, which is larger than the prediction. The predictions for the downward movements were similar to the upward movements: the model predicts 28% and 11% of relative increase in the peaks acceleration and velocity, respectively. Subjects behavior varied less: we observed 9% and 3% of increase in peak acceleration and velocity, respectively.

In order to compare the changes in the kinematics profiles across the two gravitational conditions, we computed the areas between the trajectories performed in the hypergravity condition and the average 1 g trajectory (used as a reference trajectory). As illustrated in Fig. 3.8A, the areas A1 and A2 were defined with respect to the sign of the difference between the reference 1 g trajectory (red trace) and the trajectories performed in hypergravity (black trace, example of one single trajectory taken from data).

Similarly, the areas between the optimal simulations were computed in order to compare the magnitude of the effect with the experimental data. Fig. 3.8B and 3.8C indicate that the areas A1 and A2 in the two directions averaged across bins of three movements and across subjects. The dotted lines in each plot indicate the areas computed on the simulations of an identical duration as the 1g-reference trajectory and were averaged across the subjects.

As shown in Fig. 3.3, for the upward movements, the optimal trajectory in hypergravity is above the optimal trajectory in the normal gravity condition. Therefore, for simulations A2 equals 0 (blue dotted line, Fig. 3.8B), and A1 is a positive constant (black dotted line). The opposite is observed for the downward movements: Fig. 3.8C indicates zero for A1 and a positive value for A2 for the simulations. The tendency observed in the data is clearly consistent with the simulations. The trajectories performed in hypergravity were neither strictly above nor under the average trajectory in normal gravity (see example in Fig.

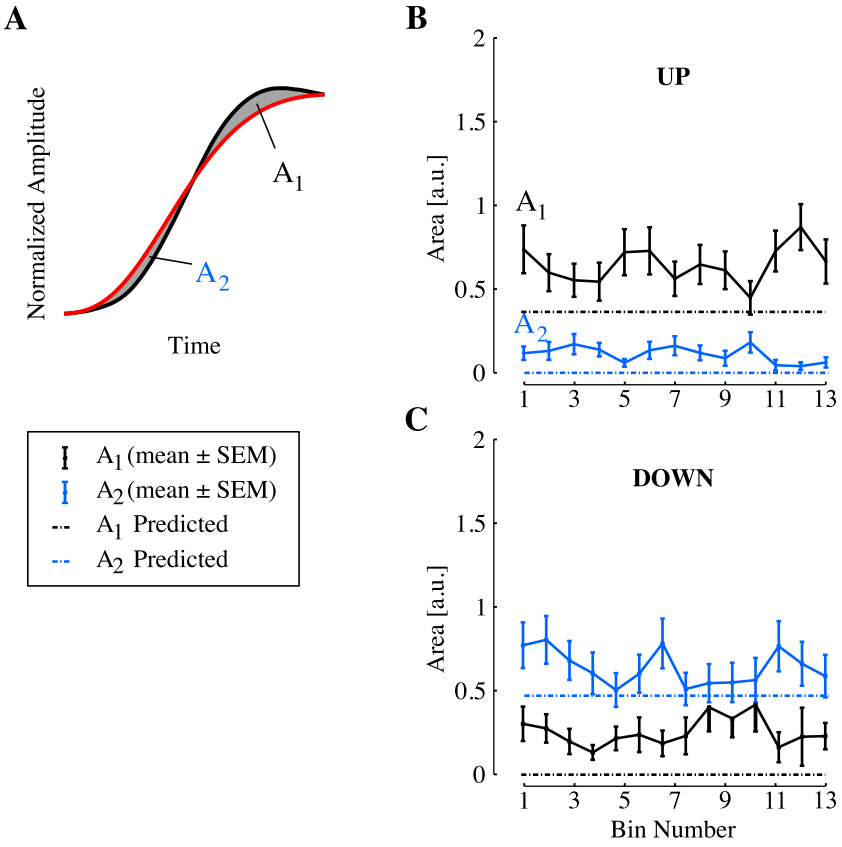


Figure 3.8: The quantitative analysis of the effect of hypergravity. A: The illustration of the computation procedure, the amplitudes were normalized to the movement amplitude from movement onset to movement end. The time was unchanged. A1 and A2 are the areas between the hypergravity traces and the reference 1 g trace when the integrated differences were positive and negative respectively. Panels B (upward) and C (downward) show the areas A1 and A2 averaged across bins of three movements and across the subjects versus the number of the bin.

3.8A, A1 and A2 are both non-zero), however the general tendency confirms the prediction of the model. According to the model simulations, for upward movements, the difference between the predicted and the observed values for A1 demonstrate that the subjects tended to overcompensate (A1 was larger in data in comparison with the simulations). Similarly, the effect of movement direction is illustrated in Fig. 3.8B

and 3.8C. The downward movements present more variability although the global tendency is in accordance with the simulations.

To further argue for a re-optimization of the motor commands, we computed the trajectories obtained when the feed forward component of the control law corresponding to normal gravity is adjusted to compensate for the increase in the arm weight (Equation 11), but not re-optimized. The simulation of this alternative model predicted that the kinematics of movements in hypergravity are the same as in normal gravity condition, yielding for A1 and A2 values very close to zero in Fig. 3.8. This demonstrates that the model based on the non-optimizing strategy can be rejected.

3.4 Discussion

Our results describe the effect of an increase in gravity on vertical pointing movements and compare the subjects behavior with the simulation of arm trajectories utilizing a model based on minimum integrated control input. The proposed model considers a first order low pass filter between the motor neuron discharge and the muscular torque as a physiological model and Newtons second law for the mechanical equation. The analysis reveals that after an adaptation to hypergravity, the subjects behavior was consistent with the model predictions. This was in accordance with the hypothesis that adaptation to altered dynamics is achieved after a re-optimization of the motor plan in the new environment (Izawa et al., 2008).

In addition, data reveal a significant effect of movement direction, which was not predicted by the model simulations. It takes more time to learn the downward movements and upon learning them, the variation in the kinematics parameters was larger for the upward movements. This was accompanied by a clear preference for the overshoot strategy reinforced in hypergravity, despite the increase in the arm weight. The fact that the subjects behavior is different depending on the direction of the movement may reflect the strategy with respect to the goal of the task, i.e., to stabilize next to the target for which gravity either enables or hinders the braking acceleration. This result suggests that re-optimization is not the only process that ensures an adaptation to altered dynamics. Rather the goal of the task and the strategies that rely on cognitive factors modulate the adaptation of the motor plan.

The model was kept as simple as possible in order to focus on the effect of a change in gravity and avoid that other factors come into play in the simulations. Several limitations can be easily removed to obtain a better match between the predictions and the data. First, one can

introduce a bias in order to account for the effect of the movement direction. Then, more sophisticated mechanical and physiological models can improve the quality of the prediction, by considering more carefully the properties of the musculoskeletal system. Finally, keeping the same simulation duration across the two gravitational conditions was a strong constraint, which can be relaxed to improve the correspondence between the predictions and the data. In particular, matching the simulation duration with the movement duration in hypergravity yields better predictions for upward movements.

Our modeling approach follows the models proposed by Gentili and colleagues (2007), which consisted of minimal torque changes and minimal commanded torque changes (Nakano et al., 1999). These models assume that the brain has an access to the joint torque, given that it is the variable being controlled. We added the physiological model (Equation 3) in order to formulate a control variable that is closer to the neural motor command, which is presumably accessible within the Central Nervous System as a corollary discharge. Our results obtained in the normal gravity condition are fully compatible with the results from Gentili and colleagues (2007), despite some differences between the protocols. The main differences were that their subjects performed reaches of various amplitudes and from various starting position, and the movements were performed in darkness without visual feedback. Our protocol was restricted to one movement amplitude from a single starting position in order to collect a sufficient number of trials per subject and per flight. Then, our subjects were provided with continuous visual feedback in order to prevent that they suffer from motion sickness. This was presumably the origin of the high success rate observed early, in particular for the upward movements. However, in normal gravity, we obtained very similar values for the AD/MD ratio. This suggests that asymmetry in the velocity profiles is a robust feature of the vertical movements

across various testing conditions. More generally, our model accounts for the difference between vertical and horizontal movements in normal gravity, in addition to the difference between the vertical movements performed in normal and hyper gravity.

Our main finding is that an increase in gravity is properly compensated in a feed forward manner in accordance with the hypothesis of minimum control input. In particular, the effect of hypergravity on the peak acceleration (precisely matched by the simulations for upward movements) is in direct support of a change in the central planning process, which must account for the effect of gravity on the limb. In addition, our results suggest that the Central Nervous System utilizes the internal representation of the gravitational torque in order to optimize the motor commands. Our sample does not permit the evaluation of whether the optimal feedback gains (L_k in Equation 10) are also re-optimized in hypergravity. However, the simulations predict distinct sensitivities to the position and speed errors across the two gravitational conditions. It follows from our result that the Central Nervous System takes into account the effect of external forces on the limb and takes advantage of the dynamic interaction between the body and the environment. White and colleagues reported a similar result in the context of oscillatory movements performed in different gravity conditions (White et al., 2008). They found that the spontaneous movement frequency was driven by gravity as the resonance phenomenon of a pendulum, which is the signature of a system maximizing energy transfer with the environment. The interaction with the environment is emphasized by the changes in the movement frequency in response to the changes in gravity. Altogether, these results provide evidence for an optimal interaction with the environment in both rhythmic and discrete movements depending on the action of gravity on the limb.

Previous studies argued for an optimization of the dynamic forces

only (Nishikawa et al., 1999; Soechting et al., 1995), which appears contradictory with the hypothesis of integration of the gravitational torque in the computation of a motor plan. Nishikawa and colleagues showed that the final arm posture after pointing movements depended on the initial position, and these postures were invariant, even for slow movements, where the antigravity component of the joint torque should be dominant in comparison to the peak joint torque. In our study, the initial and final arm postures were prescribed and the movements were constrained to one degree of freedom in the vertical plane. Therefore, for such movements, the minimization of the dynamic variations only (as supported by Nishikawa and colleagues) implies that the gravitational torque is taken into account, as supported by the present study. Other kinds of movement with horizontal components and more degrees of freedom may rely on distinct strategies.

The results of the present study have two main implications. First, the data allow us to reject the hypothesis of an invariant desired trajectory, which assumes that internal models build a new map between a desired trajectory and the motor command, taking the unperturbed trajectory as the desired trajectory. In our experiment, the optimal trajectory in normal gravity is of course a feasible solution in hypergravity but the simulations reveal that, although possible, this trajectory is no longer optimal. Accordingly, the subjects change the kinematics profile without any tendency to recover the characteristics of the movements performed in normal terrestrial gravity. However, many studies in various contexts do provide evidence for a tendency to return to the performance of the unperturbed condition (Burdet et al., 2001; Lackner and Dizio, 1994; Papaxanthis et al., 2005; Shadmehr and Mussa-Ivaldi, 1994), whereas other studies, including the present paper, suggest that re-optimization produces definitive changes in the movement kinematics (Izawa et al., 2008). It seems that question of which adaptation process

(re-calibration of the internal models or re-optimization) will be observed depending on the experimental conditions remains open to debate.

Second, under the hypothesis that the motor actions are re-optimized in response to a change in the environment, this experiment suggests that the estimation of movement costs can be based on the motor command corollary discharge and proprioceptive feedback. Indeed, gravity acting vertically with respect to the aircraft floor was not a divergent force field for vertical movements. Therefore, it is very unlikely that the re-optimization observed in hypergravity is based solely on visuomotor adjustments. The movements were visually guided and the movement control relied on visual feedback (e.g. corrective adjustments as observed in trials presenting large undershoots). However, visual feedback by itself fails to explain why the subjects changed the kinematics motor plan and performed faster movements. Therefore, the sources of information available for an estimation of the movements costs (necessary for optimization) are the motor command corollary discharge, which is represented in the model by u(t), and the proprioceptive feedback. Such an estimation of movement costs based on these variables compared to an expected cost from prior knowledge can represent a signal that generates the update of the kinematic and dynamic properties of the movement.

A potential region for the generation of this signal is the posterior parietal cortex (PPC), which plays a fundamental role in visuomotor transformations for reaching and in the planning and control of visually guided movements (Buneo and Andersen, 2006; Buneo et al., 2002). Downstream to the visuomotor transformation, PPC activity correlates with kinematics parameters such as target location, movement direction, and velocity. The PPC activity further has little effect for various load conditions for a given invariant trajectory (Ashe and Georgopoulos, 1994; Hamel-Paquet et al., 2006; Kalaska et al., 1990). In addition, the neural correlates with kinematics errors in reaching were found in the

parietal area-5 (Diedrichsen et al., 2005). It was further found that transcranial magnetic stimulations of this region alter the learning of new dynamics (Della-Maggiore et al., 2004). However, the fact that continuous visual feedback was provided suggests that the alteration of learning could be related to visuomotor transformation instead of a kinematics adaptation.

Of course, the neural correlates with kinematics parameters are present in other brain regions such as the premotor areas (Kakei et al., 2003) and the primary motor cortex whose activity is not solely related to force output (Graziano, 2006; Scott, 2003). However, in addition to the evidence that the PPC codes kinematics features of the movement, the anatomical situation of the PPC is consistent with our hypothesis that internal and proprioceptive feedback are necessary to adapt the kinematics motor plan. Indeed, the PPC receives projection from the somatosensory cortex for proprioceptive feedback, and from the cerebellum via the thalamus (Amino et al., 2001), whose activity relates to state estimation and prediction (Miall et al., 2007; Wolpert et al., 1998b), which could contribute to the prior estimate of the movement cost. Altogether, the characteristics of the PPC render it a good candidate as a sensorimotor interface for updating the kinematics motor plans.

3.5 Addendum

In the preceding discussion, we outlined that the modeling approach considered a very simple model in order to limit the number of parameters and focus on a change in gravity only. For this reason, the simulation durations were kept constant for all subjects to avoid that peaks acceleration and velocity were artificially increased by manipulating the simulation duration. Thus, we did not analyze the AD/MD ratio in hypergravity given that the simulation did not take into account the actual change in movement duration that we measured experimentally.

The simulations predict a significant reduction in AD/MD in hypergravity when the simulation duration is unchanged (average for up and down movements for each subject, Wilcoxon ranksum test, $P < 0.005$). This tendency was not observed in the data. Rather, the experimental results suggest that the ratio AD/MD was invariant across the two gravitational conditions ($P > 0.05$). In order to address this issue, we simulated the optimal trajectories in hypergravity by matching the simulation duration with the actual movement duration that was measured in this condition (plus 50 ms as explained above). The trajectories obtained by relaxing the duration constraint reproduced the fact that AD/MD did not vary in hypergravity compared to normal gravity ($P = 0.43$). In addition, the values obtained with thee simulations were not significantly different from the values measured experimentally ($P = 0.67$).

Hence, refining the model could provide more accurate quantitative prediction of the movement kinematics. This result suggests that the shape of the velocity profile may be an invariant feature of movements performed under an optimal strategy without any constraint on the duration.

Chapter 4

Sensorimotor mapping for anticipatory grip force modulation

"An expert is a man who has made all the mistakes that can be made in a very narrow field."

N Bohr.

Abstract. During object manipulation, predictive grip force modulation allows compensation for inertial forces induced by the objects acceleration. This coupling between grip force and load force during voluntary movements has demonstrated high levels of complexity, adaptability and flexibility under many loading conditions in a broad range of experimental studies. The association between grip force and load force indicates the presence of internal models underlying predictive grip force control. The present experiment sought to identify the variables taken into account during grip force modulation at the initiation of a movement. Twenty subjects performed discrete point-to-point movements under normal and hypergravity conditions induced by parabolic flights. Two control experiments performed under normal gravitational conditions compared the observed effect of the increase in gravity to the effects of a change in movement kinematics and a change in mass. In

hypergravity, subjects responded accurately to the increase in weight during stationary holding but overestimated inertial loads. During dynamic phases, the relationship between grip force and load force under hypergravity varied in a manner similar to the control test in which object mass was increased, while a change in movement kinematics could not reproduce this result. We suggest that the subjects strategy for anticipatory grip force modulation is based on sensorimotor mapping that combines the perception of the weight encoded during stationary holding with an internal representation of the movement kinematics. In particular, such combination reflects a prior knowledge of the unequivocal relationship linking mass, weight and loads under the invariant gravitational context experienced on Earth.

4.1 Introduction

The ability to predict and anticipate the consequences of ones actions is a robust and general component of the processes involved in motor control (Wolpert and Flanagan, 2001). Motor predictions and anticipatory control are evidenced in various contexts, such as the remapping of the visual field prior to a saccade completion (Duhamel et al., 1992), the compensation of self-generated Coriolis acceleration in pointing during active trunk rotation (Pigeon et al., 2003), and the synchronized modulation of grasping forces with inertial loads during object manipulation (Flanagan and Wing, 1993). In the latter context, the grip force (GF) normal to the surface of the manipulated object is modulated with self-induced variations of the load force (LF) resulting from inertial and gravitational constraints between the fingertips and the object.

GF depends on many variables, including the objects weight, the mechanical properties of the skin-object interfac (Andre et al., 2009; Johansson and Westling, 1984), the sensory feedback provided by cu-

taneous afferents (Nowak et al., 2001a; Augurelle et al., 2003b; Monzee et al., 2003; Witney et al., 2004) and the manipulated objects internal model of dynamics (Flanagan and Wing, 1997).

The coupling between GF and LF exhibits high levels of complexity and flexibility relative to distinct loading conditions. For instance, Flanagan and Wing (1995) demonstrated that the slope and intercept of the GF/LF relationship were independently adjusted in response to increased frequency of movement during rhythmic cycles. A similar result was reported in the context of multi-digit grasp with distinct conditions of movement acceleration and object mass(Zatsiorsky et al., 2005), yielding the hypothesis that gravitational and inertial constraints could be separately treated. Moreover, the flexibility of the coupling between GF and LF allows adaptation to changes in load profiles induced by changes in gravity, for both rhythmic and discrete types of movements (Nowak et al., 2001b; Augurelle et al., 2003a).

The possible dissociation between gravitational and inertial constraints encouraged us to decompose GF into static and dynamic components in order to investigate the adaptation of GF in zero-gravity conditions (Crevecoeur et al., 2009a). This approach revealed a distinct timescale of adaptation for each component, giving further support to the hypothesis that each outcome could adapt and evolve independently.

The dissociation of static from dynamic components yields the hypothesis that gravitational and inertial constraints may be independently controlled. Under this assumption, the internal representation of the manipulated objects weight should be the primary factor influencing the adjustment of GF during stationary holding, while the GF modulation should be primarily based on the prediction of inertial loads. It is therefore necessary to estimate weight and inertial load in order to produce adequate GF levels. However, the physical variables taken into account during these estimations, and the sensorimotor strategies under-

lying the prediction of inertial loads, have not to date been thoroughly investigated.

To this purpose, this study used a hypergravity environment to induce changes in weight without changing the mass of the manipulated object. We show that the factors underlying the GF modulation is based on a combination of the object weight encoded during stationary holding and an internal representation of the intended movement. In particular, this combination reflects a sensorimotor mapping between the object weight and a prior knowledge of the life-long experienced physical laws linking mass, weight and loads on Earth.

4.2 Material and Methods

Twenty healthy subjects (11 males and 9 females) without neurological disorders participated in this experiment. All subjects gave informed consent and the experimental protocol complied with the ethical requirements observed by the Medical Board of the European Space Agency (ESA) and the French Committee for the Protection of Persons. The latter organization is responsible for life-science experiments performed in France.

Each subject was seated in front of three vertically aligned visual targets (green LEDs) placed 18 cm apart, with the central target at shoulder height. S/he was asked to grasp a manipulandum (4.5 cm grip aperture; 250 g mass) with a precision grip and to align it in front of the central target. Each subjects arm was thus in horizontal position. A random sequence of targets was then generated, and the subject was asked to align the manipulandum with the current target by means of outstretched-arm rotation around the shoulder in the sagittal plane. After each upward or downward movement (from center to the top or bottom target, respectively), the subject returned the arm to central alignment prior to the next movement.

Each subject performed the experiment in a training session under laboratory conditions (normal gravity, 1 g) in order to learn the task and become familiarized with the experimental protocol. The training session was composed of 10 blocks of 16 to 20 movements. The first group of subjects (N = 10) then performed the experiment under the hypergravity conditions induced in parabolic flights. We used the 47th and 48th ESA Parabolic Flight Campaigns. One parabolic flight was composed of a sequence of 31 parabolic maneuvers. The gravity was increased to 1.8 g over a period of approximately 20 s during the first phase of each parabola. The second phase consisted of approximately

22 s of zero gravity, followed by another 20 s phase of hypergravity. The subjects performed the experimental task during the second hypergravity phase of each parabola. Two subjects were evaluated per flight, and each subject performed the task during at least 14 consecutive parabolas.

The ten remaining subjects were involved in two control experiments. After the training session, the first control group (N = 5) performed another series of 8 blocks under normal laboratory conditions. This control experiment allowed only 1 s to complete each movement, instead of the 1.25 s allowed in the training session. In addition, the subjects were explicitly requested to perform faster movements. The second control group (N = 5) performed a second series of 8 blocks without changes in movement timing or instructions regarding the velocity of the movement, but the manipulandum was loaded with an additional mass of 220 g (470 g in total). The increase in weight for this control group was similar to that experienced by the group tested in hypergravity conditions. For each control session performed under 1 g conditions, the data from the first block were systematically removed from the sample in order to avoid transient effects due to learning the task. Based on visual inspection, the second block was removed for three of the control subjects for similar reasons.

The manipulandum was equipped with force and torque sensors located under each finger (Mini 40 F/T Transducers, ATI Industrial Automation, North Carolina, USA), and with a low-g accelerometer sensitive to acceleration changes in a range of 3 g (ADXL330, Analog Devices, Massachusetts, USA). Another accelerometer of the same type was employed during the flights to sample the gravity inside the aircraft and to verify that the movements were performed during stable gravitational phases. Trials performed during unstable gravitational phases were discarded.

The data collected from the sensors and accelerometers were digitally low-pass filtered with a fourth-order zero-lag Butterworth filter and a cut-off frequency of 50 Hz. GF was defined as the mean of the absolute force components normal to the sensor surfaces. Variation in LF was collected from the accelerometer signal and multiplied by the objects mass.

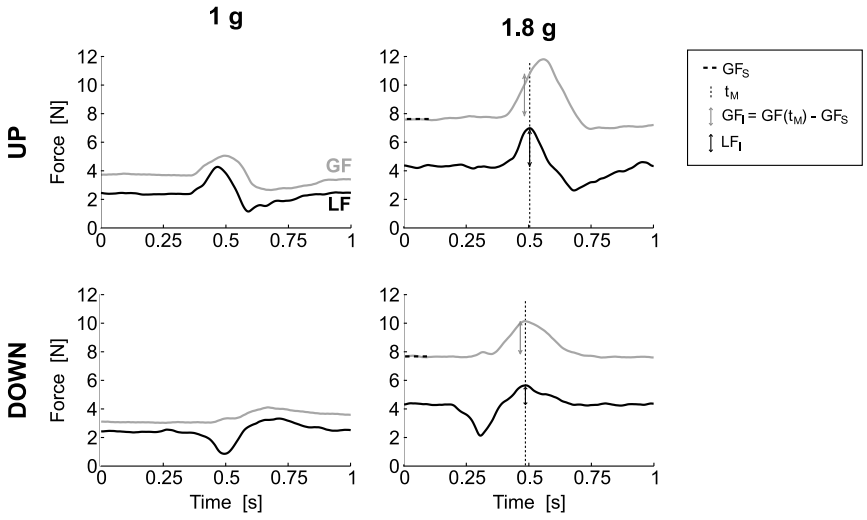


Figure 4.1: Typical traces of grip force (GF) and load force (LF) in the two gravitational conditions (1 g, left; 1.8 g, right), and in the two movements directions (upwards, up; downwards, down). The variables are represented on the examples selected from hypergravity: the static grip force measured during stationary holding prior to the movement (GF_S), the increment of GF (GF_I) measured at the time of load force peak (t_M) relative to GF_S and the increment of LF (LF_I) measured at the difference between the peak of LF and the weight of the held load.

Representative trials performed under both gravitational conditions are shown in Fig. 4.1, with the variables for the hypergravity trials illustrated (Fig. 4.1, right column). GF was decomposed into a static

component (GF_S, dashed horizontal line) measured prior to movement when the arm was stable, and a dynamic component (GF_I, grey arrow) measured as an increment of GF at the peaks of LF relative to the static component. The increment of LF (LF_I, black arrow) is the difference between maximum LF and the weight of the object. During hypergravitational conditions, weight was computed using the actual gravity measured during each trial. The decomposition was computed for each trial at maximum LF, corresponding to the acceleration phase (for upward movements) or the deceleration phase (for downward movements). This decomposition of GF is similar to the method previously utilized by Crevecoeur et al. (2009a). It is a convenient method to examine the combined estimation of object mass during static phases and dynamic modulation during dynamic phases that produce the grip motor command.

A one-way ANOVA was used to test the main effect of parabola on GF_S and on the ratio between GF_I and LF_I. Comparison between the hypergravity and normal gravity condition, and between normal and fast or loaded for the control experiments, were realized with Wilcoxon ranksum test in order to detect a change in a given variable. Finally, the relationship between LF_I and GF_I was addressed by means of classical least-square linear regressions. The R^2 statistics reported below indicate the square of the correlation between the two variables estimated on the regression.

4.3 Results

Hypergravity Experiment

Under normal gravity conditions, GF_S varied across subjects. The individual means during the training session ranged between 2.5 N and 9.6 N (with a mass of 250 g). Under 1.8 g conditions, GF_S increased in response to the weight increase induced by the change in gravity. Fig. 4.2A shows the mean GF_S, normalized for each subject to his/her normal gravity mean, and the time course of GF_S across the parabolas. There was no significant evolution of GF_S across the parabolas (one way ANOVA, $P > 0.9$). Despite some variability, the relative increase in GF_S under hypergravity corresponded to the relative increase in object weight, as evidenced by the increase in gravity shown on the same plot (red line). Both GF_S and gravity data were averaged across subjects in each block (one block corresponds to one parabola). The low variability in the gravity data (Fig. 4.2A) confirms the stability and reproducibility of experimental conditions across parabolas.

The absolute ratio between GF and maximum LF during upward and downward movement (measured at LF peaks) tended to increase under hypergravity ($P < 0.001$). This tendency was significant ($P < 0.01$) for seven subjects. The dynamic phase was analyzed to address the origin of the increase. Fig. 4.2B shows that increments of GF increased under hypergravity for a given variation of LF, as evidenced by a greater ratio between the two variables than that observed under normal gravity conditions (Fig. 4.2B, left). The ratio between increments of GF and LF increased an average of 0.44 for upward movement and 0.62 for downward movement. The ratio between GF_I and LF_I did not show significant tendency across the parabolas for both up and down movements (one-way ANOVA, $P > 0.8$).

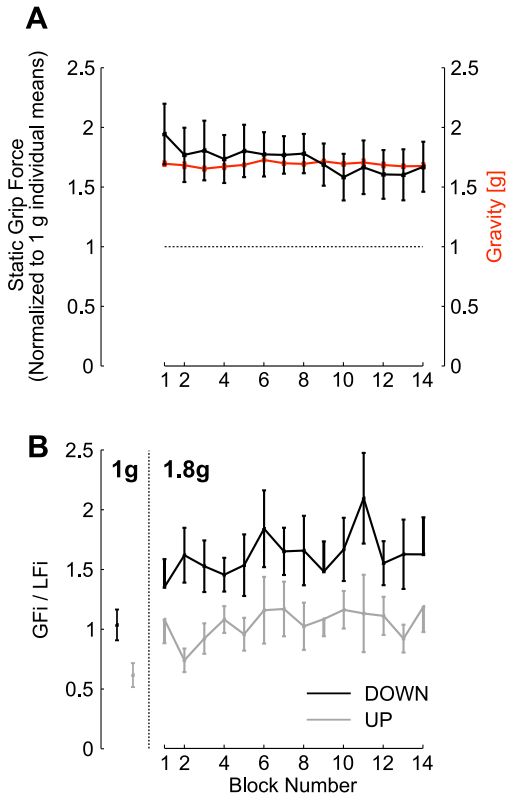


Figure 4.2: A: Evolution of the GF_S across the parabolas. The data were normalized to the individual means measured under 1 g condition. The average gravity during the measurement of GF_S is shown on the same plot (red trace). B: Ratio between GF_I and LF_I in 1 g and in hypergravity across the parabolas in each movement direction. Data from up and down trials are represented in grey and black, respectively. In panels A and B, the vertical bars indicate the standard error computed across subjects.

The origin of this effect was investigated using the following linear model for increments of GF (GF_I) as a function of the variation of LF (LF_I):

$$GF_I = a_0 + a_1 LF_I. \tag{4.1}$$

As shown in Fig. 4.3A and 4.3B, GF_I was significantly correlated with LF_I in both gravitational conditions among all subjects (all subjects

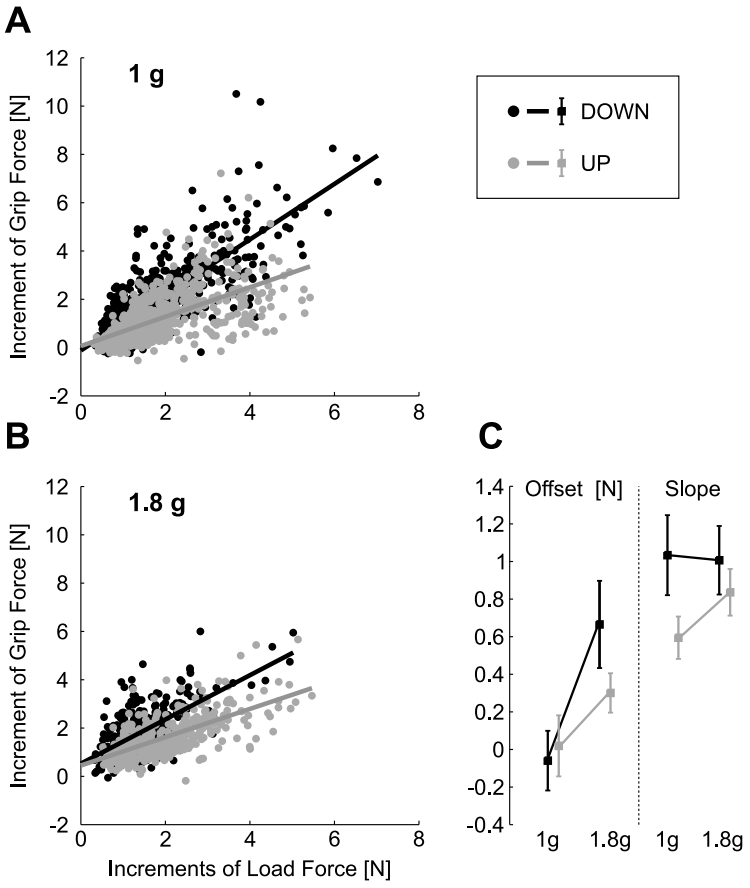


Figure 4.3: A: Linear regressions of GF_I as a function of LF_I under 1 g condition. The regression were computed on up (grey) and down (black) data separately. The data from all subjects were pooled for the illustration. B: Same plot as in Panel A with the data collected in hypergravity. C: Effect of the change in gravity on the regression parameters. The vertical bars indicate the inter subjects standard error on the estimation of the regression slope and offset in each direction and gravitational condition.

pooled, $P < 0.001$, R^2 range 0.289 - 0.621 for each regression). The upward and downward movement data were separated since the linear regression parameters were distinct. This difference in parameters between the two movement types was consistent under both gravitational conditions. The linear regressions were significant for all individual sub-

jects ($P < 0.05$), except for the downward movements of one subject in hypergravity ($P = 0.69$). Individual R^2 in both movement directions ranged between 0.08 and 0.53 under normal gravity and between 0.1 and 0.63 under hypergravity conditions. Fig. 4.3C shows the effect of the increase in gravity on the parameters of the linear regression computed for each subject. The offsets (a_0) and slopes (a_1) were averaged across subjects for each movement direction and gravitational condition. For the upward movements, the increase in the ratio between GF_I and LF_I was due to an increase in both the slope and the offset, while it was primarily due to an increase in the offset for the downward movements. Thus, the default increment of GF (a_0) increased under hypergravity for both movement directions in order to compensate for the increase in LF. The two control experiments presented below aimed to reproduce this increase in a_0 by changing the movement kinematics (first control experiment) or the objects mass (second control experiment).

Control Experiments

Several factors could underlie the above-described effect on anticipatory GF modulation. The first control experiment tested whether the change in GF adjustment could be induced by a change in movement kinematics (Crevecoeur et al., 2009b). Indeed, the movements were faster in both directions under hypergravity conditions. The average peak inertial load in the training session performed under normal gravity was 1.61 N for the ten subjects who performed the task in hypergravity, and 1.34 N for the control group. The control group showed a significant increase in LF peaks between the training session (first 8 blocks) and the session in which they were requested to perform faster movements (8 subsequent blocks, $P < 0.001$). The average increase in LF_I between the two sessions was 1.2 N, reflecting greater variation in the kinematics profile than observed for the hypergravity group (average

0.05 N increase in LF_I). When the subjects performed rapid movements, there was a significant increase in the ratio between GF_I and LF_I in both movement directions ($P < 0.01$). The average increase in the ratio was 0.05 for upward movements and 0.31 for downward movements.

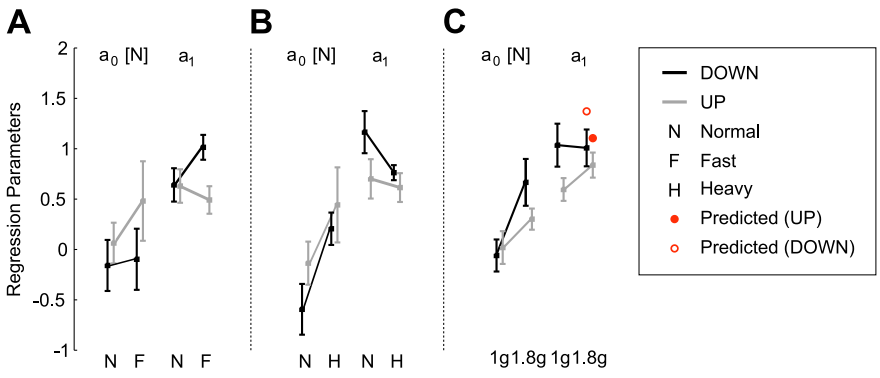


Figure 4.4: A: Effect of the change in movement kinematics on the parameters of the coupling between GF_I and LF_I in the first control group with identical mass across the two testing sessions. B: Effect of the change in movement kinematics on the parameters of the coupling between GF_I and LF_I in the second control group with an additional mass on the held load and similar instruction relative to the movement speed across the two testing sessions. C: Same plot as Fig. 3 C for comparison with the results of the control experiments. The red open and filled circles show the results of the second control experiment in the heavy condition multiplied by the average relative increase in gravity across subjects and parabolas in each movement direction.

The increments of GF correlated with the increments of LF in both movement directions and movement speed conditions in 18 of 20 computed regressions for the first control group (2 directions $\times$ 2 speed conditions $\times$ 5 subjects, $P < 0.05$). The remaining non-significant regressions were for downward movements in the training session of one subject ($P = 0.25$), and upward movements in the rapid session of another subject ($P = 0.44$). Individual R^2 ranged between 0.06 and 0.69. Fig. 4.4A shows the mean effect of the increase in peak acceleration (and therefore LF) on the parameters of the linear regressions. This effect cannot explain the change in regression parameters observed in

hypergravity conditions. Indeed, we observed no increase in the offset for downward movements, which suggests that a change in movement kinematics cannot account for the increase in a_0 measured under hypergravity for both movement directions.

The second control group revealed that the subjects strategy during exposure to hypergravity could be attributed to the effect of the change in weight on anticipatory GF modulation. The average peak inertial load during the first 8 blocks performed by the second control group was 1.6 N, similar to the average of 1.61 N observed during training sessions for the group who performed the experiment in hypergravity. The peak inertial loads were logically greater due to the change in the objects mass ($P < 0.001$). The effect on peak acceleration was reduced in the session performed with the heavier manipulandum ($P < 0.001$). The average decrease in peak acceleration for both directions in this session was 0.57 ms^{-2} and the average increase in peak inertial loads was 1.14 N. Thus, the increase in inertial loads represented 81% of the increase in loads that would correspond to movements realized with identical peak acceleration across the two sessions. This suggests that the change in movement kinematics for this control group had a limited effect relative to the variation in inertial loads induced by the change in mass. This control experiment also produced a significant increase in the ratio between GFI and LFI for upward (0.12) and downward (0.13) movements ($P < 0.01$).

GF_I correlated with LF_I for all subjects ($P < 0.05$), excepting upward movements in the loaded condition of one subject. The relationship approached significance in this case ($P = 0.06$). Individual R^2 ranged between 0.08 and 0.71. In this control experiment (Fig. 4.4B), the change in mass produced an increase in the offset in both movement directions, consistent with the effect of hypergravity on these parameters (Fig. 4.3C).

The results of the second control experiment suggest that the increase in a_0 could be due to the change in the objects weight. However, although the two control experiments reproduced the increase in the ratio between GF_I and LF_I, neither was in quantitative agreement with the increase in this ratio measured under hypergravity conditions. This suggests that inertial loads may be overestimated in hypergravity. We show below that such overestimation is consistent with the application in hypergravity of the strategy revealed by the second control group.

Under normal gravity conditions, a change in weight is necessarily due to a change in mass. However, the ten subjects who performed the experiment in hypergravity faced an increase in weight that was due to gravity rather than mass. By erroneously attributing the increase in weight to mass under hypergravity conditions, the subjects would expect an inertial load equal to:

$$LF_I \cong \alpha m a(t_M), \tag{4.2}$$

where α is the increase in gravity, m is the mass of the manipulated object and $a(t_M)$ is the peak acceleration of the intended movement. Based on the static GF developed under hypergravity (Fig. 4.2A), we can hypothesize that the subjects had a good internal estimate of α. However, the actual inertial load for this movement would be equal to $ma(t_M)$. Consequently, if the predicted inertial load is equal to α times the actual inertial load, then we expect that Eqn. 4.1 becomes:

$$GF_I = a_0 + a_1 \alpha LF_I, \tag{4.3}$$

where a_1 corresponds to the gain of the modulation applied to the internal estimate of the upcoming LF_I when manipulating an object of mass α.

The second control experiment provided us with an estimate of a_1 applied by the subjects who experienced a change in weight due to mass.

By multiplying this value (average a_1 in the heavy condition of the second control experiment) by α (average increase in gravity), we estimated the slopes of the modulation in hypergravity that corresponded to a strategy based on estimation of weight combined with an internal representation of movement kinematics. Fig. 4.4C shows the slopes obtained in this situation for upward (solid circle) and downward (open circle) movements. The increase of GF modulation in hypergravity showed a consistent tendency toward these values, under the assumption that the subjects who experienced the increase in gravity used a similar strategy as the subjects tested during the second control experiment.

4.4 Discussion

Our results describe the GF adjustments to LF variation during voluntary movements realized under hypergravity conditions. First, the increase in weight was properly compensated for by an increase in the level of GF developed during stationary holding. Second, the increase in the ratio between the increments of GF and LF revealed that the magnitude of the predicted inertial loads could be overestimated. The control experiments determined that such changes were likely due to the increase in weight that could be treated as an increase in mass in agreement with the invariant relationship between mass and weight on Earth.

These results reflect a coherent sensorimotor strategy under the hypotheses of optimal feedback control (Todorov and Jordan, 2002; Liu and Todorov, 2007; Izawa et al., 2008) and Bayesian integration of state and parameter estimation in motor control (Kording and Wolpert, 2004). Optimal feedback control posits that the state estimate is mapped into motor commands in a way that optimizes a performance index. In the present study, the observed increase in GF modulation following an increase in object weight is fully compatible with the presence of a sensorimotor loop in which the anticipatory control of GF is modulated by the sensory inflow that conveys information about the objects weight.

A possible mechanism for such modulation is that the neural structures controlling the grip force receive proprioceptive input from the fingers in addition to the arm, and that the encoding of weight is based on the force developed to maintain a stable grip. This proposed mechanism is based on the overlapping of sensory and motor representations in a given body part. This local sensorimotor association forms the basis for the default strategy or prior estimate used by the central nervous system (CNS) during motor learning (Asanuma, 1981; Singh and Scott,

2003).

The exchange of modulation gain for a constant offset under an increased load is compatible with the motor systems tendency to minimize motor output variability in the presence of signal-dependent noise (Harris and Wolpert, 1998; Todorov, 2002). Higher loads are necessarily associated with higher arm or grip motor commands. Thus, the internal prediction of inertial loads suffers from greater uncertainty in these situations, which is compensated for by applying a constant increment of grip force and a lower modulation gain based on prediction. We suggest that this strategy minimizes the variability in grip modulation when the magnitude of the inertial load increases.

Our results also suggest that the encoding of weight is combined with an internal representation of the intended movement, yielding the correlation between the grip force and load force increments. The increase in the ratio between these two variables shows that this combination is based on a Bayesian prior corresponding to the unequivocal relationship between weight, mass and inertial loads experienced on Earth. However, in hypergravity, the sensory feedback must inform the CNS that the actual loads are smaller than expected, as compared to the expected load while assuming only an increase in mass. Under this assumption, we hypothesize that the adjustments in grip modulation parameters are based on whether the difference between the expected and actual loads is most likely due to a change in the body or in the environment. Indeed, such Bayesian inference for estimating the origin of motor errors was demonstrated to be a very powerful model for motor adaptation and generalization (Berniker and Kording, 2008). We suggest that a similar inference was processed in hypergravity, and that the persistent overestimation of inertial loads reflects the strength of our internal prior knowledge of an environment in which gravity never changes.

The Bayesian inference is reinforced by the fact that the increase

in modulation could not be explained by a strategy exclusively based on the perception of the objects weight. Several factors could be at the origin of this effect. First, a sensorimotor map based on the arms weight could yield excessive arm motor commands for upward acceleration since the inertial force would be overestimated. Such an effect would counter the overerestimation of actual inertial force, since acceleration would be underestimated even when mass was overestimated. However, this factor could not account for the effect of hypergravity on the kinematics of downward movements; these movements were faster and there was a sharp reduction in target overshooting (Crevecoeur et al., 2009b). These results contradict the suggestion that arm motor commands were calibrated to overcome a force that was smaller than expected. We may thus conclude that the internal models of arm dynamics were adapted and that the internal representation of movement kinematics was reliable. This is further supported by the good correlations (similar to 1 g conditions) between increments of the grip force and the load force in hypergravity.

Second, the first control experiment revealed that the effect of a change in movement kinematics may contribute to the hypergravity results for upward movements, but it fails to fully explain the upward movement results. We therefore suggest that the increased GF modulation under hypergravity was partially corrected by sensory feedback on the actual inertial loads experienced in previous trials. However, the prediction was strongly biased toward the prior expectation that combined the perception of the objects weight and a reliable internal representation of movement kinematics, in agreement with the life-long physical law experienced under stable gravitational conditions.

Despite this bias, our results demonstrate that arm and grip motor commands are dissociated. Similar results were reported in the context of oscillatory movements by White et al. (2005), who showed that the

grip force was adjusted to the actual load despite the fact that the variation of load force resulted from a distinct combination of object mass, movement acceleration and gravity. In the present context of discrete movements, independent prediction must be estimated for each trial, which presumably hardens a fine GF adjustment relative to the actual load. In addition, our subjects were experiencing a change in gravity for the first time, while the subjects tested by White and colleagues had extensive experience with parabolic flights (> 300 parabolas). Thus, we expect that after a longer and stable exposure, humans are able to learn an unbiased mapping between weight and loads that corresponds to a novel gravitational context.

Chapter 5

Forward models of inertial loads in weightlessness

"If people do not believe that mathematics is simple,
it is only because they do not realize how complicated life is."

JL von Neumann.

[1]**Abstract.** In this experiment, we investigated whether the Central Nervous System uses internal forward models of inertial loads to maintain the stability of a precision grip when manipulating objects in the absence of gravity. The micro-gravity condition causes profound changes in the profile of tangential constraints at the finger-object interface. In order to assess the ability to predict the micro-gravity-specific variation of inertial loads, we analyzed the grip force adjustments that occurred when naive subjects held an object in a precision grip and performed point-to-point movements under the weightless condition induced by parabolic flight. Such movements typically presented static and dynamic phases, which permitted distinction between a static component of the grip force (measured before the movement) and a dynamic component of the grip force (measured during the movement). The static component tended to gradually decrease across the parabolas, whereas the dynamic component was rapidly modulated with the micro-gravity-

[1]Neuroscience (2009), 161: 589-598.

specific inertial loads. In addition, the amplitude of the modulation significantly correlated with the amplitude of the tangential constraints for the dynamic component. These results strongly support the hypothesis that the internal representation of arm and object dynamics adapts to new gravitational contexts. In addition, the difference in timescales of adaptation of static and dynamic components suggests that they can be processed independently. The prediction of self-induced variation of inertial loads permits fine modulation of grip force, which ensures a stable grip during manipulation of an object in a new environment.

5.1 Introduction

Motor actions are a fundamental mode of interaction between the human body and the external world. The mechanisms that underlie movement control are commonly described in terms of internal inverse and forward models (Wolpert and Kawato, 1998; Kawato, 1999; Wolpert and Ghahramani, 2000). Inverse models invert the dynamics of the limb in order to map a desired trajectory onto a motor command, whereas forward models predict the sensory consequences of a motor command (Miall and Wolpert, 1996; Davidson and Wolpert, 2005). The modulation of grasping forces with self-induced loads is an example of predictive control mechanisms based on forward models. When the object is held in a precision grip, i.e. between the thumb and the index finger, the grip force (GF) is synchronously modulated with variations in tangential constraints due to the sum of the objects weight and inertial forces (LF, load force). In this case, the absence of a delay in the response of GF to changes in LF is the signature of a predictive mechanism that is conceptualized as a forward model. Adaptation of motor control in general can be seen as an acquisition of appropriate internal models (Wolpert et al., 2001). To date, adaptation of forward models of inertial

loads in the absence of gravity has not been demonstrated. Therefore, to address specifically the adaptation of forward models, this study focuses on the GF response to a variation of LF in a micro-gravity condition (0 g).

The tight coupling between GF and LF has been thoroughly studied on Earth in various paradigms, such as grip lift (Johansson and Westling, 1984; Westling and Johansson, 1984), horizontal and vertical point-to-point movements (Flanagan and Wing, 1993), and cyclic arm movements (Flanagan and Wing, 1995; Blank et al., 2001; Descoins et al., 2006). Modulation of GF with LF is also very efficient in other contexts such as multi digit grasp (Zatsiorsky and Latash, 2008), or when variations of LF are induced by locomotion (Gysin et al., 2003). In the context of precision grip, the coupling between GF and inertial, elastic and viscous loads induced by linear motors has provided evidence for a forward model of the manipulated object dynamics (Flanagan and Wing, 1997; Flanagan et al., 2003). Similarly, previous studies on the coupling between GF and LF in altered gravity have shed light on the adaptability of GF control in a new gravitational context. Stationary holding (Hermsdorfer et al., 1999) and cyclic arm movements (Hermsdorfer et al., 2000; Augurelle et al., 2003a; White et al., 2005) were performed under a 0 g condition induced by parabolic flights. Under the normal gravity condition, a downward acceleration usually does not produce a negative peak of LF (except in very fast movements where the held load is accelerated faster than gravity); however, it does generate a decrease in tangential constraints resulting from the weight of the manipulated object. Consequently, there is no increase in GF in phase with the downward acceleration. In contrast, under the 0 g condition, negative acceleration produces a negative LF since the weight of the held load equals zero. Therefore, the risk to lose grip stability associated to both positive and negative peaks of LF is specific to the 0 g condition.

In a preliminary study, Nowak and colleagues (Nowak et al., 2001b) performed point-to-point movements in combination with other protocols in micro-gravity and emphasized a change in the pattern of GF in response to LF variations. This finding proves that an adaptation occurs in 0 g condition, but the nature of the adaptive mechanism remains unknown. In particular, the ability to predict the positive and negative peaks of LF was not addressed and it remains unanswered whether the amplitude of the GF modulation is based on a prediction of the inertial loads. There is, to date, no formal proof that such changes in GF modulation in weightless condition rely on internal forward models of inertial loads adapted to the novel gravitational context. The aim of the present study was to provide a quantitative analysis of GF adjustments to variations of LF under the 0 g condition in order to elucidate whether the adaptation is due to an internal forward model.

To this end, we varied the amplitude and direction of discrete point-to-point movements (see Hogan and Sternad (2007) for a definition) and investigated both the time course of GF responses to the variations of LF and the amplitude of the response with respect to the amplitude of LF. In the previous studies investigating oscillatory movements in changed gravity, the change in GF reflected a fine adaptive control, but sensory feedback continuously drove the GF modulation through the repeated cycles of identical amplitude. In addition, the mechanisms controlling rhythmic and discrete movements in altered gravity are different (White et al., 2008). In the context of point-to-point movements performed in 0 g, if the load force was predicted in a time-varying fashion and the grip force was adjusted accordingly, we expect to uncover distinct GF responses to positive and negative peaks of LF leading to biphasic GF profiles with appropriate timing and amplitude for each individual movement.

5.2 Experimental Procedures

Subjects

Eight healthy human subjects (24 - 37 years old), naive to the purpose of the study and to 0 g conditions, participated in this experiment. All subjects gave their informed consent and received the approval to participate in parabolic flights from their National Centre for Aerospace Medicine (class II medical examination). The experiment complied with the ESA ethical and biomedical requirements for experimentation on human subjects (ESA Medical Board Committee) and was approved by the local French CPP committee (*Comité pour la Protection des Personnes*) in charge of reviewing the life science protocols in accordance with the French law.

Parabolic Flight

These experiments were performed during the 43^{rd} and 44^{th} ESA Parabolic Flight Campaigns on board the A-300 ZERO-G aircraft (Bordeaux-Mrignac, France). A parabolic manoeuvre is composed of three distinct phases: 20 s of hyper gravity (1.8 g, pull up phase) followed by 22 s of weightlessness (0 g) before another period of around 20 s of hyper gravity (pull out phase). The beginning of each 0 g phase is announced by the pilot as the injection point. The aircraft ran a sequence of thirty parabolas per flight organized in six groups of five parabolas separated by 5 to 8 minutes pauses. Each subject typically performed the task during 15 parabolas, but due to the unforeseeable nature of the experimental conditions, data could be collected during only 8 parabolas for subject S6.

Experimental Procedure

The task, illustrated in Fig. 5.1A, was performed only in the 0 g

phases. Four target light emitting diodes (LEDs) were placed along a structure that was vertically aligned with respect to the aircraft floor. The target LEDs were positioned every 15 cm. Data acquisition began at the injection point. The program generated a random sequence of targets at a frequency of 1 Hz. The target sequence was generated such that, at any time, the transition probability from the current target to any of the three remaining targets was equal to 1/3. The subjects were seated in front of the target axis and, during data acquisition, held a manipulandum in a precision grip (mass 800 g, grip aperture 4.5 cm). They were asked to align and stabilize the manipulandum with the current target as fast as possible until the next target was illuminated. Head, eye, and arm movements were not constrained. The subjects were allowed to touch the manipulandum only during the 0 g phases to reduce cues to its mass. On return to normal gravity condition, all the subjects were very surprised when they lifted the manipulandum and felt the actual weight. It appeared that their estimation of object mass from experienced load force variation was much smaller than the actual mass. The randomized sequence of targets yielded twelve possible movements. For the purpose of this analysis, the movements were separated into six different categories: upward or downward movements of one, two, or three steps, regardless of the initial hand position. A block of 18 point-to-point movements was performed during each parabola. In the following text, one block refers to the set of trials performed during one parabola. The subjects tested in the second half of each flight were not involved in tasks involving object manipulation during the first half of the flight.

Apparatus and Data Collection

The manipulandum was equipped with two force-torque sensors, one under each finger (40 mm diameter, Mini 40 F/T transducers, ATI Industrial Automation, NC, USA). The contact surface between the fingers

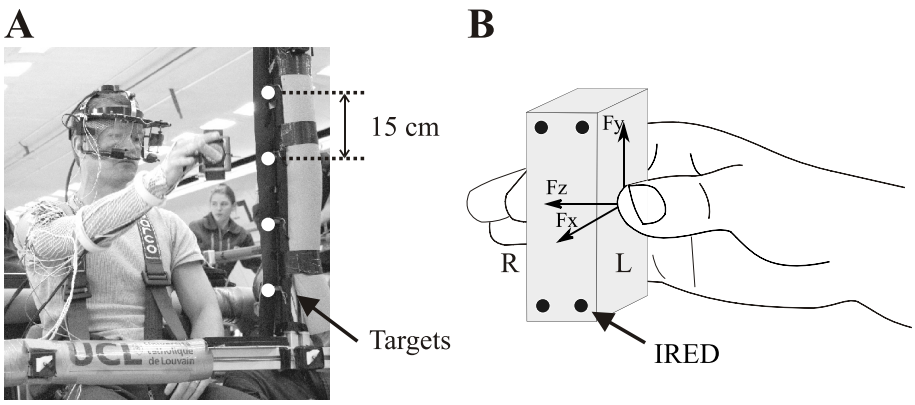


Figure 5.1: A: A subject performing the task. The white disks represent the position of the targets. B: The subjects held the manipulandum in a precision grip between the thumb and the index finger. Fx, Fy, and Fz are the normal and tangential constraints between the fingers and the manipulandum measured by the left and right sensors ($R\&L$). The four IREDs used to track the position and orientation of the manipulandum are represented by black disks.

and the manipulandum were disks of brass pasted on each sensor. These sensors measured the forces and torques in three dimensions, as illustrated in Fig. 5.1B. The sampling rate for acquisition by the sensors was 800 Hz. Three-dimensional position signals of four infrared markers (IRED) placed on the manipulandum as shown in Fig. 5.1B were sampled at 200Hz with a motion-tracking device (Codamotion System, Charnwoods Dynamics, Leicestershire, UK).

Data Post Processing

Forces and position signals were digitally low-pass filtered with a zero phase-lag Butterworth filter of order four with a cut-off frequency set to 15 Hz. Let (Fx_R, Fy_R, Fz_R) and (Fx_L, Fy_L, Fz_L) be the force components in the three directions of space, measured in the right and left sensors reference frame, respectively (Fig. 5.1B). The GF was

defined as the mean of the components normal to the sensors surfaces:

$$GF = \frac{|Fz_R| + |Fz_L|}{2}. \tag{5.1}$$

The LF was defined as the projection of the resulting tangential constraint ($\vec{TC}$) on the vertical axis of the aircrafts reference frame ($\vec{I}_y$). More precisely, $\vec{TC}$ and LF were computed as follows:

$$\vec{TC} = \Big((Fx_R + Fx_L)\,\vec{e}_x + (Fy_R + Fy_L)\,\vec{e}_y \Big), \tag{5.2}$$

$$LF = \vec{TC} \cdot \vec{I}_y, \tag{5.3}$$

where $\vec{e}_x$ and $\vec{e}_y$ represent the unit vectors of the sensors reference frame, in which Fx_R, Fx_L, Fy_R and Fy_L were measured. Given that the norm of $\vec{I}_y$ is equal to one, the dot product comes down to the product of the norm of $\vec{TC}$ and a correction term equal to the cosine of the angle between this vector and $\vec{I}_y$. This procedure allowed for correction of cases in which the manipulandum was slightly tilted or when the trajectories were not strictly vertical. We verified that this correction did not exceed 5% of the norm of $\vec{TC}$ across all blocks and subjects. The onset of the movement was detected when the arm velocity exceeded 5% of the peak velocity computed on each trial. The end of the movement was defined similarly when the arm velocity dropped below the same threshold. The movement duration and amplitude (i.e., the displacement between the movement onset and end), as well as the peak velocity, were used to characterize the subjects performance with respect to the arm trajectory.

Data Analysis

According to Newtons second law, the resulting tangential constraints at the finger-object interface when the manipulandum is held and moved vertically is equal to the sum of the weight and the inertial load:

$$LF = m(g + a(t)), \tag{5.4}$$

where m is the mass of the manipulandum, $a(t)$ is its acceleration and g is gravity. Since g equals zero in this experiment, LF is directly proportional to the acceleration (Fig. 5.2C and 5.22-D), provoking positive and negative peaks of LF corresponding to acceleration and deceleration phases of the movements in both directions. Therefore, we distinguished four different types of tangential constraints, in accordance with the profile of LF. For upward movements (Fig. 5.2D, left), LF first reached a maximum and then a minimum. These two extrema were defined as U^+ (Up-Positive) and U^- (Up-Negative) constraints, respectively. Similarly, the constraints D^+ (Down-Positive) and D^- (Down-Negative) were defined for the extrema of LF that occurred during a downward movement (Fig. 5.2D, right). In the analyses, the sign of LF was preserved to allow differentiating the phases of the movement presenting negative tangential constraints usually not experienced on Earth, and which are different in up (final phase) and down movements (initial phase). For each trial, the static level of GF (GF_S) was defined as the average GF in a 100 ms time window after the target onset. It represents the level of GF exerted by a subject when the arm was at rest. The increment of GF was defined as the difference between GF and GF_S measured at the time of LF extrema. Thus, for each trial, there was one measurement of GF_S and two measurements of increments, one relative to the positive maximum of LF (U^+ or D^+) and the other relative to the negative minimum of LF (U^- or D^-). Fig. 5.2D illustrates these parameters. The brackets represent the time window in which GF_S is computed and the dotted vertical lines joining LF and GF illustrate that GF increments (GF_I) were measured with respect to GF_S at the extrema of LF.

Statistical Analysis

The values of GF_S inside each block were pooled after verifying that there was no effect of initial hand position for any of the subjects, and

no significant tendency within the blocks (ANOVA, $P > 0.05$). This observation motivated the analysis of the evolution of GF_S across the blocks. When ANOVA revealed significant effect across the blocks, classical least-squares linear regressions were computed on raw data from individual trials to identify the nature of the effect based on the sign of the slope. The ratio between GF increments and corresponding extremum of LF was utilized to address the stabilization of the dynamic component. The analyses were performed across the blocks for consistency with the analysis of the adaptation of the static grip force. The stabilization across the blocks was assessed for each subject by comparing the data obtained from a sliding window that contained three blocks with the data obtained in the next block. The non-parametric Wilcoxon rank sum test was employed to test the hypothesis that block i was not significantly different from blocks $i-1$ to $i-3$ pooled together. A lack of any significant difference indicates that the four blocks under examination could be considered as stable. This method permits to assess the stabilization of static and dynamic components of GF with an identical criterion without any hypothesis on the learning curve. The Levene test was used to assess variance homogeneity. The analysis of the modulation of GF during the dynamic phase of the movement is based on classical least-square linear regression. For all statistical tests, a P level inferior to 0.05 was considered to be statistically significant. Finally, cross correlations between the grip force and the absolute load force were used to provide an index of synchrony.

5.3 Results

Two typical trials are shown in Fig. 5.2, three steps upwards (Fig. 5.2, left) and three step downwards (Fig. 5.2, right). In both directions, the subjects performed trajectories with bell-shaped velocity profiles (Fig. 5.1B). The arm trajectories performed by the subjects were rapidly adapted. Indeed, subjects had continuous visual feedback and could therefore correct the movement and stabilize the manipulandum accurately. For the movements of one step in both directions corresponding to movements of 15 cm, the average absolute amplitude after four blocks was 15.17 cm with a standard deviation of 1.71 cm (averaged across subjects), which shows that subjects performed accurate movements. The movement duration, amplitude, and peak velocity did not show any significant trend across the trials and blocks, suggesting a fast adjustment of internal inverse models. It can be observed that GF profiles shown in Fig. 5.2D are synchronously modulated with positive U^+ and D^+ constraints and also with the negative U^- and D^- constraints. Therefore, GF has two distinct peaks for one single point-to-point movement. The following sections separately assess the evolution of the static and dynamic components of GF.

Static Component of GF

The static component GF_S represents the baseline of GF exerted when the subjects arm is at rest for each trial. The following analysis investigates the evolution of GF_S across the blocks. There was no evidence that the performance of subjects tested during the last 15 parabolas was different from the performance of the subjects tested in the first 15 parabolas. The tendency for a decrease in GF_S, shown in Fig. 5.3A for one subject, was significant for seven out of eight subjects (linear regressions, R ranged between 0.38 and 0.65 across subjects). Fig. 5.3A

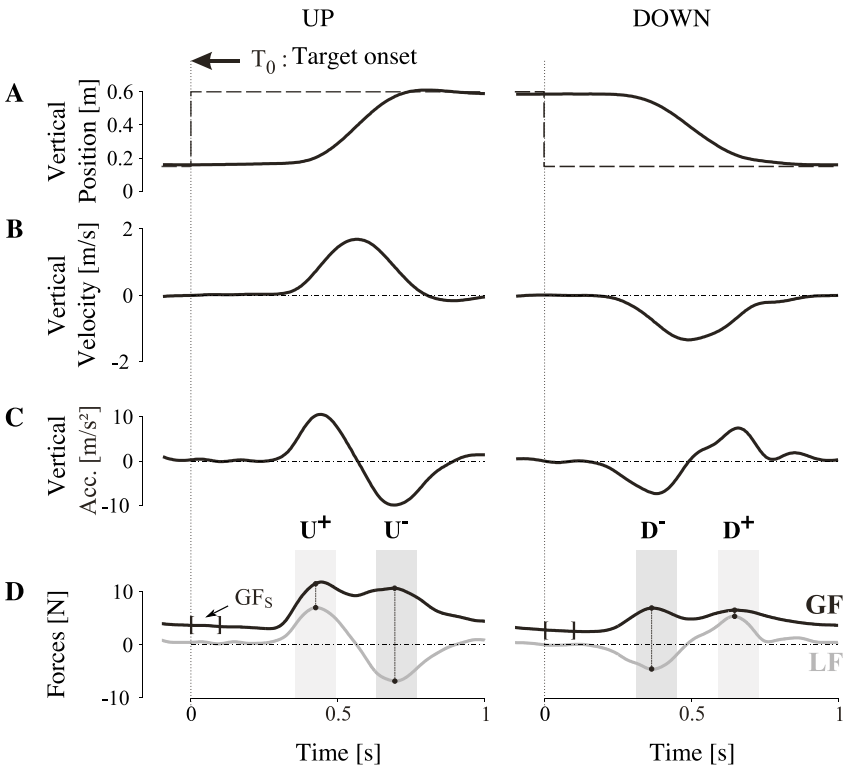


Figure 5.2: Typical upward and downward movements under the 0 g condition as a function of time are shown in the left and right panels, respectively. All of the traces are synchronized with the target onset. A: Trajectory of the held load (solid) and position of the target (dashed). B: Velocity profiles. C: Acceleration profiles. D: GF (black) and LF (grey). The static component of GF is illustrated.

also shows the result of the sliding window analysis (see methods) revealing that, for this subject, the last four blocks surrounded by the grey rectangle may be considered stable. It should be emphasized that the values of GF_S shown for this subject are already rather low from the first block, at least with respect to the minimum grip force required to hold an object of 800 g in normal gravity condition. However, low GF_S were not observed for all the subjects and some of them developed static grip forces up to 20 N. Similar analyses of the remaining subjects

revealed that six out of eight subjects showed stabilization for at least the last four blocks. The earliest stabilization across the subjects was observed for the last seven blocks (subject S7). It is worth mentioning that one of the two subjects who did not show any stabilization was S6, who performed only 8 blocks. The decrease in GF_S was accompanied by a significant reduction of variance inside the blocks, as shown in Fig. 5.3B for the same subject. This significant reduction of variance across blocks was observed for all of the subjects. Given the variability of the range of GF_S across the subjects, the means were normalized for each subject with respect to the largest mean across all of the blocks before the data were pooled for illustration. Fig. 5.3C and 5.3D clearly show for all subjects that adaptation of the static component could be characterized by a decrease across the blocks, a stabilization around the 10^{th} block, and a reduction of variance across the blocks.

Dynamic Component of GF

The analysis of the dynamic component of GF in response to LF variations describes firstly the time course of the modulation and secondly the amplitude of the modulation. Particular interest is given to the negative LF for the update of internal models, since the risk that the object slips due to a negative LF is specific to the 0 g condition. Fig. 5.4A shows LF traces of two typical up (left) and down movements (right). Three events, which correspond to the vertical dotted lines, were defined with respect to the profile of LF: first extremum occurring at t_1, zero of LF occurring at t_2 and second extremum occurring at t_3. The solid traces in Fig. 5.4B show the dynamic component of GF ($GF - GF_S$) for the corresponding trials. The events defined above were used to compute the slopes of linear fits of $GF - GF_S$ as a function of time for the periods between t_1 and t_2 and between t_2 and t_3 (see α_1, α_2, α_3 and α_4 in Fig. 5.4B). It is important to mention that there is no

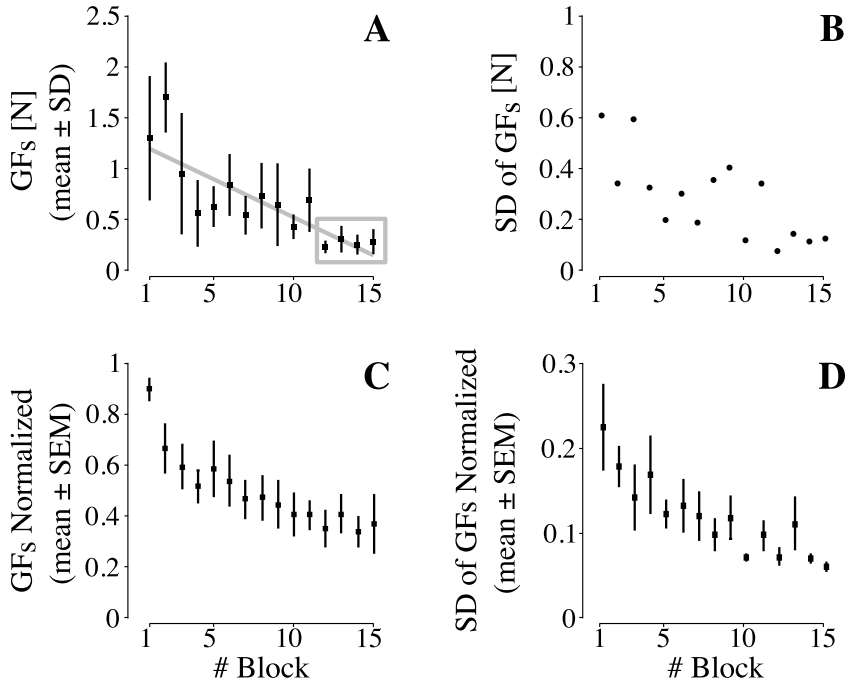


Figure 5.3: Evolution of GF_S across the blocks. A: Mean ± SD of GF_S inside each block as a function of the number of the block for one subject (S3). The grey lines show the linear regressions and the grey rectangle illustrates the stable blocks. B: Standard deviation of GF_S inside each block as a function of the number of the block for the same subject. C: Means of normalized GF_S averaged across the seven subjects presenting significant decreases (mean ± standard error of the mean). D: Intra-block standard deviations of normalized GF_S averaged across the subjects (mean ± standard error of the mean).

increment of GF with a negative LF under the normal gravity condition. For the sake of illustration, the dashed lines represent the putative profiles of GF that are expected on earth (freehand sketch, see Flanagan and Wing (1993) for real data). Therefore, for upward movements, a 1 g strategy would produce negative α_1 and α_2 slopes, whereas α_3 and α_4 would be positive for downward movements. In contrast, double peak responses of GF, such as those shown in Fig. 5.4B, change the signs of α_2 and α_3 with respect to the normal gravity condition: α_2 becomes

positive and α_3 becomes negative. As a consequence, the change in the signs of slopes provides evidence for a biphasic grip force response. The analyses revealed that α_2 was significantly positive for seven subjects out of eight (all but S6, individual values between 0.21 and 0.84) and α_3 was significantly negative for all of the subjects (individual values between -0.72 and -0.04). As expected, α_1 and α_4 remained significantly negative and positive, respectively, for all the subjects. As illustrated in Fig. 5.4C, α_2 and α_3 had opposite signs with respect to those in the 1 g profiles from the first bin of four blocks, and the slopes and correlations (Fig. 5.4D) were relatively stable across the blocks. These findings suggest that biphasic responses of GF to the variations of LF can be observed very early and that this tendency is already significant within the first four blocks.

Following our analysis of the time course of the modulation, we investigated whether the amplitude of GF_I was scaled with the amplitude of LF variations. To this end, we computed the relationship between the increments of GF (i.e., $GF - GF_S$ in Fig. 5.4B measured at t_1 and t_3) and the corresponding maximum or minimum of LF, namely U^+, U^-, D^+, and D^-. The increments significantly correlated with the D^- constraint for all of the subjects and for all but one subject (S6) with the U^- constraint. Slopes and R statistics of the linear regressions for each subject are listed in Table 5.1. More importantly, the significant correlation between the increments of GF and the maximum or minimum of LF remained significant when we considered only the movement of one amplitude in each direction (R ranged between 0.24 and 0.83 across subjects). This was observed for all the subjects but S6 who did not significantly modulate GF with the U^+ and U^- constraints, as was already observed for correlations computed on the data including all the movement categories (see Table 5.1). Fig. 5.5 shows the relationship between GF_I and the corresponding extremum of LF for one subject (S5). Only

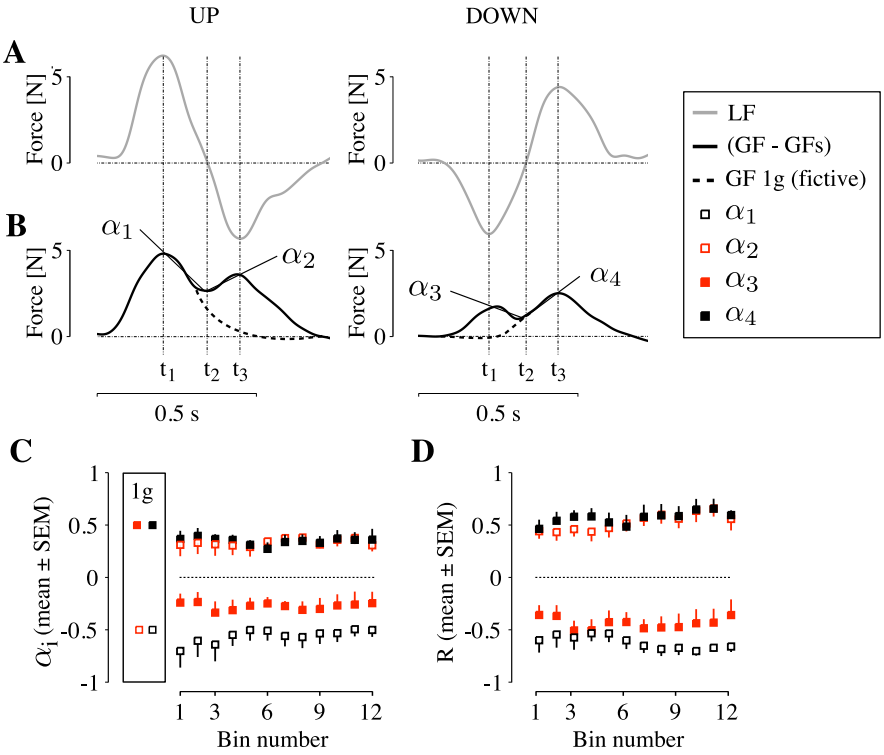


Figure 5.4: Modulation of GF as a function of time. A: LF traces for selected upward (left) and downward (right) movements as a function of time. B: GF as a function of time after subtracting the static component of GF for each trial (solid trace) and GF traces expected under the 1 g condition (dashed traces, freehand sketch). The extrema and zero of LF permitted definition of the events t_1, t_2, and t_3 for movements in both directions. The α parameters are the slopes of linear fits computed on GF as a function of time in the two time intervals $[t_1, t_2]$ and $[t_2, t_3]$. C: time course of the slopes (α_1, α_2, α_3, and α_4 computed on data grouped by bins of four blocks as a function of the bin number (number of the first block inside each bin). The 1 g squares (inset) are free-hand sketch data shown for the purpose of illustration to enhance the change in sign of α_2 and α_3 (red squares). D: time course of the R statistics of the linear regressions computed on the bins as a function of the bin number.

the movements corresponding to one step upwards and downwards are represented. This significant relationship within one single movement category (± 15 cm) demonstrates that the actual motor command of each individual movement is taken into account for the generation of an

increment of grip force.

Table 5.1: Slopes and R statistics of the linear regression of GF_I as a function of the corresponding peak of LF.

	U^+		U^-		D^+		D^-	
	slope	R						
S1	0.51	0.48	-0.41	0.33	0.61	0.56	-0.65	0.54
S2	0.82	0.63	-0.77	0.52	0.73	0.42	-0.64	0.67
S3	0.55	0.65	-0.5	0.54	0.46	0.5	-0.56	0.73
S4	0.66	0.71	-0.36	0.53	0.42	0.56	-0.18	0.46
S5	0.7	0.73	-1.13	0.75	0.9	0.76	-0.77	0.73
S6	NS		NS		0.61	0.54	-0.83	0.72
S7	1.68	0.75	-1.72	0.71	1.6	0.71	-1.75	0.8
S8	0.72	0.67	-0.74	0.57	0.76	0.81	-0.5	0.71

Previous analyses demonstrate a time varying prediction of the inertial loads and a significant modulation of GF with the actual LF. In order to assess when the predictions were stabilized, indicating that the dynamic component was adapted, we computed the ratio between the increments of GF and the corresponding maximum or minimum LF and applied the same sliding window analysis as for the stabilization of the static level of GF. The ratio is stable from the 3^{rd} block for U^+, from the 6th block for U^- and D^+, and from the 5^{th} block for D^- (all movements pooled, averaged across subjects). Again, there was no difference between the subjects evaluated during the first 15 parabolas and the subjects evaluated during the second 15 parabolas.

Finally, in order to test the synchrony between LF and GF profiles, the cross correlations were computed on the trials performed during the last four blocks when both static and dynamic components could be considered stable. The average time shift corresponding to the maximum correlation was very close to zero (LF lead of 19 $\pm$ 30 ms on average). The corresponding maximal correlations were equal to 0.83 $\pm$ 0.06 (mean $\pm$ standard deviation, averaged across subjects).

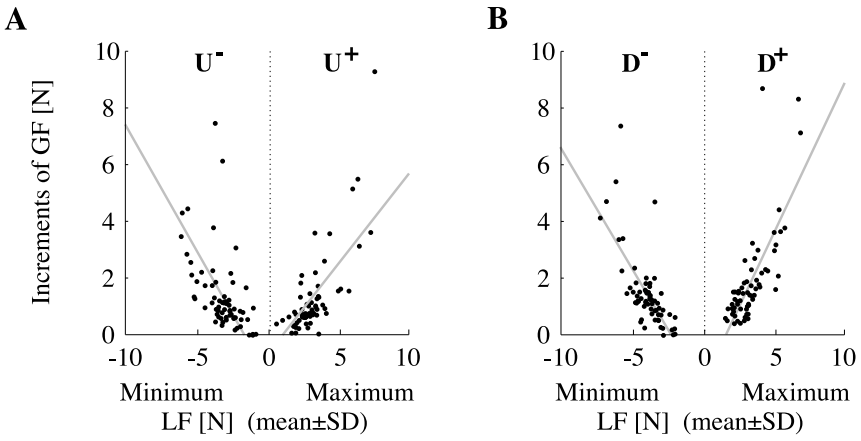


Figure 5.5: Modulation of GF as a function of the corresponding extremum of LF, data from subject S5. The grey lines correspond to linear regressions computed on raw data. Only the data corresponding to movements of one amplitude are represented. A: Upward movements. B: Downward movements.

This section provides evidence for biphasic profiles of GF in response to the positive and negative LF and demonstrates that the amplitude of the GF response of each movement is scaled with the amplitude of LF. The predictions are stable from the fifth block on average and the grip force modulation is synchronized with the load force variations.

5.4 Discussion

Our results describe the adaptation of static and dynamic components of GF. On the one hand, the static component decreases slowly, tends to stabilize late, and the variance of GF_S decreases across the blocks. On the other hand, the dynamic component is quickly modulated by the tangential constraints, and the modulation is significantly correlated with the positive and negative peaks of LF.

Our results appear to be fully compatible with those reported in earlier studies. In an analysis of stationary holding of an object under the 0 g condition, Hermsdörfer and colleagues (1999) observed a continuous decrease of GF during the first 5 parabolas dedicated to this task (subsequent parabolas were dedicated to other protocols). They concluded that longer exposure is needed in order to observe stable performance. The results of the present study indicate that around 10 parabolas are required before stabilization of GF_S occurs. In a previous study, which investigated oscillatory movements performed in parabolic flights by naïve subjects, Augurelle and colleagues (2003a) reported stabilization of the baseline of GF in 0 g from the 5^{th} parabola. The nature of the movement (rhythmic oscillations) probably facilitates this earlier stabilization of the baseline GF. In addition, the subjects performed the task during other gravitational contexts (in particular in 1 g), which could contribute to provide the subjects a good estimate of the object mass and help to produce and adequate grip force.

Our main finding is that GF modulation reflects a fine prediction of the specific inertial loads experienced under the 0 g condition. The double-peak responses of GF (see Fig. 5.2D and Fig. 5.4) and significant correlations between GF_I and the extrema of LF (Fig. 5.5) demonstrate a predictive control mechanism, which takes into account the variation of LF as a function of time for each particular movement,

and produces an increment of GF that is proportional to the predicted constraint. Analysis of the one-step category (Fig. 5.5C and 5.5D) confirms that the prediction is realized on a trial-by-trial basis. This implies that the prediction takes the actual motor command sent to the limb into account in order to produce an appropriate grip response. This mechanism, which is well characterized under the normal gravity condition for point-to-point movements (Flanagan and Wing, 1993), is rapidly adapted to the 0 g condition and allows for fine prediction of positive and negative constraints, as well as prediction of their amplitude. In 0 g, Nowak and colleagues (2001) reported that GF remained elevated during the whole movement in order to counteract both peaks of LF. They concluded that the control of GF was highly flexible and able to integrate changes in load profile that were induced by changes in gravity. However, their study involved only two subjects with different experiences of weightlessness who performed the task during only two parabolas. The protocol consisted of movements of one amplitude (corresponding to two steps in our experiment) without randomization. Their preliminary data permitted enhancement of a change in GF control but fell short of explaining the mechanism that underlies the adaptation to micro-gravity. In contrast, we provide evidence for a biphasic response of GF proving a time-varying prediction of LF, and we demonstrate that the amplitude of the modulation of GF is scaled as a function of the predicted LF. Altogether, our results permit to conclude that LF is predicted in a time varying fashion and GF is adjusted accordingly, proving the existence of a forward model of inertial loads adapted to weightless condition.

The point of performing this experiment in weightlessness is that the nature of the perturbation (the change in gravity) obliges the subjects to learn appropriate arm motor command through sensory signals of force and motion from muscles and tendons (Lackner and DiZio, 2005).

This is due to the fact that there is no external contact point between the limb and a perturbing device like a robot. This distinction in the nature of the perturbation led Lackner and DiZio to emphasize distinct adaptation processes when identical forces were applied on the limb, depending on the nature of the perturbing force: Coriolis forces in one case (without contact) and forces induced by a robot in another case. Concerning object manipulation, it was previously demonstrated that the CNS can predict the effect of various force fields induced by linear motors (Flanagan and Wing, 1997), which proves that a forward model of inertial loads is available when the manipulated object presents altered dynamics experienced through contact between the object and the fingers, whereas the arm is moved in normal condition. In addition, performing horizontal movements on Earth generates a similar profile of load force in the direction of the movement (Flanagan and Wing, 1993), but the relative variation of the total load force for an acceleration in the range observed in the present study would be small in comparison with the constant offset due to the object weight (less than 8% variation of total LF for an acceleration of 4 m/s^2). On Earth, the weight of the object can be counterbalanced by an external support, leading to pure acceleration dependent loads for horizontal movements. A fine coupling between grip force and load force can be observed in such contexts (Flanagan and Lolley, 2001; Descoins et al., 2006) providing evidence for a good anticipation of inertial loads related to the manipulated object dynamics. However, similar range of load force variation as observed under 0 g condition cannot be experienced in normal gravity without artificially neutralizing the object weight. Moreover, the whole system (arm-object) undergoes the perturbation induced by a change in gravity without contact on the limb or on the object. Therefore, the forward models must take into account the change in arm dynamics in addition to changes in the object dynamics.

The main difference between the adaptation processes uncovered by Lackner and DiZio concerned the time course of adaptation and the presence of an after effect, which was greater after the Coriolis perturbation than after the robots perturbation. It was not possible to investigate the presence of an after effect in our experiment given the context of parabolic flight (short exposure separated by hyper and normal gravity phases with short pauses), thus the question of de-adaptation after longer exposure remains an open question and would provide further indication of the nature of the adaptive process. Indeed, it has been shown that context-specific adaptation to an expected Coriolis force field does not require de-adaptation upon return to normal condition (Cohn et al., 2000). The investigation of subjects performances after a long-term flight should indicate whether a similar kind of adaptation would occur in 0 g condition. In particular, the presence (or absence) of after effect should allow dissociating whether the internal forward models of inertial loads are adapted to the weightless condition, or whether a new context specific internal model is built in absence of gravity.

Based on the hypothesis of distinct control processes for posture and movement (Kurtzer et al., 2005), our results confirm that GF can be decomposed into static and dynamic components with different timescales of adaptation. Indeed, the dynamic component of GF was found to be stable from the fifth blocks on average, whereas the static component gradually decreased across the blocks. This finding suggests that the two components of GF can independently adapt and evolve. This additive model for static and dynamic components of GF is in accordance with previous hypotheses that gravitational and inertial loads are treated separately in order to program GF (Hermsdorfer et al., 2000; Nowak et al., 2001b; White et al., 2005; Zatsiorsky et al., 2005). A dissociation between static and dynamic components has also been reported in trunk postural and bending adjustments under prolonged exposure

to weightlessness (Baroni et al., 2001). In precision grip, the decoupling between static and dynamic components can also be related to the observation made by Flanagan and Wing (1995) that the intercept and gain of GF as a function of LF during oscillatory movements independently adapt in response to an increase in the movement frequency. However, the analogy must be considered with caution because there are known differences between rhythmic and discrete movements (Ronsse et al., 2008b,a, 2009). In particular, it has been shown that neural circuitries underlying the control of rhythmic and discrete tasks are distinct (Schaal et al., 2004).

More generally, we propose that the static component is the output of a mechanism that depends on the context and on an internal estimation of the object mass. In our experiment, the sensory feedbacks contributing to the general perception of a change in the environment (e.g. blood pressure variations and vestibular signals) probably encouraged the subjects to apply high levels of grip force in the beginning in order to face stress, excitement or uncertainty. Cutaneous feedback is also crucial to the generation of the static grip force as well as for the adjustments of grip force modulation and calibration of forward models through an estimation of skin-object coefficient of friction. (Johansson and Westling, 1984; Westling and Johansson, 1984; Augurelle et al., 2003b; Witney et al., 2004). Concerning the modulation of grip force, we showed that LF is continuously predicted in order to generate the grip modulation, which must take into account the estimation of the mass and frictional properties of the held load in addition to an estimation of the arm acceleration. In this framework, the modulation of the increment may differ depending on the nature of the movement and its specific underlying mechanism (rhythmic, discrete, reflex, etc.). Our data suggest that the static component and the increment are additively combined to produce the grip motor command.

Further studies should investigate the neural circuitry of both components. It is tempting to speculate that GF_S based on cutaneous feedback and subject to volitional control would result from high-level cortical control, including the primary sensorimotor cortex, ventral premotor cortex, supplementary and cingulated motor area, and inferior parietal cortices (Kuhtz-Buschbeck et al., 2001), whereas the increments, which are unconsciously adapted and highly automated, would result from lower level control, including the cerebellum (Miall et al., 1993; Kawato et al., 2003; Nowak et al., 2007). Indeed, accumulating evidence in the literature suggests that this region could store forward models underlying the control of precision grip.

Chapter 6

Improving the state estimation for optimal control of stochastic processes subject to multiplicative noise

"In mathematics you do not understand things.
You just get used to them."

JL von Neumann.

[1]**Abstract.** Computational models for the neural control of movement must take into account the properties of sensorimotor systems, including the signal-dependent intensity of the noise and the transmission delay affecting the signal conduction. For this purpose, this paper presents an algorithm for model-based control and estimation of a class of linear stochastic systems subject to multiplicative noise affecting the control and feedback signals. The state estimator based on Kalman filtering is allowed to take into account the current feedback to compute the current state estimate. The optimal feedback control process is adapted accordingly. The resulting estimation error is smaller than the estima-

[1]Submitted to Automatica.

tion error obtained when the current state must be predicted based on the last feedback signal, which reduces variability of the simulated trajectories. In particular, the performance of the present algorithm is good in a range of feedback delay that is compatible with the delay induced by the neural transmission of the sensory inflow.

6.1 Introduction

The control of stochastic processes is a challenging problem that requires efficient methods for estimating the state of the system and compute an appropriate feedback control policy. Recent results on the neural control of movement suggest that the control process used by the brain presents many features of an optimal feedback controller (Todorov, 2004; Scott, 2004; Shadmehr and Krakauer, 2008). Therefore, the modeling approach in computational neuroscience has motivated the design of optimal feedback controllers that integrate the properties of the sensorimotor system, including the presence of multiplicative noise affecting the plant dynamics and the state feedback, and a significant delay in the feedback signal. Indeed, the variability of neural signals increases with the intensity of the signal, and this property modeled as multiplicative noise is known to be a determinant factor in sensorimotor coordination (Harris and Wolpert, 1998).

The Linear Quadratic Gaussian regulator (LQG, (Aström, 1970)) provides a solution for the optimal control of stochastic systems with linear dynamics, additive Gaussian noise and quadratic costs. In this context, the problems of control and estimation, based on Kalman filtering, are independent and can be solved separately. This result, known as the separation principle, no longer holds when the control and feedback signals are affected by multiplicative noise (Phillis, 1985).

Todorov (2005) modified the LQG control algorithm to take into

account the presence of multiplicative noise under the assumption that the state of the system at time k is estimated based on the information available until time $k-1$. This state estimate corresponds to the predictive case. In order to improve the performance of the estimation process, the present paper extends the control algorithm to the filtering case (Brown, 1983): we allow the controller to use the feedback information at time k to estimate the state of the system at time k. Due to the presence of multiplicative noise, this assumption modifies the control and estimation processes.

The following sections present the adaptation of the control and estimation algorithms to the filtering case. The full control algorithm is validated on a model for biological motor control. The controller must achieve a simple reaching movement. The system is affected by additive and multiplicative noise, and the state feedback is delayed. The noise amplitude and feedback delay are compatible with physiological data. We show on this example that in the presence of an unmeasured perturbation, the state estimator is better in the filtering case, which improves the performance of the controller in terms of end-point error. In addition, for larger feedback delays, the total expected cost is smaller in the filtering case.

6.2 Problem Definition and Assumptions

We consider the following class of stochastic systems:

$$x_{k+1} = Ax_k + Bu_k + \xi_k + \sum_{i=1}^{n_c} \varepsilon_{i,k} C_i u_k, \tag{6.1}$$

$$y_k = Hx_k + \omega_k + \sum_{i=1}^{n_d} \delta_{i,k} D_i x_k, \tag{6.2}$$

where $x_k \in \mathbb{R}^n$ is the state of the system, $u_k \in \mathbb{R}^m$ is the control input, ξ_k and ω_k are multivariate Gaussian random variables with zero mean and

covariance $\Omega_\xi \in \mathbb{R}^{n\times n}$ and $\Omega_\omega \in \mathbb{R}^{p\times p}$, respectively ($p$ is the dimension of the output feedback, y_k). The matrices C_i and D_i are scaling factors employed to introduce the control and state dependent noises; $\varepsilon_{i,k}$ and $\delta_{i,k}$ are Gaussian random variable with zero mean and variance equal to 1. We assume that the different sources of noise are uncorrelated.

The cost-per-step is:

$$\begin{aligned} J_k(x_k, u_k) &= x_k^T Q_k x_k + u_k^T R u_k, \qquad k = 1, 2, \ldots, N-1, \\ J_N(x_N) &= x_N^T Q_N x_N. \end{aligned}$$

It is further assumed that R is symmetric positive definite and that the matrices Q_k are symmetric positive semidefinite. The control problem is defined as follows: find a control policy which minimizes the total expected cost defined as follows:

$$J = E\left[J_N(x_N) + \sum_{k=1}^{N-1} J_k(x_k, u_k)\right]. \tag{6.3}$$

The delay situation is postponed until section 3.4.

The state estimate at time k is computed as follows. We assume that the prior estimate has the following form:

$$x_k^p = A\hat{x}_{k-1} + Bu_{k-1} + \eta_{k-1},$$

where η_k is a multivariate Gaussian random variable with zero mean and covariance matrix $\Omega_\eta \in \mathbb{R}^{n\times n}$. It expresses that the controller may compute a prior estimate that also suffers from uncertainty. The prior estimate is then updated by a feedback correction term:

$$\hat{x}_k = x_k^p + K_k(y_k - Hx_k^p). \tag{6.4}$$

The sequence of Kalman gains (K_k) must be computed. The state estimate in the predictive case, defined as:

$$\hat{x}_k = x_k^p + K_k(y_{k-1} - H\hat{x}_{k-1}), \tag{6.5}$$

will be used to compare the performance of the full controllers in the predictive and filtering cases, respectively.

In principle, the filtering estimate is better since a more recent information is available in order to estimate the current state of the system. However, the presence of multiplicative noise has the consequence that the Kalman gains and the optimal feedback gains depend on each other. Hence, the use of Equation 6.4 instead of Equation 6.5 has a major impact on the mathematics of the solution, which is derived in the following section.

6.3 Control Algorithm

Let e_k be the estimation error computed as the difference between the true state and the estimated state at time k. By plugging Equation 6.2 into Equation 6.4, one finds the following stochastic dynamics for the state and estimation error:

$$x_{k+1} = Ax_k + Bu_k + \xi_k + \sum_{i=1}^{n_c} \varepsilon_{i,k} C_i u_k, \tag{6.6}$$

$$\begin{aligned} e_{k+1} &= \Delta_{k+1} \left[Ae_k + \xi_k - \eta_k + \sum_{i=1}^{n_c} \varepsilon_{i,k} C_i u_k \right] \\ &\quad -K_{k+1} \left[\omega_{k+1} + \sum_{i=1}^{n_d} \delta_{i,k} D_i x_{k+1} \right], \end{aligned} \tag{6.7}$$

where $\Delta_{k+1} = I - K_{k+1}H$.

6.3.1 Optimal Controller

We follow the classical approach introduced in the LQG control framework (Aström, 1970). Let us first introduce Lemma 1, which will be useful for the derivation of the optimal control policy (see Ref. Aström, 1970, Lemma 3.2, pp. 261):

Lemma 1 *Let $E[\,\cdot\,|y]$ denote the conditional mean given y. Assume that the function $f(y,u) = E[l(x,y,u)]$ has a unique minimum with respect to $u \in U$ for all $y \in Y$. Let $u^\circ(y)$ denote the value of u for which the minimum is achieved. Then*

$$\begin{aligned} \min_{u(y)} E\left[l(x,y,u)\right] &= E\left[l(x,y,u^\circ(y))\right], \\ &= E_y\left[\min_u E(l(x,y,u)\,|\,y)\right], \end{aligned}$$

where E_y denote the mean value with respect to the distribution of y.

We decompose the sum in Equation 6.3 and apply Lemma 1 in order to compute the conditional expected cost from time k until the final time, given the output feedback at time k:

$$\min_{u_k,\, u_{k+1},\, \ldots} E\left[J_N(x_N) + \sum_{s=k}^{N-1} J_s(x_s,u_s)\right] = E\left(v_k\,|\,y_k\right),$$

where v_k satisfies:

$$\begin{aligned} v_k &= \min_{u_k} E\Big(x_k^T Q_k x_k + u_k^T R u_k \\ &\quad + E[v_{k+1}|x_k,\, \hat{x}_k,\, u_k,\, y_{k+1}]\Big). \end{aligned} \tag{6.8}$$

Equation 6.8 is the classical Bellman equation (Aström, 1970) and v_k, called the cost-to-go, represents the expect remaining cost from time k under the optimal control policy. Theorem 1 gives a recursion formula for v_k and permits us to deduce the optimal control policy.

Theorem 1 *Under the optimal control policy, the cost-to-go is given by:*

$$v_k = x_k^T S_k^x x_k + e_k^T S_k^e e_k + s_k,$$

where S_k^x and S_k^e are symmetric positive semidefinite and s_k is non negative.

Proof. From assumptions, the claim is true when $k = N$, with $S_N^x = Q_N$, $S_N^e = 0$ and $s_N = 0$. To compute the conditional cost-to-go given x_k, $\hat{x}_k$ and u_k, we must evaluate the expected value of v_{k+1}. This is computed using the state and error dynamics given in Equations 6.6 and 6.7. The error dynamics can be written as:

$$e_{k+1} = q_{k+1} - \Theta_{k+1} x_{k+1},$$

where q_{k+1} brings together the terms in Equation 6.7 that do not depend on x_{k+1}, and Θ_{k+1} is defined as follows:

$$\Theta_{k+1} = K_{k+1} \sum_{i=1}^{n_d} \delta_i D_i. \tag{6.9}$$

Using Equation 6.9 to compute the expected cost-to-go at time $k+1$, we obtain:

$$\begin{aligned} v_{k+1} &= x_{k+1}^T \left(S_{k+1}^x + \Theta_{k+1}^T S_{k+1}^e \Theta_{k+1} \right) x_{k+1} \\ &\quad + q_{k+1}^T S_{k+1}^e q_{k+1} - 2 x_{k+1}^T \Theta_{k+1}^T S_{k+1}^e q_{k+1}, \end{aligned} \tag{6.10}$$

that must be developed by taking into account that the expected values of the cross products of uncorrelated noises are zero. We also use the property that, for any multivariate Gaussian random vector w with expected value $\bar{w}$ and covariance matrix Σ and any dimension-compatible matrix U, we have $E(w^T U w) = \bar{w}^T U \bar{w} + \mathrm{tr}(U\Sigma)$. In order to simplify the notations, we define:

$$U_{k+1} = S_{k+1}^x + \sum_{i=1}^{n_d} D_i^T K_{k+1}^T S_{k+1}^e K_{k+1} D_i,$$

and

$$\Gamma_{k+1} = \sum_i C_i^T (U_{k+1} + \Delta_{k+1}^T S_{k+1}^e \Delta_{k+1}) C_i.$$

The development of the expected value of Equation A.14 plugged into Equation 6.8 gives:

$$v_k = \min_{u_k} \Big(x_k^T \left(A^T U_{k+1} A + Q_k \right) x_k$$

$$
\begin{aligned}
&+u_k^T \left(B^T U_{k+1} B + R + \Gamma_{k+1}\right) u_k \\
&+e_k^T \left(A^T \Delta_{k+1}^T S_{k+1}^e \Delta_{k+1} A\right) e_k \\
&+2u_k^T B^T U_{k+1} A x_k \\
&+\mathrm{tr}\left(U_{k+1}\Omega_\xi\right) \\
&+\mathrm{tr}\left(S_{k+1}^e(\Delta_{k+1}(\Omega_\xi+\Omega_\eta)\Delta_{k+1}^T + K_{k+1}\Omega_\omega K_{k+1}^T)\right) \\
&+s_{k+1}\Big).
\end{aligned}
$$

The cost-to-go is a quadratic form in u_k. Given that the control policy is only allowed to be a function of the state estimate, the best control strategy is to apply the gain that minimizes the quadratic form on the current state estimate:

$$
\begin{aligned}
u_k &= -\left(B^T U_{k+1} B + R + \Gamma_{k+1}\right)^{-1} B^T U_{k+1} A \hat{x}_k, \\
&:= -L_k(x_k - e_k).
\end{aligned}
$$

Using the definition of u_k in the expressions of cost-to-go, we obtain:

$$
\begin{aligned}
v_k &= x_k^T \left(A^T U_{k+1}(A - BL_k) + Q_k\right) x_k \\
&\quad +e_k^T \left(A^T U_{k+1} B L_k + A^T \Delta_{k+1}^T S_{k+1}^e \Delta_{k+1} A\right) e_k + s_k,
\end{aligned}
\tag{6.11}
$$

where s_k is the sum of s_{k+1} and the trace of the covariance terms, which is positive. Equation 6.11 is the required expression for v_k and the induction is complete.

It remains to prove that the matrices S_k^x and S_k^e are symmetric positive semidefinite. This is direct for S_k^e by observing that:

$$
A^T U_{k+1} B L_k = L_k^T \left(B^T U_{k+1} B + R + \Gamma_{k+1}\right) L_k.
$$

To prove that S_k^x is symmetric positive semidefinite, we complete the square and obtain the following identity:

$$
\begin{aligned}
S_k^x &= Q_k + (A - BL_k)^T U_{k+1}(A - BL_k) \\
&\quad +L_k^T B^T U_{k+1} A - L_k^T B^T U_{k+1} B L_k,
\end{aligned}
$$

$$\begin{aligned} &= Q_k + (A - BL_k)^T U_{k+1}(A - BL_k) \\ &\quad + L_k^T (R + \Gamma_{k+1}) L_k, \end{aligned}$$

which completes the proof. ■

6.3.2 Optimal State Estimator

We start from the expression of the cost-to-go to derive the optimal Kalman gains. The following theorem uses the property that for any dimension compatible matrices, we have $\mathrm{tr}(UV) = \mathrm{tr}(VU)$. Hence, we have the following identity for any multivariate random variable x with covariance matrix $E(xx^T) = \Omega_x$:

$$E\left(x^T A^T B A x\right) = \mathrm{tr}\left(A \Omega_x A^T B\right). \tag{6.12}$$

The proof for the derivation of optimal Kalman gains follows Todorov (2005).

Theorem 2 *Let us define the following covariance matrices:* $\Sigma_k^e = E(e_k e_k^T)$, $\Sigma_k^x = E(x_k x_k^T)$ *and* $\Sigma_{k+1}^p = A\Sigma_k^e A^T + \Omega_\xi + \Omega_\eta$. *Then, the optimal sequence of Kalman gains is given by:*

$$K_{k+1} = \Sigma_{k+1}^p H^T (H \Sigma_{k+1}^p H^T + \Omega_\omega + M_{k+1})^{-1},$$

where M_{k+1} *is the following matrix:*

$$M_{k+1} = \sum_{i=1}^{n_d} D_i \left((A - BL_k)\Sigma_k^x A^T + BL_k \Sigma_k^e A^T + \Omega_\xi\right) D_i^T.$$

Proof. We decompose the matrix U_{k+1} introduced in the previous theorem and define:

$$N_{k+1} = \sum_{i=1}^{n_d} D_i^T K_{k+1}^T S_{k+1}^e K_{k+1} D_i.$$

The terms in the Equation 6.11 that depend on K_{k+1} are:

$$\begin{aligned} a(K_{k+1}) &= x_k^T A^T N_{k+1} (A - BL_k) x_k \\ &\quad + e_k^T \left(A^T N_{k+1} B L_k + A^T \Delta_{k+1} S_{k+1}^e \Delta_{k+1} A \right) e_k \\ &\quad + \mathrm{tr} \left(N_{k+1} \Omega_\xi + S_{k+1}^e \right) \\ &\quad + \mathrm{tr} \left(\Delta_{k+1} (\Omega_\xi + \Omega_\eta) \Delta_{k+1}^T + K_{k+1} \Omega_\omega K_{k+1}^T \right). \end{aligned}$$

The expression of $a(K_{k+1})$ is transformed using Equation 6.12 as follows:

$$\begin{aligned} a(K_{k+1}) &= \mathrm{tr} \left(\Delta_{k+1} \left(A \Sigma_k^e A^T + \Omega_\xi + \Omega_\eta \right) \Delta_{k+1}^T S_{k+1}^e \right) \\ &\quad + \mathrm{tr} \left(K_{k+1} \left(\Omega_\omega + M_{k+1} \right) K_{k+1}^T S_{k+1}^e \right). \end{aligned}$$

This expression is minimized over K_{k+1} when the gradient of $a(.)$ with respect to K_{k+1} is equal to zero. Taking into account the definition of Σ_{k+1}^P and that the matrices multiplying Δ_{k+1} and K_{k+1} are symmetric, we obtain:

$$\nabla_{K_{k+1}} a(K_{k+1}) = 2 S_{k+1}^e \left(\Delta_{k+1} \Sigma_{k+1}^p H^T - K_{k+1} (\Omega_\omega + M_{k+1}) \right),$$

which is equal to zero when the following holds:

$$K_{k+1} = \Sigma_{k+1}^p H^T \left(H \Sigma_{k+1}^p H^T + \Omega_\omega + M_{k+1} \right)^{-1}.$$

This completes the proof. ■

6.3.3 Recursion Formulas

The two preceding theorems allow us to build a full controller in the filtering case. The induction proof for the optimal controller provides the following backward recursion for L_k, for the given sequence of Kalman gains K_k:

$$\begin{aligned} L_k &= \left(B^T U_{k+1} B + R + \Gamma_{k+1} \right)^{-1} B^T U_{k+1} A, \qquad (6.13) \\ S_k^x &= A^T U_{k+1} (A - BL_k) + Q_k, \end{aligned}$$

$$
\begin{aligned}
S_k^e &= A^T U_{k+1} B L_k + A^T \Delta_{k+1}^T S_{k+1}^e \Delta_{k+1} A, \\
s_k &= s_{k+1} + \mathrm{tr}\left(U_{k+1}\Omega_\xi\right) \\
&\quad + \mathrm{tr}\left(S_{k+1}^e(\Delta_{k+1}(\Omega_\xi + \Omega_\eta)\Delta_{k+1}^T + K_{k+1}\Omega_\omega K_{k+1}^T)\right).
\end{aligned}
$$

The backward recursion is initialized with $S_N^x = Q_N$, and $S_N^e = s_N = 0$ (Γ_{k+1} and U_{k+1} were defined in Theorem 1).

The sequence of Kalman gains is obtained in a forward recursion. In addition to the error and state covariance matrices, we introduce the estimation covariance matrix $\Sigma_k^{\hat{x}} = E(\hat{x}_k \hat{x}_k^T)$ that will be necessary to update Σ_k^x and Σ_k^e. In order to initialize the recursions, it is assumed that the initial covariance matrices $\Sigma_0^{\hat{x}}$, Σ_0^x and Σ_0^e are known. In practice, these matrices can be set to any initial value depending on the initial conditions. The covariance matrices are updated by using the system and error dynamics (Equations 6.6 and 6.7). To simplify the notation, we use:

$$
\begin{aligned}
V_k &= \sum_i C_i L_k \Sigma_k^{\hat{x}} L_k^T C_i^T, \\
W_{k+1} &= \sum_{i=1}^{n_d} D_i \Sigma_{k+1}^x D_i^T.
\end{aligned}
$$

The forward recursion to compute the Kalman gains is:

$$
\begin{aligned}
\Sigma_{k+1}^p &= A\Sigma_k^e A^T + \Omega_\xi + \Omega_\eta, \qquad (6.14) \\
K_{k+1} &= \Sigma_{k+1}^p H (H\Sigma_{k+1}^p H^T + \Omega_\omega + M_{k+1})^{-1}, \\
\Sigma_{k+1}^x &= (A - BL_k)\Sigma_k^x (A - BL_k)^T + \Omega_\xi + V_k, \\
\Sigma_{k+1}^e &= \Delta_{k+1}\left(A\Sigma_k^e A^T + \Omega_\xi + \Omega_\eta + V_k\right)\Delta_{k+1}^T \\
&\quad + K_{k+1}\left(\Omega_\omega + W_{k+1}\right)K_{k+1}^T, \\
\Sigma_{k+1}^{\hat{x}} &= \Delta_{k+1}\left((A - BL_k)\Sigma_k^{\hat{x}}(A - BL_k)^T + \Omega_\eta\right)\Delta_{k+1}^T \\
&\quad + K_{k+1}\left(H\Sigma_{k+1}^x H^T + \Omega_\omega + W_{k+1}\right)K_{k+1}^T.
\end{aligned}
$$

The algorithm for the full controller works as follows: initialize a guess for the sequence of Kalman gains and iterate the recursions 6.13 and

6.14 until the decrease in the total expected cost, v_1, is inferior to an arbitrary limit considered as satisfactory. The total expected cost is strictly positive (S_1^z and S_1^e are positive definite and s_1 is a sum of variance terms), and each iteration should decrease the total expected cost. It guarantees the convergence.

The assumption that the current feedback is available to compute the current state estimate modifies both control and estimation formulas through the presence of Δ_{k+1}. In particular, Δ_{k+1} multiplies the terms of the error covariance related to the prior estimate. This shows how the covariance related to the prediction is reduced by using the current feedback. Another consequence of this assumption is that the covariance of the multiplicative feedback noise at time k is integrated in L_k through the matrix U_{k+1}.

6.3.4 Feedback Delay

We now assume that the feedback is:

$$y_k = Hx_{k-h} + \omega_k + \sum_{i=1}^{n_d} \delta_{i,k} D_i x_{k-h}, \tag{6.15}$$

where h is the delay expressed in number of sample times. This delay is assumed to be fixed and known. Therefore, it can be treated by augmenting the system and letting the controller observe only the most delayed state. This technique reduces Equation 6.15 to the non-delayed case corresponding to Equation 6.2.

Let A and B define the state-space representation of the system dynamics (Equation 6.1). The augmented matrices are:

$$\bar{A} = \begin{bmatrix} A & \dots & 0 & 0 \\ I_n & \dots & 0 & 0 \\ \vdots & \ddots & \vdots & \vdots \\ 0 & \dots & I_n & 0 \end{bmatrix}, \qquad \bar{B} = \begin{bmatrix} B \\ 0 \\ \vdots \\ 0 \end{bmatrix}$$

$$\bar{H} = \begin{bmatrix} 0 & 0 & \dots & H \end{bmatrix}.$$

The scaling factors C and D were augmented like B and H, respectively. The dynamics and cost of the augmented system are equivalent.

The presence of time delays is often at the origin of poor control performances in a wide range of applications. The method based on system augmentation for the control of stochastic systems has been successfully utilized in other contexts such as networked control systems (Nilsson et al., 1998; Hu and Zhu, 2003) or teleoperated systems (Sirouspour and Shahdi, 2006).

6.4 Application: Reaching Movement under Perturbation

6.4.1 Model

The proposed controller design is illustrated on a simple model of a point mass in the plane. The force exerted on the mass is controlled through a first order lag. In cartesian coordinates, the dynamics of the moving mass are:

$$\begin{aligned} \ddot{x} &= -k_v \dot{x} + F_x, \\ \ddot{y} &= -k_v \dot{y} + F_y, \\ \tau \dot{F}_x &= u_x + \alpha u_y - F_x, \\ \tau \dot{F}_y &= u_y + \alpha u_x - F_y, \end{aligned}$$

where the constant τ is set to 40 ms, the friction parameter k_v is set to 0.1 Nsm^{-1} and where the parameter α, set to 0.1, models some coupling between the two control actions.

The control action is computed to transfer the mass from $[x_0, y_0] = [0, 0]$ to a target $[x_N, y_N] = [0, 0.1]$ (the distances are in meters). The

external perturbation is modeled as an additive step input on F of amplitude $F_{\text{ext}} = [3, -3]$ N at time $t = 150$ ms. The feedback measurement is available only after a delay of 120 ms. The discrete time stochastic model results from Euler integration with discretization step equal to 10 ms. The state of the discrete system was augmented with the target location:

$$\begin{aligned}\mathbf{x}_k &= [x(k\delta)\ \ y(k\delta)\ \ \dot{x}(k\delta)\ \ \dot{y}(k\delta)\ \ F_x(k\delta)\ \ F_y(k\delta)\\ &\quad x_N\ \ y_N\ \ \dot{x}_N\ \ \dot{y}_N\ \ F_{x,N}\ \ F_{y,N}]^T,\end{aligned}$$

where the variables indexed by N represent the prescribed final state. The covariance matrices are $\Omega_\xi(5,5) = \Omega_\xi(6,6) = 0.001$, and $\Omega_\xi(i,j) = 0$ otherwise (i.e. the additive noise only affects the control input). The covariance of the feedback noise is

$$\Omega_\omega = \begin{bmatrix} 10^{-3} I_6 & \mathcal{O}_{6\times 6} \\ \mathcal{O}_{6\times 6} & 10^{-10} I_6 \end{bmatrix}.$$

The scaling factor C_i are chosen as follows:

$$C_1 = B \begin{bmatrix} \sigma & 0 \\ 0 & 0 \end{bmatrix}, \quad \text{and} \quad C_2 = B \begin{bmatrix} 0 & 0 \\ 0 & \sigma \end{bmatrix},$$

with $\sigma = 0.4$. Hence, the multiplicative noises affecting u_x and u_y have the same amplitude but are uncorrelated. The matrix H is the identity and the state dependent feedback noise was proportional to $D = 0.05H$ ($n_d = 1$).

In order to model a reaching phase during 400 ms followed by a stabilization phase during 300 ms, we choose a state weighting $Q_k = 0$ for $1 \leq k < 40$. For $k > 40$, the cost per step is:

$$\begin{aligned}\mathbf{x}_k^T Q_k \mathbf{x}_k = w_1 \parallel x(k\delta) - x_f \parallel^2 + w_2 \parallel y(k\delta) - y_f \parallel^2 \\ + w_3 \parallel \dot{x}(k\delta) - \dot{x}_f \parallel^2 + w_4 \parallel \dot{y}(k\delta) - \dot{y}_f \parallel^2 .\end{aligned}$$

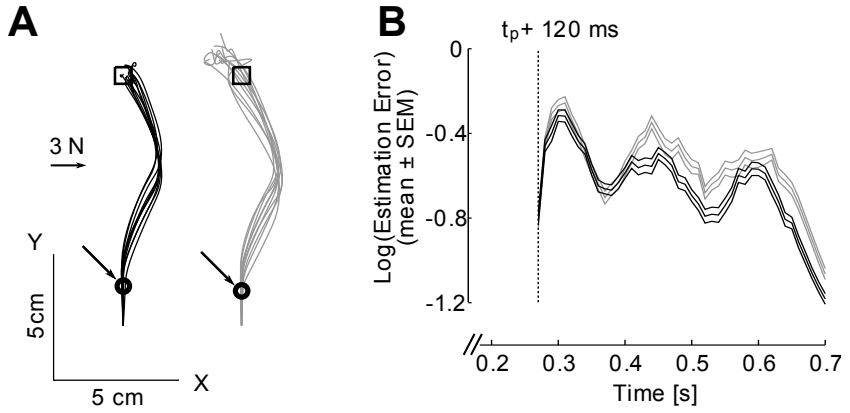


Figure 6.1: A: 2-Dimensional representation of 10 reaching movements computed in the filtering (black traces) and predictive cases (grey traces). The black dots are approximately the time of perturbation and the black squares represent the target. B: Evolution of the estimation error as a function of time computed with the two control algorithms. The estimation error is plotted from the time when the controller notices the deviation ($t_p + 120$ ms).

The weighting factors are $w_1 = w_2 = 1$ and $w_3 = w_4 = 10^{-3}$. The prescribed final velocity is zero in both directions. The control cost was $r(u_x^2 + u_y^2)$, with $r = 10^{-5}/(N-1)$.

6.4.2 Simulation Results

Figure 1 A shows 10 simulations of reaching movements in the filtering case (Figure 1 A, black), and in the predictive case (Figure 1 A, grey). Figure 1 B shows the logarithm of the norm of the estimation error as a function of time computed across 100 simulations with the same color code as in Figure 1 A. It can be seen that the error tends to be smaller in the filtering case. As a consequence, the resulting trajectories present less variability. The difference in estimation errors shown in Figure 1 B directly illustrates the benefits of using the filtering estimate.

For the two control algorithms, the recursions were stopped when the decrease in v_1 was inferior to 10^{-10}, and the forward recursion for the computation of the Kalman gains were initialized with $\Sigma_0^{\hat{x}} = \Sigma_0^x = 0$, and

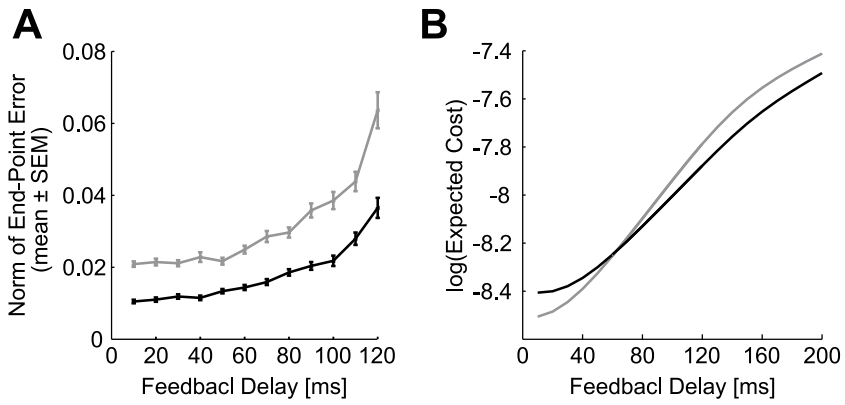


Figure 6.2: A: Evolution of the norm of the end-point error as a function of the feedback delay. Mean ± Standard Error were computed across 100 simulations for each value of the feedback delay. B: Total expected cost in the two control algorithms as a function of the feedback delay. The black and grey traces correspond to the filtering and predictive cases, respectively.

$\Sigma_0^e = \mathrm{diag}(10^{-8})$ (i.e. the initial state and estimates are static but there is a small random estimation error). It can be observed experimentally that the norm of the Kalman gains increases with the norm of the initial covariance matrices. This has an intuitive justification: if the initial state and estimated state are less certain, then the output feedback becomes the most reliable information and the controller should rely more heavily on this signal.

The performances of the full controller in the filtering case are further illustrated by the average end-point error induced by the feedback delay. Figure 2 A shows that the norm of the end-point error increases with the delay in the feedback loop both in predictive and filtering cases, but that the average error remains smaller in the filtering case (same color code as in Figure 1). The norms in Figure 2 B were computed on the final position and speed only (there was no penalty on the final forces). Finally, Figure 2 B shows that the total expected cost (v_1) is smaller in the filtering case for larger values of the feedback delay.

6.5 Conclusion

This paper extends the optimal control and state estimation problems for stochastic systems affected by multiplicative noise to the filtering case, assuming that the feedback signal is available to compute the current state estimate. The design of the control algorithm in the filtering case was motivated by the performance of the estimation process: the estimation error is smaller, which reduces the average end-point error. Our simulation results illustrate the advantage filtering, in order to limit the variability induced by time delays.

The control algorithm designed in this paper is potentially a relevant tool for modeling the control of movement. Indeed, the performance is good in the range of feedback delays observed in the sensorimotor system and assuming that the current feedback is used to compute the current state estimate is reasonable in the context of physiological motor control.

Chapter 7

Compensation for sensory feedback delays during motor adaptation

"Mathematics consists in proving the most obvious thing in the least obvious way."

G Polya.

Abstract. Sensory feedback delay is a potential source of instability and variability for the online control of movement. Thus, the central nervous system (CNS) makes predictions based on internal models to compensate for feedback delays. However, during motor learning and exposure to new environments, these predictions can be altered. Therefore, the CNS must have a distinct strategy to compensate for feedback delays. The present paper tests the hypothesis that in such situations, the CNS reduces control gains to preserve movement stability. This hypothesis was tested by asking subjects to hold a manipulandum in precision grip and perform single joint discrete arm rotations during short-term exposure to weightlessness (0 g), where the internal models of the limb dynamics must be updated. The subject performances from grip force adjustments indicated that the internal predictions were altered during the early exposure to the 0 g condition. Indeed, the relationship

between the grip force and the load force reflected a low modulation based on prediction. During this learning period, the movements were slower with asymmetric velocity profile and target undershooting. We used an optimal feedback controller with a feedback delay of 100 ms to investigate theoretically the change in movement kinematics when the internal prediction was altered. A reduction in control gains efficiently limited the increase in end-point variability following the introduction of a prediction noise in the model. The resulting simulated movements were in direct support to the hypothesis of reduction in control gains during the early exposure to a novel environment. These results suggest generalizing the optimal feedback control theory to the transient effects of motor adaptation, assuming that the control gains are modulated depending on the reliability of the internal prediction.

7.1 Introduction

The central nervous system (CNS) has two sources of information to estimate the current state of the body: a prediction based on internal models, which allows for the computation of a prior estimate from the corollary discharges of the motor commands (Kawato, 1999; Miall and Wolpert, 1996; Wolpert and Flanagan, 2001); and sensory feedback, which conveys information from the peripheral nervous system (e.g., vision, proprioception, etc). A promising hypothesis suggests that these sources are combined in a Bayesian integration process, in which each signal is given a relative importance proportional to its reliability (Kording and Wolpert, 2004; Vaziri et al., 2006). The resulting estimate is optimal in the sense of minimal estimation variance. However, there is a fundamental problem in using sensory feedback to monitor an online movement: the presence of time delays in the feedback loop causes instability (Mehta and Schaal, 2002; Miall et al., 1993). Nevertheless,

during motor adaptation, the internal prediction can be altered while the CNS acquires an internal model of the novel tool or limb dynamics (Wolpert et al., 2001), forcing the control strategy to rely on sensory feedback. Therefore, during the transient effects of learning, there must be a mechanism that compensates for uncertainty in the internal prediction despite significant delay in the sensory feedback signal.

In the present paper, we propose that impairment in the internal prediction is compensated for by decreasing the control gains to preserve movement stability. This was tested by asking human subjects to hold a manipulandum in precision grip and perform single joint point-to-point rotation in the vertical plane while transiently exposed to weightlessness. Gravity is known to play a central role in motor control (Bock, 1998; McIntyre et al., 1998), and experimental evidence suggests that 0 g is a singular condition to which adaptations observed at other gravity levels do not generalize (Mierau et al., 2008; White et al., 2008). Thus, the mechanism that compensates for uncertainty in the internal prediction was investigated during transient exposure to weightlessness, where the internal model of arm dynamics must be updated.

A clear reduction in control gain was evidenced by the changes in movement kinematics. The possibility that it arises from the uncertainty in the internal prediction was validated by subjects performances in grip force adjustments to self-induced variation of inertial loads, which typically reflects the quality of the internal prediction (Flanagan and Wing, 1993).

From a theoretical point-of-view, the reduction in control gain finds a direct interpretation in the context of optimal feedback control. Such controllers capture most properties of motor behavior, including flexibility and adaptability (Braun et al., 2009; Izawa et al., 2008; Izawa and Shadmehr, 2008; Liu and Todorov, 2007; Todorov and Jordan, 2002). In this context, a control gain reduction is achievable by decreasing the

cost of error in position and increasing the cost of motor commands. The simulated movements were quantitatively in direct support to our hypothesis of control gain reduction during the adaptation to the novel dynamics of the weightlessness condition. In addition, such mechanism is applicable to any situation of exposure to novel dynamics and can therefore be a general model for control strategies during motor learning and internal model acquisition.

7.2 Material and Methods

Subjects

Ten right-handed volunteers (four males and six females; aged 25-52 years) with no neurological disorders participated in the experiment. All subjects gave informed consent and complied with the medical requirements for parabolic flights. The medical board committee of the European Space Agency (ESA) and the French CPP (Comité pour la Protection des Personnes), responsible for all life science experiments performed in France, approved the experimental protocol.

Parabolic flights

Parabolic flight experiments were launched on board the 47^{th} and 48^{th} ESA parabolic flight campaigns. Each flight was composed of thirty parabolas organized in six groups of five parabolas separated by short pauses. Two subjects were evaluated per flight. In practice, all the subjects performed the task during at least 14 consecutive parabolas.

The parabolas can be decomposed into three phases. First, the aircraft accelerates upwards for ~ 20 s, and the gravity inside the aircraft is raised to 1.8 times terrestrial gravity (1.8 g). Second, the engine thrust is reduced to only compensate for the air drag, and the aircraft follows the parabolic trajectory of a free fall, during which time the gravity inside the aircraft is close to zero (0 g). This phase lasts ~ 22 s. At the end of the parabola, the power is turned up again and the acceleration redressing the trajectory generates another period of hypergravity (1.8 g).

Experimental procedures

Subjects were evaluated in a training session performed in normal Earth gravity several days before the flights. Subjects were seated in

front of three visual targets aligned vertically and separated by 18 cm. The center target was approximately in front of the subjects shoulders, so that when they pointed towards this target their arm was in the horizontal position.

At the beginning of the 0 g phase of each parabola (or each block in normal gravity), the subjects grasped a manipulandum of 250 g with a precision grip, i.e. between the thumb and the forefinger, and aligned the manipulandum with the center target. The grip aperture was 4.5 cm. A sequence of targets was generated and the subjects were asked to align the held load with the current target with arm-outstretched rotation of the shoulder. Movements up (from center to top) and down (from center to bottom) were randomly interweaved to avoid anticipatory movements. Subjects aligned their arm in front of the center target after each trial. Subjects were provided with continuous visual feedback throughout the movements in both normal and zero gravity conditions. In flight, the subjects performed the same task during the 0 g phase and subsequent 1.8 g phase of each parabola. Data collected during the hypergravity phases were published in a previous study (Crevecoeur et al., 2009b).

Data collection

The positions of infrared markers placed on the manipulandum and the shoulder were sampled at 200 Hz (Codamotion, Charnwoods Dynamics, Leicestershire, UK). During flight, the gravity inside the aircraft was sampled at 800 Hz with a three dimensional (3-D) accelerometer (ADXL330, Analog Devices). Gravity measurements were used to remove trials performed at the beginning or end of the 0 g phases, where gravity was sometimes unstable. Trials performed in flight were included in the data set when the average absolute gravity across the movement was < 0.1 g.

After visual inspection of all trials and validation based on gravity signals and the performance of the subjects (removal of movements triggered in the wrong direction), the total number of valid trials was 1172 in 0 g and 1655 in 1 g, equally distributed between up and down directions (range: 88-138 trials per subject in 0 g and 134-192 in 1 g). The number of valid trials represented 89% and 94% of the total number of trials collected in 0 g and 1 g, respectively.

The manipulandum was equipped with two force and torque sensors, one under each finger, which allowed us to measure the normal and tangential forces at the interface between the manipulandum and the fingers (40 mm diameter, Mini 40 F/T transducers, ATI Industrial Automation, NC, USA) with a resolution ≤ 0.02 N. Force signals were sampled at 800 Hz.

Data post-processing

The position and force signals were digitally low-pass filtered with a zero phase-lag Butterworth filter of the fourth order. The cut-off frequencies for the position and force signals were set at 20 Hz and 50 Hz, respectively. The segment joining the shoulder position and the held load was used to compute the elevation angle of the arm as a function of time [$\theta(t)$, Fig. 7.3A]. Angular velocity and acceleration were computed from numerical differentiation of the position signals. The movement duration was estimated based on linear approximation of the speed profiles at the threshold equal to 10% of its peak value computed for each individual trial. The crossing of the linear regressions with the horizontal axis were used as estimates of movements onset and end as illustrated in Fig. 7.3 (t_0 and t_f).

For some movements, the subjects made corrective adjustments. These trials were identified by looking at the acceleration profile: corrections for target overshooting (Fig. 7.3, left) or undershooting (Fig.

7.3, right) were detected when the angular acceleration presented a local maximum after or before the end of the movement, respectively (Fig. 7.3C). To avoid ambiguities in movement classification, overshoots were detected only for trials presenting no undershoot. The corrective displacement $\Delta\theta$ was defined as the displacement percentage from the time of the local maximum (t^*) to the movement end with respect to the total displacement from the movement onset to the movement end:

$$\Delta\theta = 100 \times \frac{\theta(t_f) - \theta(t^*)}{\theta(t_f) - \theta(t_0)}. \tag{7.1}$$

There was no overshoot recorded when the local maximum occurred after $t_f + 150$ ms, to avoid accounting for late corrections.

An important feature of pointing movements addressed in the present study is the velocity profile skewness. Based on the estimation of movement duration, the skewness is defined as the ratio between the durations of the acceleration and total movement. This variable is equal to the time from movement onset until peak velocity when the movement duration is normalized to 1.

The grip force (GF) was defined as the mean of the absolute force components normal to the two sensor surfaces. Load force (LF) was defined as the vertical component of the tangential constraints relative to the manipulandum reference frame (Fig. 7.3A). In zero gravity, the LF is proportional to the tangential acceleration, and the ratio between the LF and the acceleration equals the mass of the manipulandum.

The method for analyzing GF modulation is similar to that used previously (Crevecoeur et al., 2009a). However, in the present study we restricted the analysis to the positive LF peak, which allowed us to compare the performances of the subjects in the two gravitational conditions. For a single point-to-point movement, the absence of weight in 0 g provokes a negative LF peak (Fig. 7.3B) corresponding to negative acceleration. In normal gravity, the downward acceleration only

decreases the LF, and there is little to no GF modulation in phase with the downward acceleration (except for very fast movements, when the downward acceleration is greater than gravity). For this reason, a comparison of GF modulations in both gravitational contexts could only be based on the positive LF peaks.

Model

The system is composed of the arm, forearm, and hand. We computed the mass and length of each segment as ratios to the mass and size of each subject. These ratios were obtained from classical anthropometric tables (Winter, 1979). The manipulandum mass was added to the hand mass, and the hand length was divided in half to mimic the grasp posture. These parameters permitted us to evaluate the inertia of the whole system (arm-manipulandum) for each subject relative to the shoulder rotation axis.

In zero gravity, we assumed that two torques were acting on the system: the shoulder muscular torque (T) and a viscous friction torque proportional to the angular velocity. The viscous friction constant G_v was equal to $0.63 + 0.095T_M$ (the linear model was taken from (Nakano et al., 1999)), where T_M is the average joint torque across the movement. For the simulations, T_M was estimated a priori as a function of the system inertia and movement amplitude and duration:

$$T_M = 4I\frac{\theta(t_f)}{(t_f - t_0)^2}. \tag{7.2}$$

T_M corresponds to the average shoulder torque when the absolute angular acceleration is constant during the movement.

In addition to the mechanical equations, we introduced a simple physiological model to express T as a first order low-pass response to the motor command (control input to the system, u). The time constant τ for the muscular response to the control input was set to 40 ms

(Winter, 1979). Differential equations describing the dynamic system in continuous time are:

$$I\ddot{\theta} = T - G_v\dot{\theta}, \tag{7.3}$$

$$\dot{T} = \frac{1}{\tau}(u - T) \tag{7.4}$$

This system is linear, which allows us to design an optimal feedback controller in the presence of additive and signal-dependent noise sources.

Optimal Feedback Control

The CNS must be able to compensate for noise affecting the motor commands and sensory feedback. In addition to additive noise, multiplicative noise should also be considered in a model of the signal-dependent motor noise properties. Most importantly, the brain must also compensate for the presence of time delays in the sensory feedback loop. All of these features are expressed in the following state-space representation of the stochastic dynamics:

$$x_{k+1} = Ax_k + B(1 + \varepsilon_k)u_k + \xi_k, \tag{7.5}$$

$$y_k = x_{k-h} + \omega_k. \tag{7.6}$$

In Eqns. 7.5 and 7.6, x_k represents the vector of the state variable at time k, including the elevation angle, angular velocity, and shoulder torque; and h is the feedback delay expressed in number of sample times. The matrices A and B were obtained from the Euler integration scheme and from the system dynamics described in Eqns. 7.3 and 7.4.

The time step (δt) for the simulations of the discrete dynamics was equal to 10 ms and the feedback delay was set to 100 ms ($h = 10$). The prescribed final position, velocity, and shoulder torque were embedded in the state variable. Thus, the state vector had six dimensions: the three first entries are the state of the original system and the last three are the prescribed final state. The noise terms ξ_k and ω_k are multivariate Gaussian random variables with zero mean and covariance matrices

$\Omega_\xi = \text{diag}(0\,0\,\sigma^2\,0\,0\,0)$ and $\Omega_\omega = \sigma^2\text{diag}(1\,1\,1\,1\,1\,1)$. With these definitions, ξ_k affects only the control signal, whereas ω_k affects the entire state feedback, including the perception of the target location embedded in the state. The amplitude of the additive noise is $\sigma = 0.001$. The multiplicative noise ε_k is a Gaussian random variable with zero mean and variance equal to 0.04. The variance of the different noise sources is compatible with physiological data (Liu and Todorov, 2007).

The optimal feedback control theory postulates that motor commands sent to the limb will seek a maximum reward (i.e., successful attainment of the task objective) at minimal motor costs. The cost of the movement was assumed to depend on both the state and control at each time step through the following equation (recall that the control is a scalar quantity):

$$J_k = x_k^T Q_k x_k + r u_k^2. \tag{7.7}$$

The parameter r was used to penalize high control signals. The matrices Q_k permit us to express the constraints on the state variables related to the prescribed final state, representing the target. In practice, we defined a running period equal to $N_1\delta t$, corresponding to the movement execution, during which Q_k $(k = 1, 2, \ldots, N_1)$ were set to 0 (i.e., the system was free to move during the running perior). We also defined a stabilization period, $(N_2 - N_1)\delta t$, following the running time, during which time the cost matrices were defined such that:

$$x_k^T Q_k x_k = w_1 \left(\theta(k\delta t) - \theta_f\right)^2 + w_2 \dot{\theta}(k\delta t)^2, \quad k = N_1 + 1,\, N_1 + 2, \ldots, N_2. \tag{7.8}$$

The constraints in Eqn. 7.8 express that the system must stay close to the prescribed final position (θ_f), and the velocity during the stabilization period should remain close to 0.

The design of the optimal controller and state estimator in the presence of signal dependent noise and delayed state feedback is provided

in the supporting information. We assumed that the current feedback, being a delayed measurement of the state, was available to compute the current state estimate, which differed from the estimation algorithm considered by Todorov (2005). This assumption required adaptation of the recursion formulas for the optimal control and estimation processes.

In short, the system was driven by:

$$u_k = -L_k \hat{x}_k, \tag{7.9}$$

where L_k was the optimal gain applied to the current belief about the system state ($\hat{x}_k$). The system and estimation dynamics were reduced to the non-delayed case by system augmentation (see Chapter 5). Let $\mathbf{x}_k$ represent the augmented state containing the history of x_k until x_{k-h}. The current state estimate was updated in two steps by computing the prior belief about the state:

$$\mathbf{x}^p_{k+1} = A\hat{\mathbf{x}}_k + Bu_k + \eta_k, \tag{7.10}$$

where η_k was a multivariate Gaussian random variable representing the internal uncertainty related to the prediction based on the internal model. Then, the prior estimate was updated by a correction based on the feedback measurement (Kalman filter):

$$\hat{\mathbf{x}}_{k+1} = \mathbf{x}^p_{k+1} + K_{k+1}\left(y_{k+1} - \mathbf{x}^p_{k+1}\right). \tag{7.11}$$

Comparison between model and data

The system inertia for the simulations was set to the mean inertia evaluated for all individual subjects (0.568 Kgm^2). The end-point variance was computed from the angular position and velocity at the estimated final time. The final angular position was computed relative to the measured initial position for each individual trial. To estimate

the variance of a 2-D variable, we computed the area of the ellipsoid obtained by singular value decomposition of the covariance matrix. The same method was used to estimate the final time and end point variance on the simulations and experimental data (Fig. 7.3).

The control gains (L_k in Eqn. 7.9) depend on both Q_k and r through the recursion formulas used to compute L_k (Todorov (2005); see also the Chapter 5). Therefore, simulations with low control gains were obtained by decreasing w_1 and w_2 (the cost of error in position and velocity), and increasing r (the cost of effort). The details about the setting of the cost parameters and the noise amplitude changed across the simulations are provided in the section on the simulation results.

7.3 Results

Effect of Microgravity on the Grip Force Modulation

The Grip Force (GF) and the Load Force (LF) are illustrated in Fig. 7.3A and typical traces of a trial collected in 0 g are shown in Fig. 7.3B. The absolute ratio between GF and LF at the load force peaks was markedly increased in 0 g for all subjects and tended to decrease gradually across the parabolas (Fig. 7.2A). This could be mainly attributed to the fact that subjects initially applied static grip forces (GF_S in Fig. 7.3B) that were comparable to the levels measured under 1 g condition. The static grip force across subjects ranged between 2.5 N and 9.6 N in 1 g condition, and between 1.7 N and 13 N during the 4 first parabolas in 0 g condition. This value decreased towards about 50% of this level at the end of the exposure to 0 g: the average GF_S across the 4 last parabolas ranged between 0.8 N and 6 N. The decrease in GF_S was significant ($P < 0.01$, computed form linear regression of the subjects individual means versus the block number).

In order to address the quality of the internal prediction and its evolution, we computed the linear regressions between GF and LF at the times of load force peaks (t_M in Fig. 7.3B). The data were grouped in bins of three consecutive blocks to ensure that the regressions were computed on a sufficient number of trials. The relationship:

$$GF(t_M) = a_0 + a_1 LF(t_M), \tag{7.12}$$

was significant for all but one subject ($P < 0.05$, computed on the whole data set, data of up and down movement were pooled). However, the evolution of a_0 and a_1 across the bins of blocks revealed a change in strategy in the anticipatory grip force control. Fig. 7.2B shows the parameters of the regressions from the second bin, including the parabolas number 2, 3 and 4. The offset (a_0) was clearly elevated compared to the

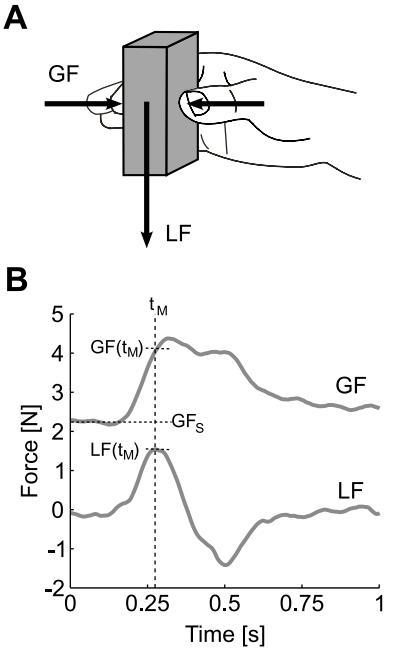


Figure 7.1: Analysis of the precision grip forces. A: Representation of the manipulandum held in precision grip between the thumb and the index finger. Black arrows are the grip force (GF, normal to the contact surfaces) and load force (LF, tangential to the contact surfaces). B: Example of GF and LF as a function of time for one selected trial. The vertical dashed line is the time of maximum LF (t_M). Panel B illustrates the static grip force (GF_S), measured prior to movement when the arm was stable. GF_S was measured as the average grip force during a time interval of 100 ms after target onset. The analysis of GF modulation focused on the value of GF measured at the time of LF peaks.

slope (a_1) for the regressions computed until the bin number 5.

Based on this result, we defined the early exposure time as the 7 first parabolas, during which the grip force is characterized by an elevated offset and a low-gain modulation (Fig. 7.2A and 7.2B, the bin number 5 contains the blocks number 5, 6 and 7). The change in strategy for grip force control is schematically illustrated in Fig. 7.2C. During the early exposure, the offset (a_0) tends to be elevated and the slope (a_1) reflects a low control gain based on prediction. This tendency changes with time and evolves towards lower offset and greater modulation based on prediction. This is compatible with the presence of noise and uncertainty affecting the internal prediction during the early exposure to weightlessness. Accordingly, the subsequent analysis of movement control mainly focuses on this period of learning (early exposure, 7 first parabolas).

Effect of 0 g on Movement Kinematics

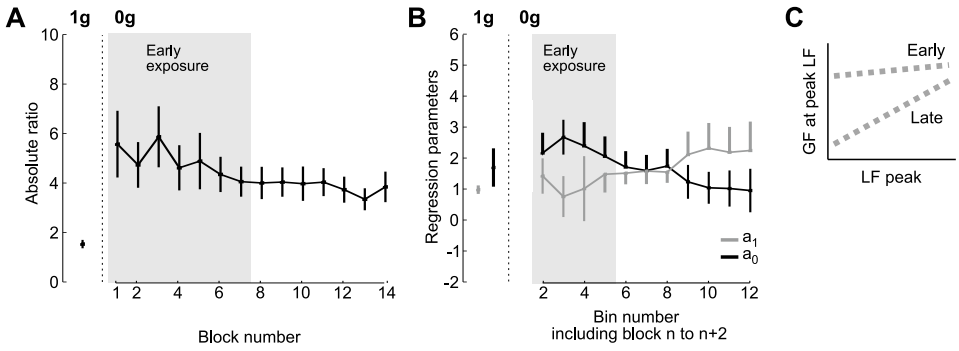


Figure 7.2: A: Absolute ratio between GF and LF measured at the load force peaks in 1 g and across the blocks in 0 g condition. B: time course of the regression parameters a_0 (black) and a_1 (grey). Due to an important variability at the beginning of exposure to 0 g, the linear regressions could not be computed on the data including the first bin. The early exposure time includes the blocks during which a_0 is greater than a_1 (grey rectangle). The error bars in panel A and B indicate the inter subject standard error of the mean. C: Schematic illustration of the change in strategy for anticipatory grip force adjustment between early and late exposure to 0 g.

A typical trial is shown in Fig. 7.3 with illustrations of the kinematics parameters analyzed hereafter (see the Materials and Methods section). During the early exposure period, the 2-D end-point variability measured on position and velocity signals was increased by a factor 1.9 relative to the variability observed in normal gravity (data of up and down movement pooled, averaged across subjects). There was a significant tendency for a decrease in end-point variability during the whole exposure but without reaching the variability measured in 1 g ($P < 0.05$, linear regression of subjects data versus the block number).

Compared to normal gravity, the movements were slower in microgravity and presented reduced peak acceleration, peak velocity and increased movement duration (Wilcoxon ranksum test computed on raw data, $P < 0.01$). This tendency is shown in Fig. 7.4A to 7.4D for one representative subject. In both directions, the velocity profiles di-

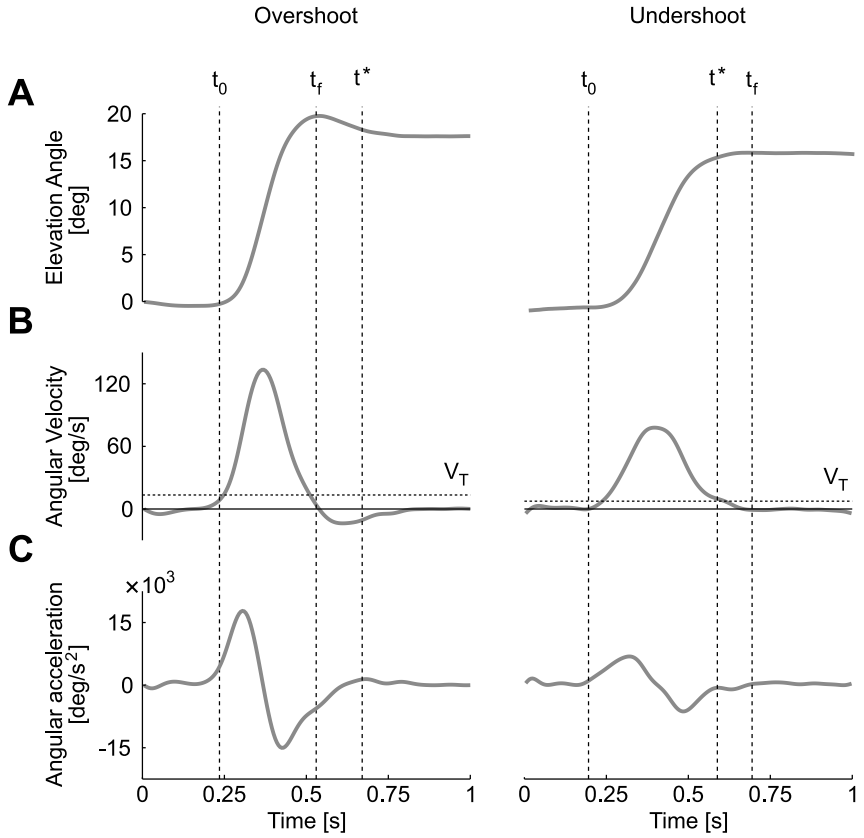


Figure 7.3: Plots of the elevation angle (A), angular velocity (B), and angular acceleration (C) as a function of time for two selected trials. Typical overshoot (left) and undershoot (right) profiles are illustrated. Panel B and C represent the velocity and acceleration profiles computed from numerical differentiation of the position signals. The speed was approximated by linear regressions at points where it exceeded or dropped below the threshold of 10% of its peak value (V_T horizontal dotted line, computed for each individual trial). The movement onset and end (t_0 and t_f) were estimated by the crossing the linear regressions and the horizontal axis (solid trace). The vertical dashed traces show the estimation of movement onset (t_0) and movement end (t_f) for these trials. The detection of overshoots and undershoots was based on the presence of local maxima in the acceleration profile (t^*).

verged early from the average trajectory performed in normal gravity (Fig. 7.4B, 7.4D). This reflects an important decrease in the initial shoulder torque, particularly for upward movements. Fig. 7.4B and

7.4D also illustrate that the velocity profiles in 0 g presented a significant skewness in both directions (t-test, raw data compared to 0.5, $P < 0.01$).

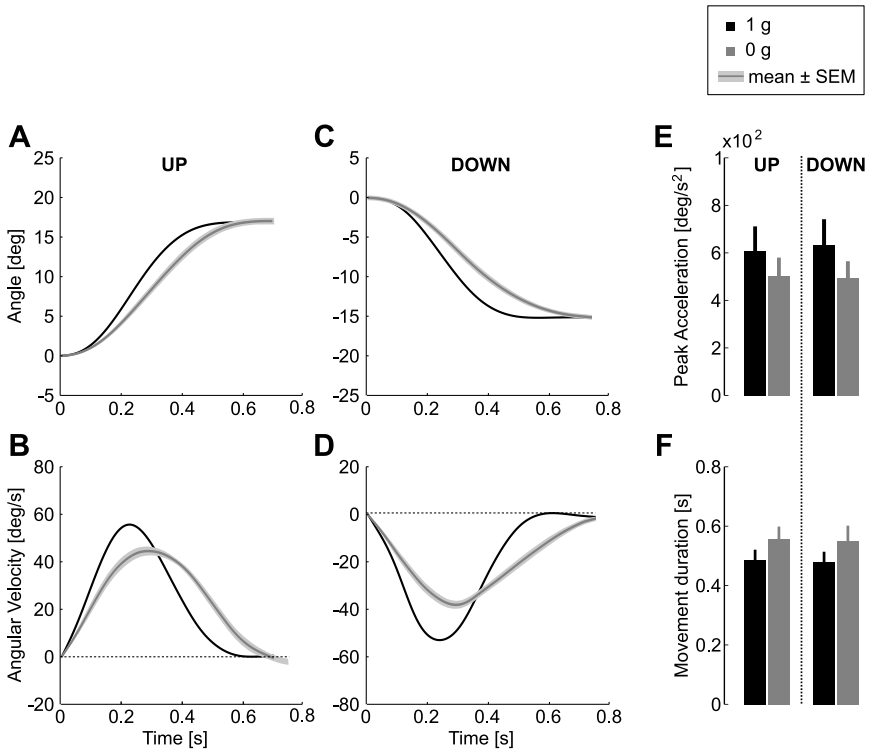


Figure 7.4: Average trajectories in 1 g (black) and during the early exposure to 0 g (grey) from one representative subject. Shaded areas represent the standard error of the mean, computed at each time step. Panels A and B show the elvation angle and the angular velocity as a function of time for upward movements. Panels C and D show the same plots for downward movements. Pooled subjects data, showing the effect of 0 g on the peak angular acceleration and movement duration are shown in panels E and F, respectively. In panels E and F, the vertical bar indicates the inter subject standard error of the mean.

Analysis of individual subjects revealed that, for upward movements, the decrease in peak angular acceleration and increase in movement duration in 0 g was significant for seven subjects (Wilcoxon ranksum test, $P < 0.05$). The same tendency was observed for one of the three re-

maining subjects, but did not reach the level of statistical significance ($P = 0.13$ and 0.16 for peak angular acceleration and movement duration, respectively). For the downward movements, the decrease in peak angular acceleration was significant for six subjects ($P < 0.01$). Two of the remaining four showed the same tendency, but did not reach statistical significance ($P = 0.15$ and 0.11 for these two subjects). In this direction, the increase in movement duration in 0 g was significant for seven subjects ($P < 0.01$), and two of the remaining three showed a similar tendency without reaching the level of significance (P = 0.12 and 0.11). The analysis of the peak velocity for individual subjects revealed a weaker effect than the peak angular acceleration and the movement duration. Subjects data are shown in Fig. 7.4E and 7.4F for the two latter kinematics variables for which the effect of 0 g was the strongest. There was no evidence for clear evolution of the kinematics parameters after the early exposure period although the parameters of the grip force modulations seemed to stabilize. The end-point variability was the only variable for which we could extract a significant trend across the blocks.

Analyses of the overshoots and undershoots of the subjects revealed an increased tendency to undershoot the target in 0 g in both movement directions, logically accompanied by a decrease in the tendency to overshoot the target (which was the dominant strategy in 1 g). The proportion of trials presenting overshoots or undershoots is shown in Table 7.1. This proportion was evaluated on the data from all blocks in order to estimate percentages on a sufficient number of trials. There was no evidence that the trials presenting undershoot profiles were not uniformly distributed across the blocks. The change in gravity did not significantly affect the over/undershoot amplitudes. The average $\Delta\theta$ for up and down movements was equal to 12.3%.

Table 7.1: Percentage of trials presenting an overshoot (OSH) or undershoot (USH) in the two gravitational conditions for up and down movements (averaged across subjects ± standard error).

	Movements Up		Movements Down	
	1 g	0 g	1 g	0 g
OSH	$63 \pm 5.7\%$	$41 \pm 5.5\%$	$64 \pm 6\%$	$49 \pm 7\%$
USH	$24 \pm 6.5\%$	$39 \pm 7.3\%$	$16 \pm 5.1\%$	$33 \pm 8.5\%$

Simulation Results

The results concerning the grip force modulation strongly indicate that the internal prediction was less reliable during the early exposure to microgravity. This supports the presence of a prediction noise in the context of Bayesian integration. A prediction noise was retained instead of a prediction bias. Indeed, if the subjects were using an internal model adapted to 1 g to control the movement in 0 g, the motor commands would aim at fighting against a force that is no longer acting on the limb. This would produce excessive shoulder torque and target overshooting for upward movements, which is in contradiction with our data. Regarding the noise parameters, the variances of the additive and multiplicative motor noises were kept constant across the simulations (ξ_k and ε_k in Materials and Methods, Eqn. 7.5). The exposure to 0 g may affect the sensory feedback, and proprioception in particular. However, the movements were visually guided, providing the subjects with reliable feedback on the limb position and velocity. In addition, increasing the covariance of the output feedback noise (ω_k, Eqn. 7.6) by a factor 100 produced an increase in end-point variability inferior to 5% relative to baseline, which could not account for the increase that we measured experimentally from subjects data. Thus the output feedback noise was also kept constant across the simulations. The detailed list of the pa-

rameters changed across the simulations can be found in Table 7.2.

Table 7.2: List of the parameters across the simulations. Simulations with decreased control gains were obtained by varying α. Parameters that do not appear in the Table below were kept constant in all simulations.

	Baseline	Low Gain
Ω_η	0	0.2×10^{-4}diag(1 1 1 0 0 0)
r	10^{-5}	$\alpha 10^{-5}$
w_1	1	$1/\alpha$
w_2	0.1	$0.1/\alpha$

The results of the simulations are shown in Fig. 7.5A and 7.5B. For each simulation, the running period was set to the subjects average movement duration measured in 1 g condition (480 ms) and the stabilization period was set to 500 ms (from 480 ms to 980 ms). The baseline trajectories (black) were obtained without prediction noise ($\Omega_\eta = 0$), corresponding to a movement executed with a very good internal model. The red trajectories were obtained after introducing the prediction noise ($\Omega_\eta \neq 0$) while keeping constant the cost of error and the cost of effort. The issue of movement stability in this situation is obvious. The blue trajectories, corresponding to our hypothesis of reduction in control gain, were obtained by decreasing the cost of errors in position and velocity (Q_k, Eqn. 7.7) and increasing the cost of motor commands (r, Eqn. 7.7) by a factor α. The kinematics parameters evaluated on the simulated trajectories continuously depended on α. Fig. 7.5C to 7.5E show the effect of α on the 2-D end-point variability, skewness, peak angular acceleration (PA), peak angular velocity (PV), movement duration (MD) and undershoot (US). The latter was estimated on the simulations as the percentage of angular displacement achieved at the end of the run-

ning time. For each value of α, the parameters were averaged across 500 simulations.

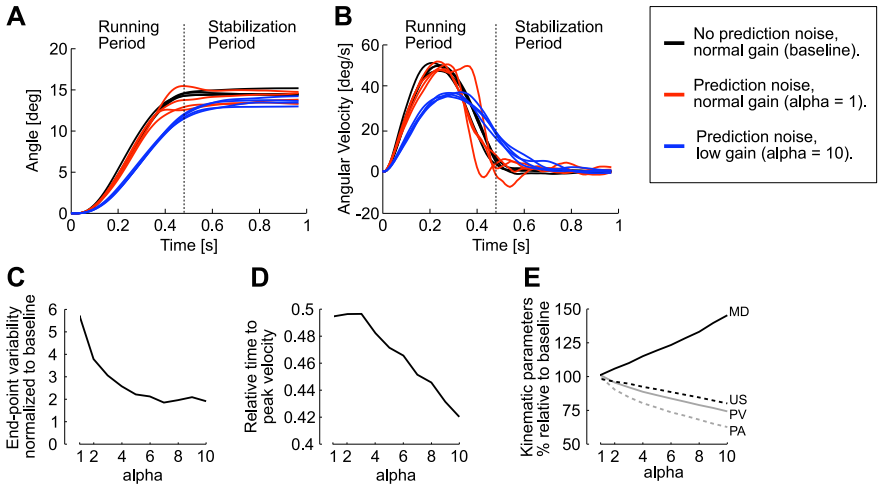


Figure 7.5: A: Angular displacement as a function of time for three simulation conditions; baseline (black), with prediction noise and normal control gain (red), with prediction noise and low control gain (blue). Four trajectories are represented for each simulation condition. B: Corresponding angular velocity as a function of time. C: Estimated 2-D end-point variability measured in the simulations as a function of α. Simulation variability was normalized to the end-point variability of the baseline simulation. D: Skewness in the velocity profiles of the simulated movements as a function of α. E: Kinematics parameters of simulated movements expressed as percentage relative to baseline. For each value of α, the kinematics parameters were estimated on 500 simulations.

Despite its simplicity and the fact that we only varied α for decreasing the control gain, the model achieves good quantitative predictions of the kinematics parameters that we observed experimentally. Fig. 7.6 show the average parameters after introducing the prediction noise with normal control gains (red squares), and with low control gains obtained with $\alpha = 5$ (blue diamond). With that value of α, the 2-D end-point variability was similar to the experimental results (Fig. 7.6A). Subjects end-point variability was normalized to their individual level of variability measured in 1 g condition. The red trajectories with normal gains achieve performances that are equal to the baseline on average, but the

end-point variability of these simulations allows us to reject that hypothesis (Fig. 7.6A). Fig. 7.6B shows that the percentage of change in the kinematics parameters relative to baseline is in agreement with the percentage of variation that we measured in 0 g relative to the 1 g data (considered as baseline). In addition, our model also captures the tendency for asymmetric velocity profiles, and a precise quantitative match is achievable with higher values of α (see Fig. 7.6C). Hence, simulations with low control gains capture quantitatively all features of the effect of 0 g on the movement kinematics.

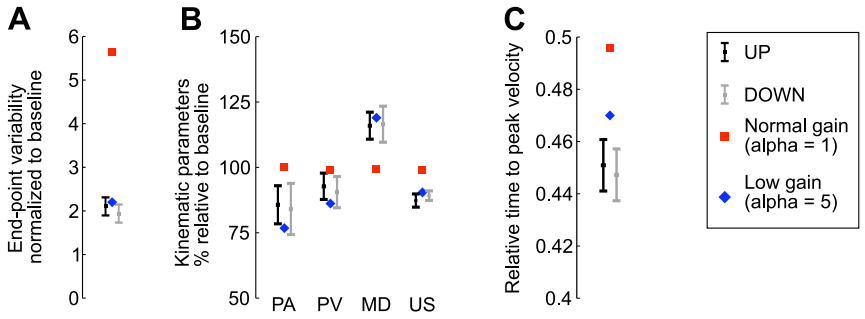


Figure 7.6: Comparison between experimental data and model for $\alpha = 1$ (red square) and $\alpha = 5$ (blue diamond). A: End-point variability. B: Percentage of change for the peak acceleration (PA), peak velocity (PV), movement duration (MD) and target undershooting (US). Simulation results and experimental data were normalized to baseline and to 1 g, respectively. C: Relative time to peak velocity. The vertical bars indicate the inter subject standard error of the mean.

7.4 Discussion

The brain must solve numerous complex problems to control movements, including the sensory feedback time delay that is compensated by internal forward models predicting the consequences of motor commands. However, during the transient effects of motor adaptation, these internal models may be inaccurate. Thus, the CNS must also compensate for feedback delays in this situation. This paper uses experimental and modeling approaches to test the hypothesis of reduction in control gains as compensatory mechanism to stabilize the movement during early exposure to a novel environment. The early exposure period was defined based on subjects performances in grip force modulation. During this period, the grip force control was characterized by an elevated offset and low modulation. This effect is compatible with the presence of noise affecting the internal prediction. The movements performed during the early exposure were slower, lasted longer, the velocity profile was asymmetric, and the subjects increased their tendency to undershoot the target. In addition, the end-point variability was increased in 0 g. From the theoretical point of view, the reduction in control gain after introduction of a prediction noise, implemented in the context of optimal feedback control, reproduced the changes in movement kinematics in quantitative agreement.

The experimental GF modulation results motivated our theoretical approach. The time course of compensation of the load force peaks enhanced the change in strategy for anticipatory grip force scaling. Clearly the modulation based on prediction is kept at a low level during the early exposure time. In the context of Bayesian integration theory (Kording and Wolpert, 2004), these results are consistent with the hypothesis that exposure to 0 g induces a prediction noise: the CNS should be less confident in the prediction and apply higher constant level of grip force

in order to compensate for the uncertainty. This is exactly what we implemented by introducing a prediction noise to simulate the internal prediction impairment. The weighting of the predicted and actual sensory feedbacks was through the Kalman filter, which accounted for the feedback delay.

Although we introduced a prediction noise, we know that forward models adapt in 0 g, and that an inertial load prediction stabilizes within four to five parabolas for nave subjects, in both rhythmic and discrete movements (Augurelle et al., 2003a; Crevecoeur et al., 2009a). This suggests that the internal prediction is processed in 0 g, but it may be less accurate, or considered as less reliable by the controller. The GF modulation results of the present study agree with our previous experimental results (Crevecoeur et al., 2009a): the GF_S decreased slowly, whereas the GF modulation correlated early with LF variations.

Besides the possible presence of a prediction noise, we should mention that the exposure to 0 g may have an effect on proprioceptive feedback and limb impedance (Fisk et al., 1993). However, as explained above, increasing the uncertainty related to sensory feedback could not explain our experimental results; hence we kept it constant in order to focus on the prediction noise. Our assumption that the sensory feedback did not change is of course a strong assumption that could be relaxed in further studies addressing this issue more specifically. Concerning the limb impedance, the adjustment of stiffness and damping parameters was proposed as a mechanism for stabilizing the movements and during motor adaptation to force fields (Burdet et al., 2001; Franklin et al., 2008). The control strategy proposed in the present study could be combined with the learning mechanism proposed by (Franklin et al., 2008): our approach considers the net motor command, which is independent from possible changes in the level of co-contraction at the shoulder joint. The reduction in control gains and the optimal setting

of limb impedance may be two cooperative mechanisms for maintaining the stability in both postural and movement control.

The results of the present study are consistent with previous results collected under a 0 g condition (Mechtcheriakov et al., 2002): peak acceleration and velocity were reduced and movement duration increased. In addition, the authors of this previous study showed that the movements realized without visual feedback presented greater errors. It was hypothesized that the slow down of movements in weightlessness and the use of visual feedback permitted to preserve the movement accuracy. However, Mechtcheriakov and colleagues failed to explain how the CNS could compensate for sensory feedback delays if the movement accuracy was ensured by the visual feedback. We solve this puzzle in the context of optimal feedback control and give a computational argument for the effect of 0 g on the control of movement.

In the context of parabolic flights, Papaxanthis et al. (2005) reported a similar increase in movement duration at the beginning of exposure to 0 g for self-paced movements, but this difference vanished after training. This result differs from our observations, as we observed no tendency to recover the movement duration of the Earth gravity condition. Our relative times to peak velocity also differed from their results. However, a common point is that the values for upward movements remained < 0.5 s, suggesting that the skewness also persisted across the parabolas. Differences in the protocols may account for the differing results; we restricted the movements to a single joint rotation, had no changes in pace, our target sequence was random, and our subjects performed the task in hypergravity after each exposure to 0 g, which could provoke washout between two consecutive parabolas. Despite these differences, our hypothesis of a reduction in control gains provides an explanation for the movement slow-down in 0 g observed by Papaxanthis et al. These authors suggested that the persistence of asymmetric velocity profiles in

0 g reflected a strategy based on the reproduction of movement kinematics observed under the normal gravity condition (Gentili et al., 2007). Indeed, such an adaptive mechanism has been observed in other experimental contexts (Papaxanthis et al., 2005; Lackner and Dizio, 1994; Shadmehr and Mussa-Ivaldi, 1994). The hypothesis that we propose in the present study provides an alternative explanation in the framework of optimal feedback control. Although asymmetric trajectories are suboptimal in 0 g, we suggest that they reflect an optimal strategy in the presence of feedback delay under the hypothesis of control gains reduction.

In addition, optimal control models based on the minimization of movement jerk (Flash and Hogan, 1985) or joint torque (Nakano et al., 1999) predict that optimal trajectories in 0 g should present symmetrical profiles in 0 g. Similarly, the optimal feedback controller with normal gain generates symmetrical trajectories on average. The presence of skewed velocity profiles in 0 g enhances the insufficiency of the models based on re-optimization to account for the transient effects of short exposure to novel dynamics such as the 0 g condition.

Artificial feedback delays alter the performances of subjects in a tracking task (Foulkes and Miall, 2000; Miall and Jackson, 2006): the tracking error is increased and corrective movements present a reduced frequency content of the motor responses to target jumps. Such a strategy could be explained by a reduction in control gain, producing stable corrective movements, although the resulting tracking is slow and sluggish (Miall et al., 1993). This effect is similar to the effect of 0 g observed in the present study. Our approach interprets this behavior in the context of flexible optimal feedback control with adaptive state and control-related costs. It generalizes the similarity between motor control and optimal feedback control to the transient effects of motor learning, during which the movements appear suboptimal.

A model based on optimal feedback control was a natural choice, given the behavioral and neurophysiological evidences for similarities with movement control (Scott, 2004; Shadmehr and Krakauer, 2008). This model allowed us to test the hypothesis of reduction in control gain, and its effect on movement kinematics, in a relevant and well-defined computational framework. In this framework, the reduction in control gain can be obtained by the setting of state and control costs, which has an intuitive justification. Decreasing the cost related to the state (Q_k, Eqn. 7.7) allows reduction of the movement accuracy without triggering abrupt corrective motor commands. Increasing the motor costs (r) penalizes high control gains, which slows down the movement and preserves the stability, despite a possible loss of movement accuracy following the decrease in the cost of position errors. In particular, we showed that adapting these parameters limited the increase in end-point variance, which is known to be a determining factor in motor control (Harris and Wolpert, 1998). In the presence of a feedback delay, complex movements with high requirements on task precision (Q_k elevated) and execution speed (r low) can only be achieved after long-term training and acquisition of a very good internal representation based on prediction.

Our approach also explains why good predictions are achieved before accurate or optimal trajectories in motor learning (Flanagan et al., 2003): in the presence of sensory feedback delays, restoring the control performances corresponding to the unperturbed condition is not possible before a good internal representation of the dynamics for online movement control is available. Thus, learning to predict before to control is a necessary condition for maintaining the movement stability in novel environments.

The optimal feedback control model makes a direct link between three fundamental neural processes: prediction, estimation and control. At a neural level, specific brain regions and their interaction support

each process: internal prediction and state estimation in the cerebellum (Miall et al., 1993; Miall and Reckess, 2002; Miall et al., 2007), integration of sensory feedback for online state estimation in the parietal cortex (Filimon et al., 2009; Wolpert et al., 1998a), and control in the premotor cortex, motor cortex and spinal interneurons (Todorov, 2000; Yanai et al., 2008). The present study shows theoretically that these processes are inseparable and that the introduction of a noise at a specific point potentially affects all stages of sensorimotor integration for feedback control. In this context, we show that the adaptation of the whole network to preserve the movement stability is achievable by a modulation of the requirements on movement precision and speed.

The attribution of costs and rewards to the intended motor actions could be performed by the basal ganglia as proposed by Mazzoni et al. (2007). Therefore, any input to the basal ganglia could modulate the control of movement in terms of motor performances. In particular, we suggest that the projections from the prefrontal cortex to the striatum (Parent and Hazrati, 1995) provide high-level and voluntary contribution to the modulation of costs and rewards, and stabilize the movement in a novel environment.

We did not find any evidence for stable adaptation to the 0 g condition after testing the subjects across 15 parabolas. This observation differs from adaptation to the hypergravity condition, where we observed a re-optimization of the motor plan within a similar exposure time to hypergravity (Crevecoeur et al., 2009b). As explained above, such adaptive scheme does not account for subjects behavior in 0 g condition. Conversely, the hypothesis of reduction in control gain does not apply to the hypergravity experiment. According to our assumptions, this difference is consistent with the fact the hypergravity has a limited effect on the state estimation and on predictive grip force control (Lackner and DiZio, 2009; Nowak et al., 2001b) contrarily to the effect of 0 g. We hypothe-

size that the good internal prediction and state estimation achieved in hypergravity allowed for the re-optimization.

The fact that the subjects also performed the task during the periods of hypergravity presumably hardened the adaptation and placed the subjects in a situation where the uncertainty at each entrance in 0 g was maximum. Hence, the question of arm movement adaptation after long-term exposure to 0 g remains open. Assuming that the CNS optimizes the motor commands in all contexts, we expect that the parameters of the GF modulation as a function of LF should recover performances similar to normal gravity, suggesting that an identical level of confidence in the internal prediction would be restored. We also expect that the velocity profiles become symmetrical with practice. Alternatively, if the CNS does not fully re-optimize after long-term exposure to 0 g, this would suggest that the presence of external constraints, and the interaction between the limb and environmental dynamics, are necessary conditions for the optimization of the motor commands.

Chapter 8

Conclusions and Future

"Either mathematics is too big for the human mind
or the human mind is more than a machine."

K Gödel.

8.1 Major Contributions

This work inserts in the general topic of motor adaptation applied to the particular context of changes in gravity. We have addressed the adaptation of sensorimotor coordination for the control of arm movements and precision grip forces in hyper and microgravity conditions. Motor prediction is efficiently processed in hypergravity and in microgravity. However, they are not equivalent: the prediction was very good in hypergravity whereas the strategy for anticipatory grip force modulation in 0 g revealed a greater uncertainty. The consequences are straightforward under the assumption that prediction, estimation and control operate in a single sensorimotor process: a good internal prediction in hypergravity provides the subjects with an accurate state estimate, allowing, in turn, high control performances and re-optimization of the motor commands. To the contrary, although forward models adapt to the 0 g condition, predictions that are less accurate, or considered so, potentially alter the

state estimate and, in turn, the control performances. Thus, in this situation, we suggest that the control strategy is adapted by decreasing the control gain to ensure the movement stability.

By analyzing the dynamics of prehension, we validated the hypothesis formulated relative to the control of movement under the assumption that the latter process depends on the quality of the internal models for online movement control. It gives a coherent framework for understanding the effect of changes in gravity on the control of movement. However, it does not explain why increasing the gravity by 1 g does not have the same effect as decreasing it by the same amount. In Chapter 4, we suggested that the anticipatory grip force modulation was based on a sensorimotor mapping that takes as input the perception of the object weight encoded during stationary holding, and that this variable is combined with an internal representation of the kinematics of the intended movement. We want to further extend this hypothesis and suggest that the weight of the limbs and/or the tools that we are interacting with, is used by the central planning process as a calibration signal for sensorimotor coordination. As a consequence, 1 g and 1.8 g become similar conditions. In both gravitational contexts, the CNS adjusts the motor gains according to the intensity of the sensory input, which depends on the actuators weight. To the contrary, 0 g is a singular environment in which no calibration signal is available for setting adequate forces and joint torques. This can be the reason why the confidence in the internal prediction is impaired with the consequences on the control performances analyzed above.

The present thesis generalizes the hypothesis that the gravitational forces drive the movements as formulated in the context of rhythmic movements (White et al., 2008). We recast the gravitational forces as a fundamental input for calibrating the sensorimotor loops and put forward the necessity of acquiring good internal models prior to achieving

good control performances. This necessary condition is implied by the natural tendency of the physiological systems to avoid instability and variability. Indeed, it would be extremely frustrating to achieve successful reaches to our cup of coffee every other attempt. Then, the optimality properties of movement control captured by optimal control theory are a natural consequence of the fact that biological systems, by nature, do not like purposeless expenditures.

8.2 Limitation of Optimal Feedback Control

Despite the complexity of the equations, the optimal control framework is very restrictive. The current methods allow one to compute optimal state feedback control in the case of linear dynamics. By considering single joint rotation and linear model for the joint-torque production, we could use the optimal feedback control theory in Chapter 7. But, in Chapter 3, the gravitational torque depends on the state in a non-linear way through the presence of the cosine. Thus, the computational model in this approach was based on the equivalent of a feed-forward solution computed for the deterministic case (i.e. without noise). The state feedback policy is then computed by linearizing the system around the optimal, unperturbed path. It is similar to the approach used in previous studies (Shadmehr and Mussa-Ivaldi, 1994; Nagengast et al., 2009), and corresponds to an affine control policy (Li and Todorov, 2007). This is different from the optimal state feedback control in several ways: it assumes the presence of the feedforward control strategy and assumes that the state feedback is capable to correct the deviation of the system from the corresponding optimal trajectory. Thus, we really benefit from the optimal feedback control theory (linear sensorimotor mapping) when it is applied to linear systems.

Another factor that limits the application of this model is related to the timing of movement planning and execution. Indeed, the time

horizon must be fixed, and the sequences of feedback gains and Kalman gains depend directly on the time horizon. This is a strong limitation since the simulations are computed based on the measurement of the movement duration from experimental data, and kept constant to avoid artificial changes in movement kinematics induced by a change in timing. However, there is no evidence that the CNS works with fixed internal estimates of movement time during movement control.

Finally, the treatment of sensorimotor delays by finite system augmentation is rather artificial. This technique is required for reducing the system to the non-delayed case. However, in the "real life", the delay is probably unknown and uncertain.

8.3 Open Questions and Perspectives

8.3.1 Long-term Adaptation

The context of parabolic flights is a unique opportunity to test the effect of changes in gravity relatively easily with a sufficiently large number of subjects. However, as discussed in the previous chapters, the exposure is limited (one parabolic flight is about 11 min 20 sec in weightlessness) and the alternation of hyper- and microgravity phases makes it a quite extreme environment. This has certainly an effect on the variability of the data collected and allows one to only assess the transient effects of short-term exposure. Hence, a full description of motor adaptation to a 0 g condition must inescapably be tested during long-term and stable exposure.

Several predictions emanate from this thesis under the assumption that the CNS can fully adapt to weightlessness. First, the effect of movement direction should disappear. This effect was enhanced in Chapter 3, and was interpreted in terms of a high level strategy based on the opposition or contribution of gravity relative to the movement stabilization.

The relative time to peak velocity (ADMD ratio) analyzed in Chapter 3 in the presence of gravity and in Chapter 7 under a 0 g condition will be a determinant indicator in the analysis of long term adaptation to 0 g. If motor prediction no longer depends on the movement direction and if the control gains are re-optimized, vertical movements performed in weightlessness should become similar to the horizontal movements performed on Earth. The velocity traces should present symmetric profiles.

Finally, as discussed in Chapter 4, the analysis of after-effects should indicate whether the adaptation to weightlessness replaces the internal models acquired on Earth or whether the internal models acquired in 0 g are built in a non-competitive fashion.

8.3.2 Optimal Control vs. Impedance Adjustments

Besides the ability to adapt the control strategies to novel environments, the CNS is also able to adapt the mechanical impedance of the limb in order to stabilize the movements (Burdet et al., 2001; Franklin et al., 2004). An algorithm for motor adaptation has also been proposed that is based on adaptive changes in arm impedance depending on whether a muscle at a joint was stretched or shortened (Franklin et al., 2003, 2008). The adaptive impedance is controlled by setting the level of muscular co-contraction at a the given joint with distinct gains on agonist and antagonist muscles in response to the unexpected muscle deformation. This powerful algorithm predicted well the motor adaptation to various force fields.

This proposed algorithm assumes that the mechanical properties of the limb are changed (damping and stiffness), in addition to the control strategy in itself. The models for adaptation proposed in the present work based on optimal control address the adaptation of the control strategy only. In this way, the two approaches could be combined in

a more general model for adaptive motor behavior when facing novel dynamics.

For instance, by standing with the arm in horizontal position, increasing gravity stretches the shoulder muscles that maintain the arm in horizontal position, leading to increased co-contraction at the shoulder joint, in addition to increased motor gain for moving the arm upwards. Our model for adaptation to hypergravity considers the net torque at the shoulder joint and is, therefore, independent from muscular co-contraction at this joint. Then, depending on the parameters of the learning schemes based on impedance adjustments, the progressive decrease in co-contraction for achieving stable performance could be similar to the changes in net shoulder motor command that we obtained from simulations under the assumption of optimal control.

The context of 0 g raises conflicting predictions regarding the adjustment of limb impedance as discussed in Chapter 7: during a vertical movement, a decrease in gravity would provoke unexpected deformations of the muscles. According to Franklin and colleagues (2008), the motor system should also increase the level of co-contraction for the subsequent trials. However, it has been proposed that the reduction in tonic input from the motoneuron in 0 g produces a reduction in limb impedance (Fisk et al., 1993). Again, the modeling approach used in the present work (Chapter 7) considers the net shoulder motor command, which is independent of the level of co-contraction at this joint.

Further studies should investigate the changes in limb impedance following exposure to changes in gravity in order to generalize the adaptive processes proposed based on optimal control, with the learning algorithms based on impedance adjustments. The optimal setting of limb stiffness and damping, coupled with the re-optimization or reduction of the control gains depending on the accuracy of the internal prediction may be two cooperative mechanisms for ensuring stability and perfor-

mance in any changed dynamical context.

8.3.3 Horizontal vs. Vertical

The perception of the vertical direction is neither fully allo- nor egocentric. Rather, the representation of the vertical axis for movement planning is multimodal (Le Seac'h and McIntyre, 2007). Thus the separation between vertical and horizontal movements is a rather theoretical approach and the distinction between the two directions is not strict within the CNS. In this respect, the change in gravity may alter horizontal movements although, in theory, there should be no effect on horizontal movement if the planning process could correctly dissociate between vertical and horizontal directions.

In light of the present work, the investigation of planning and control of horizontal movements in both hyper- and microgravity should reveal interesting properties on the distinction between vertical and horizontal directions. Knowing that the increase in gravity does not disrupt the perception of the vertical axis (Lackner and DiZio, 2009), we expect that horizontal movements are not affected by exposure to hypergravity. This prediction is also supported by the fact that the CNS can adjust the limb impedance in the unstable, or perturbed, direction (Burdet et al., 2001; Franklin et al., 2004). Therefore, we expect that pre-loading the arm in the vertical direction is well compensated and controlled, while the control strategy in the horizontal direction would remain unchanged.

In contrary, the 0 g condition has a direct impact on the perception of the vertical direction from its effect on various sensory modalities (e.g. otolith, graviceptors, proprioception, etc.[1]). In this context, we predict that horizontal movements are affected by exposure to weightlessness: if the reference frame defining the vertical axis is more affected, all control

[1] In 0 g, only the knowledge of the aircraft roof and floor defines the up and down, and it is surprisingly easy to sit on the roof and convince oneself that all the crew is upside down.

gains may be reduced as default strategy (as observed in Chapter 7) in order to prevent the movement from instability in all directions.

8.3.4 Gain Up vs. Gain Down

In saccadic adaptation, the target presented at a given eccentricity (θ_0) jumps either away ($\theta_0 + \Delta\theta$) or towards the center ($\theta_0 - \Delta\theta$) of the visual space during the saccade. After adaptation, the CNS triggers saccades whose amplitude are greater (gain-up) or smaller (gain-down) than the perceived amplitude corresponding to the stimulus location. In the gain-up condition, Ethier, Zee, and Shadmehr (2008) demonstrated that the adapted saccade for a target eccentricity of θ_0 could not be differentiated from a baseline saccade responding to a target eccentricity of $\theta_0 + \Delta\theta$ (without target jump). Thus the motor systems remaps the perceived location of the initial target. These previously cited authors also demonstrated that the adaptive mechanisms in the gain-down paradigm was distinct: adapted saccades for a target presented at θ_0 did not correspond to the baseline saccades for a target presented at $\theta_0 - \Delta\theta$. The distinction between the two adaptive processes was emphasized by using optimal feedback control model. The gain-down adaptation was matched and explained by an adaptation of internal estimation rather than a target remapping.

There is a fundamental difference between saccades and arm movements: there is no contribution of sensory feedback for the online state estimate during a saccade. However, there exists a strong similarity between saccadic adaptation and the adaptation analyzed in the present work: hypergravity adaptation was attributed to a re-optimization of the motor plan similar to a remapping, whereas microgravity seems to primarily affect the state estimation and required an adaptation of the internal representation of the arm dynamics. Turning back the the relationship between estimation and control (Equation 2.5), the motor

system responds to gain-up by adapting L_k (and $\bar{u}_k$ in Chapter 3, Equation 3.10), whereas the response to a gain-down condition consists in adapting $\hat{x}_k$ first.

This comparison suggests that gain-up and gain-down processes may be a general strategy in physiology. Indeed, natural phenomena such as the fatigue or the aging of muscular tissues make the gain-up adaptation quite a familiar process (i.e. the movement falls short despite similar recruitment). In such context, the default strategy may be to attribute the motor errors to the body and tune up the motor commands accordingly. In contrary, gain down being less natural, this situation may therefore be attributed to a change in the environment rather than the body. As a consequence, adaptation should primarily update the internal models for achieving accurate predictions and state estimation prior to recover good control performances.

A straightforward line of research for investigating this issue would be to analyze human behavior at gravity levels between 0 and 1 g. One can expect that the behavior will correspond to a re-optimization given that the residual gravity will still produce an input to the sensorimotor loops. However, the gain down hypothesis suggests that the reduction in prediction-based control gain should be effective at any gravity level that is smaller than the Earth gravity. It will be possible to investigate this issue in a near future. Indeed, parabolic flights generating such intermediate gravity levels, corresponding to Mars ($\sim 0.37\ g$) or Moon gravity ($\sim 0.16\ g$), are now qualified and will be organized by the European Space Agency soon.

8.4 Concluding word

A detailed investigation of specific movement properties, kinematics and dynamics is usually realized in order to identify what mechanism underlies a particular feature. However, the most impressive conclusion that

could be drawn from this work, and from many others, is the extremely flexible ability of motor systems to adapt to novel conditions and environments. Learning complex tools is already impressive, similarly to the learning of very complex movements (the engineers are still working on the reach-for-a-cup, but humans can, for instance, play the piano with eyes closed). These considerations show to which extent the control strategies developed by the brain are unbeatable. Indeed, by exploring the world and space, humans have placed themselves in situations where probably the most fundamental property of the environment, namely the gravity, is changed. However, we are still able to adapt and efficiently control our movements in these situations.

Appendix A

Mathematical background for control theory

"Go down deep enough into anything
and you will find mathematics."
D Schlicter.

A.1 Introduction

The present chapter proposes a summary of fundamental results in control theory utilized in the modeling approach of the present work. It aims at a rigorous contextualization of the mathematical tools, but it cannot be exhaustive. The chapter starts with a general definition of a control problem for deterministic systems in continuous time. We present the necessary and sufficient condition for the controllability of linear systems. Then, we derive the Pontryagin maximum principle for optimal control and finally address the problem of the stability of systems subject to time delays. This theory provides a good starting point to control dynamical systems, but the real world is infinitely more complex than mathematics can express and the information that we can get from measurements is uncertain. Therefore, a real controller must set up a control strategy that should be able to compensate for external perturbations and face uncertainty. To express this in mathematical words,

we define the Brownian motion that models the (apparently) random motion and derive the formulation of stochastic differential equations. Then, we present the optimal feedback control algorithms for a class of stochastic systems. This chapter ends with some remarks on the limitations of the optimal feedback control theory used as a model in the context of sensorimotor coordination.

A.2 Deterministic Systems, Continuous Time

Let $x(t) \in \mathbb{R}^n$ be the vector of state variables and $u(t) \in \mathbb{R}^m$ be the control input at a given time t. The evolution of the state variables as a function of time depends on the state and on the control through the following equation:

$$\dot{x} = f(x, u), \tag{A.1}$$

where $f : \mathbb{R}^n \times \mathbb{R}^m \to \mathbb{R}^n$ represents the dynamics of the system. The trajectory of the system is the evolution of the state variables as a function of time for a given control input u and initial condition x_0:

$$x(t) = x_0 + \int_0^t f(x, u) d\tau. \tag{A.2}$$

Equation A.2 is implicit and cannot be used as it is. However, finding the trajectories of Equation A.1 can be expressed as finding a function that is a fix point of the application $A(y) = x_0 + \int f(y, u)$. It can be demonstrated that such fix point exists and is unique, provided f is Lipschitz-continuous.

The general control problem is the following: given an initial position, x_0, and a target set $S \subset \mathbb{R}^n$, find a control function $u(t) : [0, t_f] \to \mathcal{U} \subset R^m$ such that $t_f < \infty$, $x(t) \in \mathcal{X} \subset \mathbb{R}^n$, $0 \leq t \leq t_f$, and $x(t_f) \in S$. In other words, the control problem is to steer the system from x_0 to S in finite time within the constraints on the state and control: $(x(t), u(t)) \in (\mathcal{X} \times \mathcal{U})$ for $0 \leq t \leq t_f$.

A.2.1 Linear Systems

This section considers the case where f is a linear function. This can be expressed as follows:

$$\dot{x} = Ax + Bu, \tag{A.3}$$

where $A \in \mathbb{R}^{n\times n}$ and $B \in \mathbb{R}^{n\times m}$. We introduce the matrix exponentials in order to compute the solution of A.3.

Definition. *The matrix exponential e^{tA} is defined as*

$$e^{tA} = \sum_{k=0}^{+\infty} \frac{t^k A^k}{k!}. \tag{A.4}$$

One can demonstrate that $X(t) = e^{tA}$ is the unique solution of the matrix differential equation:

$$\dot{X}(t) = AX(t), \tag{A.5}$$

$$X(0) = I. \tag{A.6}$$

Observed that $X^{-1}(t) = X(-t)$. The matrix exponentials permit us to compute the general solutions as stated by the following theorem.

Theorem. *The unique solution of the ordinary differential equation*

$$\dot{x}(t) = Ax(t) + g(t), \tag{A.7}$$

$$x(0) = x_0 \tag{A.8}$$

is given by

$$x(t) = X(t)x_0 + X(t)\int_0^t X^{-1}(\tau)g(\tau)d\tau, \tag{A.9}$$

with $X(t) = e^{tA}$.

Note that this theorem does not assume a particular form for the dependency of f on the control input, represented by $g(t)$. Only linearity in the state is required, provided that $g(t)$ is integrable.

With A.9, the system A.3 is said to be totally controllable if for any initial and final conditions, x_0 and x_f, there exists some $t_f < \infty$ and some integrable control function $u(t)$ such that:

$$x_f = e^{t_f A}\left(x_0 + \int_0^{t_f} e^{-\tau A} B u(\tau) d\tau\right). \tag{A.10}$$

The equation A.10 is utilized to demonstrate the following sufficient and necessary condition for the controllability of linear systems. A proof can be found in Terrell (1999).

Theorem. *The system A.3 is totally controllable if and only if the controllability matrix* $C = [B \quad AB \dots A^{n-1}B]$ *is full rank.*

The controllability of a linear systems can be easily checked with the previous condition. Note that it does not take into account the possible constraints on the trajectory and on the control function. For non linear systems, the controllability of the linearized system is sufficient to ensure local controllability. The contrary is not true. The local controllability condition for the non linear systems depends on the span of the iterated Lie brackets (Coron, 2007).

A.2.2 Optimal Control

In this section, we are interested in solving the control problem with a control function that minimizes a cost defined along the trajectory. The general formulation is:

$$\min \quad J(u) = g\left(x(t_f)\right) + \int_0^{t_f} L(x,u)dt, \tag{A.11}$$

$$\text{s.t.} \quad x(0) - x_0 = 0, \tag{A.12}$$

$$\dot{x} - f(x,u) = 0. \tag{A.13}$$

With the precedent formulation, the requirements on the final state are expressed in the cost with the term $g\left(x(t_f)\right)$. The constraints of the optimization problem ensures the system starts from the given initial

position (A.14), and that the trajectory follows the system dynamics (A.15). A solution to the optimal control problem is given by the Pontryagin's maximum principle. The latter principle can be derived from the calculus of variations (Bryson and Ho, 1975), or from the Hamilton-Jacobi-Bellman equation (HJB). We present the derivation from the HJB equation as it will play a central role in the derivation of optimal control policy for stochastic systems. Its basic principle is that if the trajectory is optimal from $t^* > 0$ until t_f, then one should only solve the problem from 0 to t^*.

We consider a discrete time formulation of the optimal control problem with time step h and Euler integration scheme. At each time step $t_k = kh$, the cost-to-go J_k (i.e. the cost of the remaining trajectory) equals the local minimum of A.11, plus the cost-to-go from $(k+1)h$ until t_f. It yields the following backward recursion:

$$J_k(x) = \min_u \Big\{ hL(x,u) + J_{k+1}(x + hf(x,u)) \Big\}. \tag{A.14}$$

The dynamic programming starts at $t_f = Nh$ by $J_N(x) = g(x)$ and iterates backwards until $t_0 = 0$. Replacing the k index by a dependency on time, J becomes:

$$J(x,t_k) = \min_u \Big\{ hL(x,u) + J_{k+1}(x + hf(x,u), t_k + h) \Big\}. \tag{A.15}$$

Assuming that J is differentiable with respect to x and t, the first order Taylor expansion of A.15 is:

$$J(x,t) \quad = \quad \min_u \Big\{ hL(x,u) + J(x,t) + h\frac{\partial J}{\partial x} f(x,u) + h\frac{\partial J}{\partial t} + O(h^2) \Big\}, \tag{A.16}$$

or, as $h \to 0$, the HJB equation:

$$-\frac{\partial J}{\partial t} = \min_u \Big\{ L(x,u) + \frac{\partial J}{\partial x} f(x,u) \Big\}. \tag{A.17}$$

Equation A.17 provides an optimal feedback control policy by computing $u^*(x,t)$ that minimizes the right hand side. Introducing the Hamiltonian

function:

$$H(x, \lambda, u) = L(x, u) + \lambda^T f(x, u), \tag{A.18}$$

with $\lambda \in R^n$, equation A.17 becomes:

$$-\frac{\partial J}{\partial t} = \min_u H(x, \nabla J, u), \tag{A.19}$$

and the optimal control function can be derived as follows:

$$u^*(x, \lambda) = \arg\min_u H(x, \lambda, u). \tag{A.20}$$

From A.19, it appears that the optimal control function depends on the gradient of J, and not on J itself. This motivated the introduction of the adjoint variables, $\lambda^T = \nabla_x J$, in the Hamiltonian function to compute u^*.

The adjoint variables are computed by differentiation of the HJB equation with respect to x. From A.19 and the definition of λ, we get the following results:

$$-\frac{\partial \nabla_x J^T}{\partial t} = \frac{\partial H}{\partial x} + f(x, u^*)^T \nabla_x^2 J. \tag{A.21}$$

Knowing that

$$\frac{d}{dt}\nabla_x J = \frac{\partial \nabla_x J^T}{\partial t} + f(x, u^*)^T \nabla_x^2 J, \tag{A.22}$$

we finally obtain:

$$-\dot{\lambda}(t) = \nabla_x H(x, \lambda, u^*). \tag{A.23}$$

The terminal condition on λ is obtained similarly by differentiating $J(x, t_f)$ with respect to x:

$$\lambda(t_f) = \nabla_x g(x(t_f)). \tag{A.24}$$

The derivation is summarized in the following theorem, which solves a maximization problem for convention.

Theorem (Pontryagin Maximum Principle). *Assume that u^* is the solution of the optimal control problem and x is the corresponding trajectory. Then, there exists a function $\lambda : [0, t_f] \to \mathbb{R}^n, \quad t \to \lambda(t)$ such that:*

$$\dot{x} = \nabla_\lambda H(x, \lambda, u^*), \tag{A.25}$$

$$\dot{\lambda} = -\nabla_x H(x, \lambda, u^*), \tag{A.26}$$

$$\lambda(t_f) = \nabla_x g(x(t_f)) \tag{A.27}$$

$$\text{and } H(x, \lambda, u^*) = \max_u H(x, \lambda, u). \tag{A.28}$$

In addition, the mapping $t \mapsto H(x(t), \lambda(t), u^*(t))$ is constant.

Given the similarity between λ and x relative to the Hamiltonian, the adjoint variables λ are often called the co-state. For numerical solutions of the optimal control problem, the Pontryagin Maximum Principle can be used to formulate a boundary value problem with initial conditions on x, terminal conditions on λ and state dynamics for $(x,\ \lambda)$ given by the theorem. Alternatively, one can discretize the optimal control problem and transform it into a non-linear optimization problem (non-linear in the cost and in the constraints). This constitutes the direct approach utilized in Crevecoeur et al. (2009b). It is possible to discretize the control only, or the state and control simustaneously. The discretization of the state and control leads to the direct multiple shooting algorithm (Diehl et al., 2006, pp. 65-93). When the final state is prescribed ($x(t_f) = x_f$), the discretized control and state yields the following non-linear optimization problem:

$$\min_{u_i, i=0,\ldots n} \quad \sum_{i=0}^{n} L(x_i, u_i), \tag{A.29}$$

$$\text{s.t.} \quad x_0 - x(t_0) = 0, \tag{A.30}$$

$$x_f - x(t_f) = 0, \tag{A.31}$$

$$x_{i+1} - \varphi(x_i, u_i) = 0, \tag{A.32}$$

where

$$\varphi(x_i, u_i) = x_i + \int_{t_i}^{t_{i+1}} f(x_i, u_i)dt. \tag{A.33}$$

In the preceeding formulation, x_i is a guess about the state at every node of the discretized time interval $[0, t_f]$. The cost is the sum of the cost function evaluated at each point of the discretized time span. The constraints ensure that the initial and terminal condition are respected (x_0 and x_f prescribed), and the continuity of the state at each discretized point is ensured by A.33.

A.2.3 Delayed Systems

In many applications, the physical constraints on the transport of a state or control component induce time delays in the system dynamics. A typical example is the neural control of movement, where the time for biological signal conduction delays the control signal and the sensory feedback. The presence of delays has dramatic consequences for the stability of the system. Let us recall the definition of stability for a general system without delay.

Definition. *The system $\dot{x} = Ax$ is stable if for every $\epsilon > 0$, there exists a $\delta > 0$ such that if $\| x_0 \| < \delta$, then $\| x(t) \| < \epsilon$, $\forall t \geq 0$.*

It is well known that the unforced system (i.e. with $u \equiv 0$) is stable if and only if all of the eigenvalues of A have negative real parts. This criterion is no longer applicable for time delay system. The Laplace transform of $x(t-h)$ is $X(s)e^{-hs}$ and the corresponding transfer function has infinitely many poles. Therefore, the stability depends on whether the right-most pole in the complex plane has negative real part, which can be difficult to check. We present another approach for the stability of delayed systems based Lyapunov functionals and linear maxtrix inequalities (LMI).

Let us consider the following system:

$$\dot{x}(t) = A_0 x(t) + \sum_{j=1}^{m} A_j x(t-h_j) + Bu(t), \tag{A.34}$$

$$x(\tau) = \phi(\tau) \in C([-\bar{h}, 0]), \quad -h \leq \tau \leq 0. \tag{A.35}$$

The initial condition is now the function ϕ, defined between $-\bar{h}$ and 0 ($\bar{h} = \max_j\{h_j\}$). A common choice for the space of initial functions $C([-\bar{h}, 0])$ is the set of continuous functions mapping $[-\bar{h}, 0]$ into $\mathbb{R}^n$ with the norm of the supremum. The definition of stability for delayed systems is identical except that $\| x_0 \|$ should be replaced by $\| \phi(.) \|_\infty$. The following theorem provides the most general delay-independent sufficient condition for stability. A proof can be found in Boukas and Liu (2002), where many more conditions for stability of time-delay systems can be found.

Theorem. *If there exists a set of symmetric positive definite matrices $P > 0$ and $Q_i > 0$, $i = 1, 2, \ldots, m$, such that the following LMI holds:*

$$\Theta = \begin{pmatrix} A_0^T P + P A_0 + \sum_j Q_j & PA_1 & \ldots & PA_m \\ A_1^T P & -Q_1 & & \\ \vdots & & \ddots & \\ A_m^T P & & & -Q_m \end{pmatrix} \prec 0, \tag{A.36}$$

then the unforced delayed system is stable.

The previous theorem provides a sufficient condition that ensures stability for any delay $\bar{h}$. It is therefore a very conservative condition whose improvement has mobilized much of the research efforts in this area over the last years. Improvements are obtained typically by considering more general Lyapunov functionals or by derivation of delay-

dependent conditions (Fridman, 2001; Boukas and Liu, 2002; Fridman and Shaked, 2003; Richard, 2003).

This introduction on the stability of delayed systems allows us to address the following issue related to state feedback control for such systems, given the importance of state feedback control models in sensorimotor control. The following theorem shows that for a given delayed system, the set of stabilizing state feedback gains is bounded, which renders impossible the application of arbitrarily high feedback gains in order to move all eigenvalues (λ) in the left open half complex plane, as it is possible for non-delayed systems. the proof is given by Michiels et al. (2002).

Theorem. *Suppose that a feedback* $u = K^T x$ *asymptotically stabilizes the system* $\dot{x} = Ax + Bu(t - \tau)$ *for* $\tau \in [0, r]$ *with* $r > 0$. *Then, there exist constants* $\gamma, \delta > 0$ *independent of* K *such that* $\| K \| \leq \gamma$ *and, for each* $\tau \in [0, r]$, $\inf_K \sup \mathcal{R}(\lambda) \geq -\delta$.

A.3 Stochastic Dynamics, Discrete Time

The introduction of stochastic processes in the systems dynamics suggests the existence of random motion. An example of such a motion is the Brownian motion, also called Wiener process or diffusion process. The last appellation recalls that this model for random motion was constructed to describe the diffusion of an ink drop in a glass of water. Another construction based on random walk is presented hereafter.

A.3.1 Random Motion

Consider a particle located on the origin of a one-dimensional axis at time 0. At each time step, the particle is moved either forward or backward depending on the outcome of the toss of a coin. The position of

the particle after n tosses is:

$$X(n) = \sum_{k=1}^{n} Y_i, \tag{A.37}$$

where Y_i is a random variable with the set of events $\Omega = \{-1, 1\}$ and probabilities $P = \{\frac{1}{2}, \frac{1}{2}\}$. From the central limit theorem, as $n \to +\infty$, $X(n)$ tends to a Gaussian random variable of mean and variance equal to 0 and n, respectively, noted as $N(0, n)$. By setting the size of the step equal to $\sqrt{\alpha}$ and repeating the experiment every α interval of time, we obtain that $X(n\alpha)$ tends to $N(0, n\alpha)$, or as $\alpha \to 0$, that $X(t) \sim N(0, t)$. Given that the tosses are independent, knowing $X(t_0)$, we have that $X(t_0 + t_1) \sim N(X(t_0), t_1)$. The previous construction yields the following definition of a Brownian motion. In the sequel, the property that something occurs *almost surely* (a.s.) is linked to the measure theory underlying the probability theory, which we do not address here. This concepts has a direct translation in the present context: it should be understood as "with probability 1".

Definition. *$W(.)$ is a Brownian motion if the following holds:*

1. *$W(0) = 0$ a.s. (initial condition),*
2. *$W(t_1) - W(t_0)$ is $N(0, t_1 - t_0)$ (stationary increments),*
3. *for any sequence $0 = t_0 < t_1 < \ldots < t_n \leq T$, the random variables $X_i = W(t_i) - W(t_{i-1}), \quad i = 1, \ldots, n,$ are independent (independent increments).*

It can be proved that the Brownian motion defined above exists, is almost surely continuous and belongs to $L^2([0, T])$ (the set of square integrable functions defined between 0 and $T < \infty$). Consequently, an intuitive definition of the stochastic dynamics of a Brownian motion is

$$\dot{W}(t) = \xi(t), \tag{A.38}$$

where $\xi(t)$ is called a white noise. Unfortunately, the time derivative of $W(t)$, almost surely, does not exist. A proof if this statement can be found in Mandelbrot and Van Ness (1968).

As a consequence, a well-defined formulation of a stochastic differential equation is the following:

$$dX(t) = F(X, u)dt + G(X, u)dW, \tag{A.39}$$

where the differential of the Brownian Motion (dW instead of $\dot{W}$) represents the white noise. The formulation of the stochastic dynamics in discrete time is straightforward:

$$x_{k+1} = M(x_k, u_k) + N(x_k, u_k)\xi_k, \tag{A.40}$$

where ξ_k is a sequence of Gaussian random variable, independent and identically distributed with 0 mean and variance depending on the size of the discretization step.

A.3.2 Optimal Control

This section gives a solution to the optimal control problem for a class of linear stochastic systems with additive noise represented by the following equations:

$$x_{k+1} = Ax_k + Bu_k + \xi_k, \tag{A.41}$$

$$y_k = Hx_k + \omega_k. \tag{A.42}$$

The matrices A and B define the system dynamics and H is the observability matrix, describing the information that the controller gets from the state feedback. The noise is introduced in the system dynamics and in the output feedback through ξ_k and ω_k, which are multivariate Gaussian random variables with 0 mean and covariance matrices Ω_ξ and Ω_ω,

rspectively. The cost per step is:

$$J_k = x_k^T Q_k x_k + u_k^T R u_k, \quad k = 1, \ldots, N. \tag{A.43}$$

The matrices Q_k are positive semidefinite and R is positive definite. The time horizon is assumed to be finite and equal to N sample times. The optimal control problem is to minimize the total expected cost obtained by summing J_k along a sample path.

We shall first ignore A.42 for the derivation of the optimal control policy, which corresponds to the assumption that the controller knows the exact state of the system at each time step (fully observable case). In the presence of stochastic dynamics, the cost-to-go introduced in A.14 becomes (the letter v is used for convention):

$$v_k(x, u) = \min_{u_k} x_k^T Q_k x_k + u_k^T R u_k + E\left(v_{k+1}\right). \tag{A.44}$$

The notation $E(.)$ defines the expected value. We recognize the backward recursion utilized that yielded the HJB equation for the derivation of the Pontryagin's maximum principle. The following theorem gives the solution to the optimal control problem.

Theorem. *Under the optimal control policy, the cost-to-go has the following form:*

$$v_k = x_k^T S_k x_k + s_k, \tag{A.45}$$

where S_k are symmetric positive semidefinite matrices and s_k is a non negative scalar quantity.

Proof. The proof is given by induction on the backward recursion of the cost-to-go. From hypothesis, the claim is true when $k = N$ with $S_N = Q_N$ and $s_N = 0$. Assume the claim is true for $k + 1 < N$. The cost-to-go at time k that must be minimized becomes:

$$v_k = x_k^T Q_k x_k + u_k^T R u_k + E(v_{k+1}|x_k, u_k). \tag{A.46}$$

From the induction hypothesis and the system dynamics, the expected value of v_{k+1} given x_k and u_k, plugged into A.46 gives:

$$\begin{aligned} v_k &= x^T(Q_k + A^T S_{k+1} A)x_k + u_k^T(R + B^T S_{k+1} B)u_k \\ &+ 2x_k^T A^T S_{k+1} B u_k + \mathrm{tr}(S_{k+1}\Omega_\xi) + s_{k+1}. \end{aligned} \tag{A.47}$$

It is a quadratic form in u_k, which is minimized when u satisfies the following:

$$u_k = -(R + B^T S_{k+1} B)^{-1} B^T S_{k+1} A x_k. \tag{A.48}$$

The matrix being inverted is non-singular from assumptions. We define L_k such that $u_k = -L_k x_k$ in A.48. By plugging A.48 into A.46, we obtain:

$$v_k = x_k^T \left(Q_k + A^T S_{k+1}(A - BL_k)\right) x_k + s_k, \tag{A.49}$$

where we defined $s_k = s_{k+1} + \mathrm{tr}(S_{k+1}\Omega_\xi) > 0$. Using the definition of L_k, by completing the square we have:

$$S_k = Q_k + (A - BL_k)^T S_{k+1}(A - BL_k) + L_k^T R L_k, \tag{A.50}$$

which is positive semidefinite from assumptions. It completes the proof. ■

Equation A.50 is the algebraic Ricatti equation. For a controller with infinite time horizon ($N \to +\infty$), the stationary control law is obtained by dropping the index k in A.50 and solving for S.

Now, we take into account that the controller has information about the state only through y_k. Consequently, the optimal feedback control policy will be $u_k = -L_k \hat{x}_k$, where $\hat{x}_k$ is the state estimate that is to be defined. We consider the following state estimation based on a Kalman filter:

$$\hat{x}_{k+1} = A\hat{x}_k + Bu_k + K_k\left(y_k - H\hat{x}_k\right). \tag{A.51}$$

The prior estimate $(A\hat{x}_k + Bu_k)$ is the maximum likelihood estimation of x_{k+1} given $\hat{x}_k$ and u_k. The prior estimate is then corrected by the feedback measurement through the term $K_k(y_k - H\hat{x}_k)$. The feedback correction is the difference between the expected and actual feedback measurements, weighted by the Kalman gain K_k that will be defined afterwards. Remark that A.51 assumes that information up to time k is available for the computation of $\hat{x}_{k+1}$. This state estimate is known as the predictive Kalman filter.

From the definition of the feedback output, we have that $y_k - H\hat{x}_k$ is a multivariate Gaussian random variable with 0 mean and covariance matrix $\Omega_\omega + H\Sigma_{\hat{x}}H^T$ ($\Sigma_{\hat{x}}$ is the covariance matrix of $\hat{x}$). Hence, if one replaces x_k by $\hat{x}_k$ in the preceding theorem, the proof still goes through. Only the independent term is affected by the use of the state estimate instead of the true state. We have:

$$s_k = s_{k+1} + \mathrm{tr}\left(S_{k+1}K_k\left(\Omega_\omega + H\Sigma_{\hat{x}}H^T\right)K_k^T\right). \tag{A.52}$$

The same optimal feedback control policy as in the fully observable case should be applied on $\hat{x}_k$. This result is known as the Separation Principle (Aström, 1970): under the state dynamics and output feedback defined in A.41 and A.42, the problems of estimation and control are independent, and can therefore be solved separately. Let us define the estimation error:

$$e_k = x_k - \hat{x}_k. \tag{A.53}$$

By using the state estimate A.51 and the optimal feedback control policy A.48 applied on $\hat{x}_k$, we obtain the following closed loop dynamics for the state variables and the estimation error:

$$\begin{bmatrix} x_{k+1} \\ e_{k+1} \end{bmatrix} = \begin{bmatrix} A - BL_k & BL_k \\ 0 & A - K_kH \end{bmatrix} \begin{bmatrix} x_k \\ e_k \end{bmatrix} + \begin{bmatrix} \xi_k \\ \xi_k - K_k\omega_k \end{bmatrix}. \tag{A.54}$$

Again, the stability of the closed loop dynamics depends on the eigenvalues of the matrices $A - BL_k$ and $A - K_k H$ obtained from the control and estimation problems separately.

Finally, we can compute the Kalman gains K_k from the dynamics of e_k given in A.54. The covariance of e_k is a quadratic function of K_k that is minimized over K_k when the following holds:

$$K_k = A\Sigma_{e_k} H^T \left(H\Sigma_{e_k} H^T + \Omega_\omega\right)^{-1}, \tag{A.55}$$

where we introduced the error covariance at time step k under the notation Σ_{e_k}. This covariance matrix is updated in a forward recursion from the definition of the Kalman's gains and the error dynamics:

$$\Sigma_{e_{k+1}} = (A - K_k H)\,\Sigma_{e_k} A^T + \Omega_\xi. \tag{A.56}$$

A.4 Towards Neuroscience

The previous section gave the solutions for optimal feedback control and optimal state estimation for a class of stochastic systems with (1) linear dynamics, (2) Gaussian uncorrelated additive noise for the dynamics and output feedback and (3) quadratic state and control costs. It constitutes the well known Linear Quadratic Gaussian (LQG) control framework. In many practical problems, the assumptions of LQG appear very restrictive. In the context of motor control, the first assumption that the system dynamics are linear is already barely tenable if one considers realistic models for the dynamics of muscular contraction and the geometry of the musculo-skeletal system.

The assumption of additive noise in the system and feedback is also very restrictive. Indeed, the stochastic dynamics induced by the sensorimotor noise shows signal and state dependent properties: the variability increase with the intensity of the signal. This feature is easily modeled by means of multiplicative noise, but it has a major impact on the

mathematics of the solution: the separation principle no longer holds. Thus, the optimal feedback gains and the Kalman gains depend on each other and must therefore be computed simultaneously. The solution of this problem was given by Todorov (2005) in the case of predictive estimation, and adapted in Chapter 5 of the present manuscript in order to allow the controller to use the current feedback for the current estimation (filtering estimation).

Then, the complexity of delayed systems in continuous time is a considerable obstacle to the design of efficient state-feedback controllers for this class of dynamical systems. However, in the particular case of discrete time models, the delay can be introduced in the state by finite state augmentation. This technique was employed in Chapter 5 and Chapter 6 of the present work. At least, it should be emphasized that the discrete dynamics imposed by the stochastic model is a limitation of the mathematics of the stochastic processes, and it has no correspondence with the physical reality of the movement controlled by the brain. Thus, the ability to deal with time delays by finite system augmentation is also an artificial result which must be used with particular caution.

In summary, the general model is far from the physiology of arm movements. Yet, this far, we have no other choice...

Appendix B

Gravity Levels in Parabolic Flights

B.1 Introduction

The time course of changes in gravity during a typical parabolic flight was explained in each chapter presenting experimental data. However, the gravity inside the aircraft is neither strictly 0 g nor 1.8 g during the different gravitational phases. Such variation in gravity could be damageable for the quality of the experiments since both the movements and measurements can be altered by unstable gravity.

This appendix provides an analysis of the gravity levels collected during one complete sequence of 30 parabolas. This sequence corresponds to the first flight of the 48^{th} ESA Parabolic Flight Campaign (March, 2008). We show based on the variability of the gravity signals that the experimental condition inside the aircraft is stable and reproducible across parabolas.

B.2 Data collection

The gravity was sampled with an accelerometer sensitive to changes in acceleration in the three directions of space in a range of $\pm 3g$ (ADXL 330, Analog Devices, Massachusetts, USA). The accelerometer was at-

tached to the aircraft floor. For a subject seated in the aircraft watching towards the cockpit, OX is the axis directed towards the right-hand side, OY is directed towards the back of the aircraft and OZ is the vertical axis pointing downwards (in order to have positive gravity signals). The variables g_x, g_y, g_z denote the gravity signals measured in the OX, OY and OZ axis, respectively.

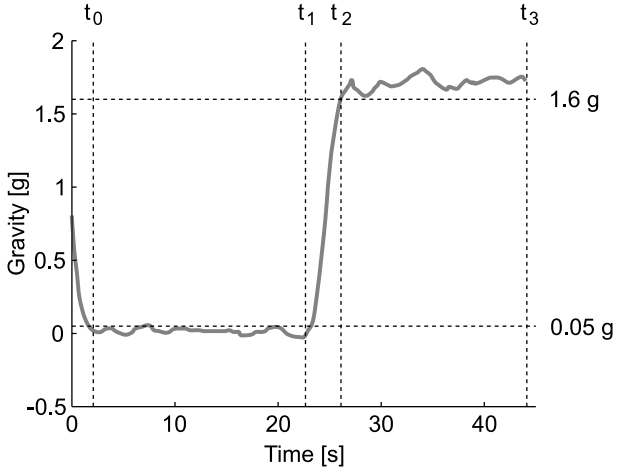


Figure B.1: g_z as a function of time for one selected parabola. The horizontal dashed lines represent the thresholds utilized for the definition of t_0, t_1, t_2 and t_3 (vertical dashed lines).

For each parabola, we computed the time when g_z dropped below the threshold of 0.05 g for the first time. We added 500 ms to this time in order to define the beginning of the 0 g phase (Fig. B.1, t_0). The end of the 0 g phase was defined similarly as 500 ms before the time when gravity exceeded 0.05 g for the last time (Fig. B.1, t_1). Then, we defined the beginning of the hypergravity phase as the moment when gravity exceeded 1.6 g for the first time (Fig. B.1, t_2), until it dropped below the same threshold of 1.6 g for the last time (Fig. B.1, t_3). In the example of Fig. B.1, t_3 was set to the end of the acquisition since gravity did not drop below the threshold of 1.6 g.

The analysis presented below gives the average ($\bar{g}_i$, $i = x, y, z$),

variance and peak-to-peak variation of g_x, g_y and g_z. In addition, it is possible that these signals co-vary and that the variance in the principal direction is greater than the variance computed for each axis independently. To verify this, we define the following covariance matrix:

$$C = \frac{1}{N-1} G^T G,$$

where $G = [g_x - \bar{g}_x \quad g_y - \bar{g}_y \quad g_z - \bar{g}_z]$, N is the number of samples collected between t_0 and t_1 for the 0 g condition and between t_2 and t_3 for the hypergravity condition. The deviation in the principal axis is the computed as the square root of the maximum eigenvalue of C (RMS standing for Root Mean Square):

$$RMS = \sqrt{\max_i \lambda_i(C)}.$$

The standard deviation, peak-to-peak variation and RMS were computed for each parabola.

B.3 Results and Conclusion

Table B.1 presents the results of the analysis. The average gravity is shown across all parabolas in each gravitational condition. Table B.1 also presents the maximum deviation, maximum peak-to-peak variation and maximum RMS across the parabolas of this flight. The maximum RMS corresponds to the maximum SD of g_z, which suggests that there is little-to-no linear covariance in the gravity signals. In general, the microgravity condition is very stable. The hypergravity condition presents more variability. However, in the worst case, the standard deviation represents 6.55% of the gravity level.

The grey traces in Figure B.2 are five typical examples of gravity signals collected in each gravity phases. The signals were aligned relative to the onset defined above: t_0 for the microgravity phases and t_2 for the

Table B.1: Results of the analysis in the microgravity (μg) and hypergravity (Hg) conditions. The maximum RMS was computed on the gravity signals collected in the three axis.

		Average	Max. SD	Max. Peak-to-peak	Max. RMS
	g_x	0.004	0.008	0.046	
μg	g_y	0.007	0.005	0.047	0.036
	g_z	0.002	0.036	0.217	
	g_x	-0.005	0.011	0.060	
Hg	g_y	0.017	0.026	0.097	0.11
	g_z	1.68	0.11	0.365	

hypergravity phases. The black traces are the worst case in peak-to-peak variation (se Table B.1). It can be seen that the worst cases are clear bumps, which can be easily identified.

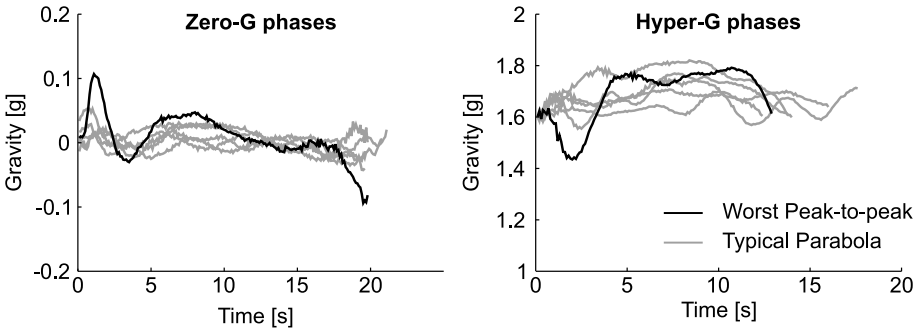


Figure B.2: g_z as a function of time for randomly selected parabolas in each gravitational phase (grey). The black curves are the worst case peak-to-peak variation.

This analysis shows that the experimental condition inside the aircraft is stable and reproducible across parabolas. Yet, the data must be analyzed with caution given the possible presence of bumps that can alter the quality of the sample.

Bibliography

Y. Amino, S. Kyuhou, R. Matsuzaki, and H. Gemba. Cerebello-thalamocortical projections to the posterior parietal cortex in the macaque monkey. *Neurosci Lett*, 309(1):29–32, 2001.

T. Andre, P. Lefevre, and J. Thonnard. Fingertip moisture is optimally modulated during object manipulation. *J Neurophysiol*, 103:402–408, 2009. doi: 10.1152/jn.00901.2009.

H. Asanuma. Functional role of sensory inputs to the motor cortex. *Prog Neurobiol*, 16(3-4):241–262, 1981.

J. Ashe and A. P. Georgopoulos. Movement parameters and neural activity in motor cortex and area 5. *Cereb Cortex*, 4(6):590–600, 1994.

K. J. Aström. *Introduction to stochastic control theory*. New York Academic Press, 1970.

C. G. Atkeson and J. M. Hollerbach. Kinematic features of unrestrained vertical arm movements. *J Neurosci*, 5(9):2318–2330, 1985.

A.-S. Augurelle, M. Penta, O. White, and J.-L. Thonnard. The effects of a change in gravity on the dynamics of prehension. *Exp Brain Res*, 148(4):533–540, 2003a.

A.-S. Augurelle, A. M. Smith, T. Lejeune, and J.-L. Thonnard. Importance of cutaneous feedback in maintaining a secure grip during

manipulation of hand-held objects. *J Neurophysiol*, 89(2):665–671, 2003b.

G. Baroni, A. Pedrocchi, G. Ferrigno, J. Massion, and A. Pedotti. Motor coordination in weightless conditions revealed by long-term microgravity adaptation. *Acta Astronaut*, 49(3-10):199–213, 2001.

A. Battaglia-Mayer, R. Caminiti, F. Lacquaniti, and M. Zago. Multiple levels of representation of reaching in the parieto-frontal network. *Cereb Cortex*, 13(10):1009–1022, 2003. ISSN 1047-3211 (Print).

M. Berger, S. Mescheriakov, E. Molokanova, S. Lechner-Steinleitner, N. Seguer, and I. Kozlovskaya. Pointing arm movements in short- and long-term spaceflights. *Aviat Space Environ Med*, 68(9):781–787, 1997.

M. Berniker and K. Kording. Estimating the sources of motor errors for adaptation and generalization. *Nat Neurosci*, 11(12):1454–1461, 2008.

B. Berret, C. Darlot, F. Jean, T. Pozzo, C. Papaxanthis, and J. P. Gauthier. The inactivation principle: mathematical solutions minimizing the absolute work and biological implications for the planning of arm movements. *PLoS Comput Biol*, 4(10):e1000194, 2008.

E. Bizzi, N. Hogan, F. A. Mussa-Ivaldi, and S. Giseter. Does the nervous system use equilibrium-point control to guide single and multiple joint movements? *Behavioral and Brain Sciences*, 15:603–613, 1992.

R. Blank, A. Breitenbach, M. Nitschke, W. Heizer, S. Letzgus, and J. Hermsdorfer. Human development of grip force modulation relating to cyclic movement-induced inertial loads. *Exp Brain Res*, 138(2):193–199, 2001.

H. G. Bock and K. J. Plitt. A multiple shooting algorithm for direct

solution of optimal control problems. *Proceedings of the 9th IFAC World Congress, Budapest*, pages 243–247, 1984.

O. Bock. Problems of sensorimotor coordination in weightlessness. *Brain Res Brain Res Rev*, 28(1-2):155–160, 1998.

E.-K. Boukas and Z.-K. Liu. *Deterministic and stochastic time delay systems*. Control engineering. Birkhauser, Boston, 2002.

D. A. Braun, A. Aertsen, D. M. Wolpert, and C. Mehring. Learning optimal adaptation strategies in unpredictable motor tasks. *J Neurosci*, 29(20):6472–6478, 2009.

R. G. Brown. *Introduction to random signal analysis and kalman filtering*. Wiley New York, 1983.

A. E. Bryson and Y.-C. Ho. *Applied optimal control : optimization, estimation, and control*. Hemisphere Pub. Corp., Washington, rev. printing edition, 1975. ISBN 0470114819.

C. A. Buneo and R. A. Andersen. The posterior parietal cortex: sensorimotor interface for the planning and online control of visually guided movements. *Neuropsychologia*, 44(13):2594–2606, 2006.

C. A. Buneo, M. R. Jarvis, A. P. Batista, and R. A. Andersen. Direct visuomotor transformations for reaching. *Nature*, 416(6881):632–636, 2002.

E. Burdet, R. Osu, D. W. Franklin, T. E. Milner, and M. Kawato. The central nervous system stabilizes unstable dynamics by learning optimal impedance. *Nature*, 414(6862):446–449, 2001.

J. V. Cohn, P. DiZio, and J. R. Lackner. Reaching during virtual rotation: context specific compensations for expected coriolis forces. *J Neurophysiol*, 83(6):3230–3240, 2000.

J. M. Coron. *Control and nonlinearity.* Mathematical Surveys and Monographs, 2007.

F. Crevecoeur, J. L. Thonnard, and P. Lefevre. Forward models of inertial loads in weightlessness. *Neuroscience*, 161(2):589–598, 2009a.

F. Crevecoeur, J.-L. Thonnard, and P. Lefevre. Optimal integration of gravity in trajectory planning of vertical pointing movements. *J Neurophysiol*, 102(2):786–796, 2009b.

L. Damm and J. McIntyre. Physiological basis of limb-impedance modulation during free and constrained movements. *J Neurophysiol*, 100 (5):2577–2588, 2008.

P. R. Davidson and D. M. Wolpert. Widespread access to predictive models in the motor system: a short review. *J Neural Eng*, 2(3): S313–9, 2005.

V. Della-Maggiore, N. Malfait, D. J. Ostry, and T. Paus. Stimulation of the posterior parietal cortex interferes with arm trajectory adjustments during the learning of new dynamics. *J Neurosci*, 24(44):9971–9976, 2004.

W. T. Dempster. *Space requirements for the seated operator.* Wright Patterson Air Force Base, WADC-TR-55-159, 1955.

W. T. Dempster, W. C. Gabel, and W. J. L. Felts. The antropometry of manual work space for the seated subject. *American Journal of Physical Anthropology*, 17:289–317, 1959.

M. Descoins, F. Danion, and R. J. Bootsma. Predictive control of grip force when moving object with an elastic load applied on the arm. *Exp Brain Res*, 172(3):331–342, 2006.

M. Desmurget, C. M. Epstein, R. S. Turner, C. Prablanc, G. E. Alexander, and S. T. Grafton. Role of the posterior parietal cortex in updating reaching movements to a visual target. *Nat Neurosci*, 2(6): 563–567, 1999.

J. Diedrichsen. Optimal task-dependent changes of bimanual feedback control and adaptation. *Curr Biol*, 17(19):1675–1679, 2007.

J. Diedrichsen, Y. Hashambhoy, T. Rane, and R. Shadmehr. Neural correlates of reach errors. *J Neurosci*, 25(43):9919–9931, 2005.

M. Diehl, H. G. Bock, H. Diedam, and P. B. Wieber. *Fast Motions in Biomechanics and Robotics*. Springer Berlin, Heidelberg, 2006.

J. R. Duhamel, C. L. Colby, and M. E. Goldberg. The updating of the representation of visual space in parietal cortex by intended eye movements. *Science*, 255(5040):90–92, 1992.

R. P. Dum and P. L. Strick. The origin of corticospinal projections from the premotor areas in the frontal lobe. *J Neurosci*, 11(3):667–689, 1991.

V. Ethier, D. S. Zee, and R. Shadmehr. Changes in control of saccades during gain adaptation. *J Neurosci*, 28(51):13929–13937, 2008.

F. Filimon, J. D. Nelson, R.-S. Huang, and M. I. Sereno. Multiple parietal reach regions in humans: cortical representations for visual and proprioceptive feedback during on-line reaching. *J Neurosci*, 29 (9):2961–2971, 2009.

J. Fisk, J. R. Lackner, and P. DiZio. Gravitoinertial force level influences arm movement control. *J Neurophysiol*, 69(2):504–511, 1993.

J. R. Flanagan and S. Lolley. The inertial anisotropy of the arm is accurately predicted during movement planning. *J Neurosci*, 21(4): 1361–1369, 2001.

J. R. Flanagan and A. M. Wing. Modulation of grip force with load force during point-to-point arm movements. *Exp Brain Res*, 95(1): 131–143, 1993.

J. R. Flanagan and A. M. Wing. The stability of precision grip forces during cyclic arm movements with a hand-held load. *Exp Brain Res*, 105(3):455–464, 1995.

J. R. Flanagan and A. M. Wing. The role of internal models in motion planning and control: evidence from grip force adjustments during movements of hand-held loads. *J Neurosci*, 17(4):1519–1528, 1997.

J. R. Flanagan, P. Vetter, R. S. Johansson, and D. M. Wolpert. Prediction precedes control in motor learning. *Curr Biol*, 13(2):146–150, 2003.

T. Flash and N. Hogan. The coordination of arm movements: an experimentally confirmed mathematical model. *J Neurosci*, 5(7):1688–1703, 1985.

A. J. Foulkes and R. C. Miall. Adaptation to visual feedback delays in a human manual tracking task. *Exp Brain Res*, 131(1):101–110, 2000.

D. W. Franklin, R. Osu, E. Burdet, M. Kawato, and T. E. Milner. Adaptation to stable and unstable dynamics achieved by combined impedance control and inverse dynamics model. *J Neurophysiol*, 90 (5):3270–3282, 2003.

D. W. Franklin, U. So, M. Kawato, and T. E. Milner. Impedance control balances stability with metabolically costly muscle activation. *J Neurophysiol*, 92(5):3097–3105, 2004.

D. W. Franklin, E. Burdet, K. P. Tee, R. Osu, C.-M. Chew, T. E. Milner, and M. Kawato. Cns learns stable, accurate, and efficient movements using a simple algorithm. *J Neurosci*, 28(44):11165–11173, 2008.

E. Fridman. New lyapunov - krasovskii functionals for stability of linear retarded and neutral type systems. *Systems and Control Letters*, 43: 309–319, 2001.

E. Fridman and U. Shaked. Delay-dependent stability and hoo control: constant and time-varying delays. *Int J Control*, 76(1):48–60, 2003.

R. Gentili, V. Cahouet, and C. Papaxanthis. Motor planning of arm movements is direction-dependent in the gravity field. *Neuroscience*, 145(1):20–32, 2007.

M. Girgenrath, S. Gobel, O. Bock, and H. Pongratz. Isometric force production in high gz: mechanical effects, proprioception, and central motor commands. *Aviat Space Environ Med*, 76(4):339–343, 2005.

H. Gomi and M. Kawato. Equilibrium-point control hypothesis examined by measured arm stiffness during multijoint movement. *Science*, 272(5258):117–120, 1996.

M. Graziano. The organization of behavioral repertoire in motor cortex. *Annu Rev Neurosci*, 29:105–134, 2006.

P. Gysin, T. R. Kaminski, and A. M. Gordon. Coordination of fingertip forces in object transport during locomotion. *Exp Brain Res*, 149(3): 371–379, 2003.

C. Hamel-Paquet, L. E. Sergio, and J. F. Kalaska. Parietal area 5 activity does not reflect the differential time-course of motor output kinetics during arm-reaching and isometric-force tasks. *J Neurophysiol*, 95(6): 3353–3370, 2006.

C. M. Harris and D. M. Wolpert. Signal-dependent noise determines motor planning. *Nature*, 394(6695):780–784, 1998.

J. Hermsdorfer, C. Marquardt, J. Philipp, A. Zierdt, D. Nowak, S. Glasauer, and N. Mai. Grip forces exerted against stationary held objects during gravity changes. *Exp Brain Res*, 126(2):205–214, 1999.

J. Hermsdorfer, C. Marquardt, J. Philipp, A. Zierdt, D. Nowak, S. Glasauer, and N. Mai. Moving weightless objects. grip force control during microgravity. *Exp Brain Res*, 132(1):52–64, 2000.

N. Hogan and D. Sternad. On rhythmic and discrete movements: reflections, definitions and implications for motor control. *Exp Brain Res*, 181(1):13–30, 2007.

S. Hu and Q. Zhu. Stochastic optimal control and analysis of stability of networked control systems with long delay. *Automatica*, pages 1877 – 1884, 2003.

J. Izawa and R. Shadmehr. On-line processing of uncertain information in visuomotor control. *J Neurosci*, 28(44):11360–11368, 2008.

J. Izawa, T. Rane, O. Donchin, and R. Shadmehr. Motor adaptation as a process of reoptimization. *J Neurosci*, 28(11):2883–2891, 2008.

A. H. Jazwinski. *Stochastic processes and filtering theory*, volume v. 64. Academic Press, New York, 1970.

R. S. Johansson and G. Westling. Roles of glabrous skin receptors and sensorimotor memory in automatic control of precision grip when lifting rougher or more slippery objects. *Exp Brain Res*, 56(3):550–564, 1984.

K. E. Jones, A. F. Hamilton, and D. M. Wolpert. Sources of signal-dependent noise during isometric force production. *J Neurophysiol*, 88(3):1533–1544, 2002.

S. Kakei, D. S. Hoffman, and P. L. Strick. Muscle and movement representations in the primary motor cortex. *Science*, 285(5436):2136–2139, 1999.

S. Kakei, D. S. Hoffman, and P. L. Strick. Direction of action is represented in the ventral premotor cortex. *Nat Neurosci*, 4(10):1020–1025, 2001.

S. Kakei, D. S. Hoffman, and P. L. Strick. Sensorimotor transformations in cortical motor areas. *Neurosci Res*, 46(1):1–10, 2003.

J. F. Kalaska, D. A. Cohen, M. Prud'homme, and M. L. Hyde. Parietal area 5 neuronal activity encodes movement kinematics, not movement dynamics. *Exp Brain Res*, 80(2):351–364, 1990.

M. Kawato. Internal models for motor control and trajectory planning. *Curr Opin Neurobiol*, 9(6):718–727, 1999.

M. Kawato, T. Kuroda, H. Imamizu, E. Nakano, S. Miyauchi, and T. Yoshioka. Internal forward models in the cerebellum: fmri study on grip force and load force coupling. *Prog Brain Res*, 142:171–188, 2003.

K. P. Kording and D. M. Wolpert. Bayesian integration in sensorimotor learning. *Nature*, 427(6971):244–247, 2004.

K. P. Kording and D. M. Wolpert. Bayesian decision theory in sensorimotor control. *Trends Cogn Sci*, 10(7):319–326, 2006.

K. P. Kording, S.-p. Ku, and D. M. Wolpert. Bayesian integration in force estimation. *J Neurophysiol*, 92(5):3161–3165, 2004.

J. Krakauer, M. Ghilardi, and C. Ghez. Independent learning of internal models for kinematic and dynamic control of reaching. *Nature Neuroscience*, 2:1026–1031, 1999.

J. P. Kuhtz-Buschbeck, H. H. Ehrsson, and H. Forssberg. Human brain activity in the control of fine static precision grip forces: an fmri study. *Eur J Neurosci*, 14(2):382–390, 2001.

I. Kurtzer, T. M. Herter, and S. H. Scott. Random change in cortical load representation suggests distinct control of posture and movement. *Nat Neurosci*, 8(4):498–504, 2005.

I. L. Kurtzer, J. A. Pruszynski, and S. H. Scott. Long-latency reflexes of the human arm reflect an internal model of limb dynamics. *Curr Biol*, 18(6):449–453, 2008.

J. R. Lackner and P. Dizio. Rapid adaptation to coriolis force perturbations of arm trajectory. *J Neurophysiol*, 72(1):299–313, 1994.

J. R. Lackner and P. DiZio. Motor control and learning in altered dynamic environments. *Curr Opin Neurobiol*, 15(6):653–659, 2005.

J. R. Lackner and P. DiZio. Angular displacement perception modulated by force background. *Exp Brain Res*, 195(2):335–343, 2009.

A. B. Le Seac'h and J. McIntyre. Multimodal reference frame for the planning of vertical arms movements. *Neurosci Lett*, 423(3):211–215, 2007.

W. Li and E. Todorov. Iterative linearization methods for approximately optimal control and estimation of non-linear stochastic system. *Int J Control*, 80:1439–1453, 2007.

D. Liu and E. Todorov. Evidence for the flexible sensorimotor strategies predicted by optimal feedback control. *J Neurosci*, 27(35):9354–9368, 2007.

B. B. Mandelbrot and J. W. Van Ness. Fractional brownian motions, fractional noise and applications. *SIAM Review*, 10(4):422–437, 1968.

P. Mazzoni, A. Hristova, and J. W. Krakauer. Why don't we move faster? parkinson's disease, movement vigor, and implicit motivation. *J Neurosci*, 27(27):7105–7116, 2007.

J. McIntyre and E. Bizzi. Servo hypotheses for the biological control of movement. *J Mot Behav*, 25(3):193–202, 1993.

J. McIntyre, A. Berthoz, and F. Lacquaniti. Reference frames and internal models for visuo-manual coordination: what can we learn from microgravity experiments? *Brain Res Brain Res Rev*, 28(1-2):143–154, 1998.

J. McIntyre, M. Zago, A. Berthoz, and F. Lacquaniti. Does the brain model newton's laws? *Nat Neurosci*, 4(7):693–694, 2001.

S. Mechtcheriakov, M. Berger, E. Molokanova, G. Holzmueller, W. Wirtenberger, S. Lechner-Steinleitner, C. De Col, I. Kozlovskaya, and F. Gerstenbrand. Slowing of human arm movements during weightlessness: the role of vision. *Eur J Appl Physiol*, 87(6):576–583, 2002.

B. Mehta and S. Schaal. Forward models in visuomotor control. *J Neurophysiol*, 88(2):942–953, 2002.

R. C. Miall and J. K. Jackson. Adaptation to visual feedback delays in manual tracking: evidence against the smith predictor model of human visually guided action. *Exp Brain Res*, 172(1):77–84, 2006.

R. C. Miall and D. King. State estimation in the cerebellum. *Cerebellum*, 7(4):572–576, 2008.

R. C. Miall and G. Z. Reckess. The cerebellum and the timing of coordinated eye and hand tracking. *Brain Cogn*, 48(1):212–226, 2002.

R. C. Miall and D. M. Wolpert. Forward models for physiological motor control. *Neural Netw*, 9(8):1265–1279, 1996.

R. C. Miall, D. J. Weir, D. M. Wolpert, and J. F. Stein. Is the cerebellum a smith predictor? *J Mot Behav*, 25(3):203–216, 1993.

R. C. Miall, L. O. D. Christensen, O. Cain, and J. Stanley. Disruption of state estimation in the human lateral cerebellum. *PLoS Biol*, 5(11): e316, 2007.

W. Michiels, K. Engelborghs, P. Vansevenant, and D. Roose. Continuous pole placement for delay equations. *Automatica*, 38:747–761, 2002.

A. Mierau, M. Girgenrath, and O. Bock. Isometric force production during changed-gz episodes of parabolic flight. *Eur J Appl Physiol*, 102(3):313–318, 2008.

J. Monzee, Y. Lamarre, and A. M. Smith. The effects of digital anesthesia on force control using a precision grip. *J Neurophysiol*, 89(2): 672–683, 2003.

A. J. Nagengast, D. A. Braun, and D. M. Wolpert. Optimal control predicts human performance on objects with internal degrees of freedom. *PLoS Comput Biol*, 5(6):e1000419, 2009.

E. Nakano, H. Imamizu, R. Osu, Y. Uno, H. Gomi, T. Yoshioka, and M. Kawato. Quantitative examinations of internal representations for arm trajectory planning: minimum commanded torque change model. *J Neurophysiol*, 81(5):2140–2155, 1999.

J. Nilsson, B. Bernhardsson, and B. Wittenmark. Stochastic analysis and control of real time systems with random time delays. *Automatica*, 34:57 – 64, 1998.

K. C. Nishikawa, S. T. Murray, and M. Flanders. Do arm postures vary with the speed of reaching? *J Neurophysiol*, 81(5):2582–2586, 1999.

D. A. Nowak, J. Hermsdorfer, S. Glasauer, J. Philipp, L. Meyer, and N. Mai. The effects of digital anaesthesia on predictive grip force adjustments during vertical movements of a grasped object. *Eur J Neurosci*, 14(4):756–762, 2001a.

D. A. Nowak, J. Hermsdorfer, J. Philipp, C. Marquardt, S. Glasauer, and N. Mai. Effects of changing gravity on anticipatory grip force control during point-to-point movements of a hand-held object. *Motor Control*, 5(3):231–253, 2001b.

D. A. Nowak, D. Timmann, and J. Hermsdorfer. Dexterity in cerebellar agenesis. *Neuropsychologia*, 45(4):696–703, 2007.

C. Papaxanthis, T. Pozzo, K. E. Popov, and J. McIntyre. Hand trajectories of vertical arm movements in one-g and zero-g environments. evidence for a central representation of gravitational force. *Exp Brain Res*, 120(4):496–502, 1998a.

C. Papaxanthis, T. Pozzo, and P. Stapley. Effects of movement direction upon kinematic characteristics of vertical arm pointing movements in man. *Neurosci Lett*, 253(2):103–106, 1998b.

C. Papaxanthis, T. Pozzo, and J. McIntyre. Kinematic and dynamic processes for the control of pointing movements in humans revealed by short-term exposure to microgravity. *Neuroscience*, 135(2):371–383, 2005.

A. Parent and L. N. Hazrati. Functional anatomy of the basal ganglia. i. the cortico-basal ganglia-thalamo-cortical loop. *Brain Res Brain Res Rev*, 20(1):91–127, 1995.

Y. A. Phillis. Controller design of systems with multiplicative noise. *IEEE Transactions on Automatic Control*, AC-30(10):1017–1019, 1985.

P. Pigeon, S. B. Bortolami, P. DiZio, and J. R. Lackner. Coordinated turn-and-reach movements. i. anticipatory compensation for self-generated coriolis and interaction torques. *J Neurophysiol*, 89 (1):276–289, 2003.

A. Polit and E. Bizzi. Characteristics of motor programs underlying arm movements in monkeys. *J Neurophysiol*, 42(1 Pt 1):183–194, 1979.

T. Pozzo, C. Papaxanthis, P. Stapley, and A. Berthoz. The sensorimotor and cognitive integration of gravity. *Brain Res Brain Res Rev*, 28(1-2): 92–101, 1998.

J. P. Richard. Time-delay systems: an overview of some recent advances and open problems. *Automatica*, 39:1667–1694, 2003.

R. Ronsse, P. Lefevre, and R. Sepulchre. Robotics and neuroscience: a rhythmic interaction. *Neural Netw*, 21(4):577–583, 2008a.

R. Ronsse, J. Thonnard, P. Lefevre, and R. Sepulchre. Control of bimanual rhythmic movements: trading efficiency for robustness depending on the context. *Exp Brain Res*, 187:193–205, 2008b.

R. Ronsse, D. Sternad, and P. Lefevre. A computational model for rhythmic and discrete movements in uni- and bimanual coordination. *Neural Comput*, 21(5):1335–1370, 2009.

H. Ross, E. Brodie, and A. Benson. Mass discrimination during prolonged weightlessness. *Science*, 225(4658):219–221, 1984.

J. Sangals, H. Heuer, D. Manzey, and B. Lorenz. Changed visuomotor transformations during and after prolonged microgravity. *Exp Brain Res*, 129(3):378–390, 1999.

S. Schaal, D. Sternad, R. Osu, and M. Kawato. Rhythmic arm movement is not discrete. *Nat Neurosci*, 7(10):1136–1143, 2004.

S. H. Scott. The role of primary motor cortex in goal-directed movements: insights from neurophysiological studies on non-human primates. *Curr Opin Neurobiol*, 13(6):671–677, 2003.

S. H. Scott. Optimal feedback control and the neural basis of volitional motor control. *Nat Rev Neurosci*, 5(7):532–546, 2004.

S. H. Scott. Inconvenient truths about neural processing in primary motor cortex. *J Physiol*, 586(5):1217–1224, 2008.

S. H. Scott and J. F. Kalaska. Reaching movements with similar hand paths but different arm orientations. i. activity of individual cells in motor cortex. *J Neurophysiol*, 77(2):826–852, 1997.

S. H. Scott, L. E. Sergio, and J. F. Kalaska. Reaching movements with similar hand paths but different arm orientations. ii. activity of individual cells in dorsal premotor cortex and parietal area 5. *J Neurophysiol*, 78(5):2413–2426, 1997.

R. Shadmehr and J. W. Krakauer. A computational neuroanatomy for motor control. *Exp Brain Res*, 185(3):359–381, 2008.

R. Shadmehr and F. A. Mussa-Ivaldi. Adaptive representation of dynamics during learning of a motor task. *J Neurosci*, 14(5 Pt 2):3208–3224, 1994.

R. Shadmehr and S. P. Wise. *The computational neurobiology of reaching and pointing : a foundation for motor learning*. MIT Press, Cambridge, Mass., 2005.

K. Singh and S. H. Scott. A motor learning strategy reflects neural circuitry for limb control. *Nat Neurosci*, 6(4):399–403, 2003.

S. Sirouspour and M. Shahdi. Model predictive control for transparent teleoperation under communication time delay. *IEEE Transactions on Robotics*, 22(6):1131 – 1145, 2006.

J. F. Soechting, C. A. Buneo, U. Herrmann, and M. Flanders. Moving effortlessly in three dimensions: does donders' law apply to arm movement? *J Neurosci*, 15(9):6271–6280, 1995.

W. J. Terrell. Some fundamental control theory 1: Controllability, observability and duality. *The American Mathematical Monthly*, 106: 705–719, 1999.

E. Todorov. Direct cortical control of muscle activation in voluntary arm movements: a model. *Nat Neurosci*, 3(4):391–398, 2000.

E. Todorov. Cosine tuning minimizes motor errors. *Neural Comput*, 14 (6):1233–1260, 2002.

E. Todorov. Optimality principles in sensorimotor control. *Nat Neurosci*, 7(9):907–915, 2004.

E. Todorov. Stochastic optimal control and estimation methods adapted to the noise characteristics of the sensorimotor system. *Neural Comput*, 17(5):1084–1108, 2005.

E. Todorov and M. I. Jordan. Optimal feedback control as a theory of motor coordination. *Nat Neurosci*, 5(11):1226–1235, 2002.

Y. Uno, M. Kawato, and R. Suzuki. Formation and control of optimal trajectory in human multijoint arm movement. minimum torque-change model. *Biol Cybern*, 61(2):89–101, 1989.

S. Vaziri, J. Diedrichsen, and R. Shadmehr. Why does the brain predict sensory consequences of oculomotor commands? optimal integration of the predicted and the actual sensory feedback. *J Neurosci*, 26(16): 4188–4197, 2006.

M. J. Wagner and M. A. Smith. Shared internal models for feedforward and feedback control. *J Neurosci*, 28(42):10663–10673, 2008.

G. Westling and R. S. Johansson. Factors influencing the force control during precision grip. *Exp Brain Res*, 53(2):277–284, 1984.

O. White, J. McIntyre, A.-S. Augurelle, and J.-L. Thonnard. Do novel gravitational environments alter the grip-force/load-force coupling at the fingertips? *Exp Brain Res*, 163(3):324–334, 2005.

O. White, Y. Bleyenheuft, R. Ronsse, A. M. Smith, J.-L. Thonnard, and P. Lefevre. Altered gravity highlights central pattern generator mechanisms. *J Neurophysiol*, 100(5):2819–2824, 2008.

D. A. Winter. *Biomechanics of human movements*. New York, 1979.

A. G. Witney, A. Wing, J.-L. Thonnard, and A. M. Smith. The cutaneous contribution to adaptive precision grip. *Trends Neurosci*, 27 (10):637–643, 2004.

D. M. Wolpert and J. R. Flanagan. Motor prediction. *Curr Biol*, 11 (18):R729–32, 2001.

D. M. Wolpert and Z. Ghahramani. Computational principles of movement neuroscience. *Nat Neurosci*, 3 Suppl:1212–1217, 2000.

D. M. Wolpert and M. Kawato. Multiple paired forward and inverse models for motor control. *Neural Netw*, 11(7-8):1317–1329, 1998.

D. M. Wolpert, Z. Ghahramani, and M. I. Jordan. An internal model for sensorimotor integration. *Science*, 269(5232):1880–1882, 1995.

D. M. Wolpert, S. J. Goodbody, and M. Husain. Maintaining internal representations: the role of the human superior parietal lobe. *Nat Neurosci*, 1(6):529–533, 1998a.

D. M. Wolpert, R. C. Miall, and M. Kawato. Internal models in the cerebellum. *Trends Cogn Sci*, 2:338–347, 1998b.

D. M. Wolpert, Z. Ghahramani, and J. R. Flanagan. Perspectives and problems in motor learning. *Trends Cogn Sci*, 5(11):487–494, 2001.

Y. Yanai, N. Adamit, Z. Israel, R. Harel, and Y. Prut. Coordinate transformation is first completed downstream of primary motor cortex. *J Neurosci*, 28(7):1728–1732, 2008.

V. M. Zatsiorsky and M. L. Latash. Multifinger prehension: an overview. *J Mot Behav*, 40(5):446–476, 2008.

V. M. Zatsiorsky, F. Gao, and M. L. Latash. Motor control goes beyond physics: differential effects of gravity and inertia on finger forces during manipulation of hand-held objects. *Exp Brain Res*, 162(3): 300–308, 2005.